Numerical Simulation of Wave Propagation in Heterogeneous and Microstructured Materials

MIHHAIL BEREZOVSKI

TALLINN UNIVERSITY OF TECHNOLOGY
Faculty of Science
Department of Mechanics and Applied Mathematics
Institute of Cybernetics

Dissertation was accepted for the defence of the degree of Doctor of Philosophy in Natural and Exact Sciences on April 26, 2010

Supervisor: Professor Jüri Engelbrecht, Department of Mechanics and Applied Mathematics, Institute of Cybernetics at Tallinn University of Technology

Opponents: Dr. Jiři Plešek, Deputy Director of the Institute of Thermomechanics AS CR, Prague, Czech Republic.

                Professor Harm Askes, Professor of Computational Mechanics, Head of Department of Civil and Structural Engineering, Sheffield, UK.

Defence of the thesis: June 21, 2010

Declaration:
Hereby I declare that this doctoral thesis, my original investigation and achievement, submitted for the doctoral degree at Tallinn University of Technology has not been submitted for any academic degree.

/ Mihhail Berezovski /

Lainelevi numbriline simulatsioon heterogeensetes ja mikrostruktuuriga materjalides

MIHHAIL BEREZOVSKI

Contents

List of Figures

Introduction

There is a considerable interest on wave propagation through naturally occurring media and man-made materials in view of widespread applications in acoustic signal transmissions, seismically induced motion, non-destructive evaluation, noise control, subsurface exploration, etc. Due to the complex structure of such media, wave propagation is accompanied by reflection, refraction, diffraction and scattering phenomena that are difficult to quantify. As a result, it becomes necessary to introduce layering as well as position-dependent moduli in the mathematical description of these problems (Baganas, 2005).

Small-scale changes in a heterogeneous material's microstructure can have major effects in its macro-scale behavior. For example, alloying elements, nano-reinforcements, and the crystalline structures of polymers all have profound effects on the parental material's macroscopic response (LaMattina, 2009).

Wave propagation in a homogenous medium is a well described phenomenon, while the situation is much more complicated if the medium is inhomogeneous. The effect of inhomogeneity manifest itself in slowing down of the propagation and in the dispersion of a wave. To describe these effects, several modifications of the wave equation are proposed for wave propagation in heterogeneous materials, like the linear version of the Boussinesq equation, the Love-Rayleigh equation, the Maxwell-Rayleigh model for anomalous dispersion (Maugin, 1995), and dispersive wave equations following from homogenization or continuation procedure (Santosa and Symes, 1991; Maugin, 1999; Wang and Sun, 2002; Fish et al, 2002; Askes and Metrikine, 2002; Engelbrecht and Pastrone, 2003; Metrikine, 2006; Askes et al., 2008) and the general one-dimensional model based on the Mindlin theory of microstructure (Engelbrecht et al., 2005).

Another approach to the description of microstructural effects is provided by internal variable theory (Berezovski, Engelbrecht and Maugin, 2009). In the framework of the internal variable theory, a fully coupled system of equations for macromotion and microstructure evolution is represented in the form of conservation laws.

However, solution of these equations is a not easy task due to their coupling and the absence of natural boundary conditions for internal variable. In addition, parameters of the microstructure model are needed to be determined in each particular case. The diagnostic numerical experiments are needed to compare results of direct numerical calculations of wave propagation in a "comparison medium" with

prescribed properties and corresponding results obtained for an effective medium with the microstructure modeling.

The aim of the thesis is to construct, validate, and implement an efficient and accurate computational method for the dynamic response of heterogeneous and microstructured materials under an impact loading.

The modification of the wave-propagation algorithm (LeVeque, 2002a) is applied as a basic tool of numerical simulations due to its physical soundness, accuracy and thermodynamic consistency (Berezovski, Engelbrecht and Maugin, 2008).

This thesis is organized as follows: Governing equations are formulated in Section 1. The numerical method of solution is introduced in Section 2. Periodic laminates represent the simplest example of microstructure. Therefore, a special attention is paid in Section 4 for wave propagation in periodic laminates, which can be also considered as the "comparison medium" for a more complex microstructure. The geometry of laminates that comes from real experiments was applied for the description of linear wave propagation in laminated composites. The introduction of nonlinearity in Section 4 allows to reproduce the shock response in laminated composites observed experimentally. Linear wave propagation in functionally graded materials is considered in next Section. Final section presents the implementation of the microstructure model in the wave propagation algorithm and the comparison of the results of numerical simulations of a pulse propagation performed by using the microstructure model and the results of the pulse propagation in a "comparison medium" with known heterogeneity properties.

The present thesis is based on seven academic papers, which are referred to in the text as "**Publication I**", "**Publication II**", "**Publication III**", "**Publication IV**", "**Publication V**" and "**Publication VI**":

Publication I

A.Berezovski, M.Berezovski and J.Engelbrecht
Numerical simulation of nonlinear elastic wave propagation in piecewise homogeneous media,
Mater. Sci. Eng A 2006, **418**, 364-369.

Publication II

A. Berezovski, M. Berezovski, J. Engelbrecht, G.A. Maugin
Numerical simulation of waves and fronts in inhomogeneous solids,
in: Multi-Phase and Multi-Component Materials Under Dynamic Loading, W.K. Nowacki and Han Zhao (Eds.) Inst. Fund. Technol. Res. Warsaw, (EMMC-10 Conference proceedings), 2007, pp. 71-80.

Publication III

A. Berezovski, M. Berezovski, J. Engelbrecht
Waves in inhomogeneous solids,
in: *Applied Wave Mathematics - Selected Topics in Solids, Fluids and Mathematical Methods*, E.Quak, T. Soomere (Eds.) Springer, 2009, pp. 55-81.

Publication IV

J. Engelbrecht, A. Berezovski, M. Berezovski

Deformation wave in microstructured materials: theory and numerics, in: Proceedings of the IUTAM Symposium on Recent advances of Acoustic Wave in Solids, May 25-28, 2009, Taipei, Taiwan. (accepted)

Publication V

M. Berezovski, A. Berezovski, J. Engelbrecht
Numerical simulations of one-dimensional microstructure dynamics, in: Proceedings of the 2nd International Symposium on Computational Mechanics (ISCM II), November 30 - December 3, 2009, Hong Kong - Macau. (accepted)

Publication VI

M.Berezovski, A.Berezovski, J.Engelbrecht
Waves in materials with microstructure: numerical simulation, *Proc. Estonian Acad. Sci.*, 2010. (accepted)

Approbation

The results of the thesis have been presented at the following conferences:

1. A. Berezovski, M. Berezovski, J. Engelbrecht
   Numerical Simulation of Non-linear Elastic Wave Propagation in Piecewise Homogeneous Media
   EUROMECH Colloquium 466 Computational and Experimental Mechanics of Advanced Materials
   July 20 - 22, 2005, Loughborough, UK.

2. A. Berezovski, M. Berezovski, J. Engelbrecht, G.A. Maugin
   Numerical simulation of waves and fronts in inhomogeneous solids
   EMMC-10 Conference
   June 11 - 14, 2007, Kazimierz Dolny, Poland.

3. J. Engelbrecht, A. Berezovski, M. Berezovski
   Deformation Waves in Microstructured materials: Theory and Numerics.
   IUTAM Symposium on Recent Advances of Acoustic Waves in Solids
   May 25-28, 2009, Taipei, Taiwan.

4. M.Rousseau, G.A.Maugin and M. Berezovski
   Elements of wave propagation in dynamic materials
   7th EUROMECH Solid Mechanics Conference (ESMC2009)
   September 7-11, 2009, Lisbon, Portugal.

5. M.Berezovski, A.Berezovski, J.Engelbrecht
   Waves in materials with microstructure: numerical simulation
   International Conference on Complexity of Nonlinear Waves
   October 5-7, 2009, Tallinn, Estonia.

6. M. Berezovski, A. Berezovski, J. Engelbrecht
   Numerical simulations of one-dimensional microstructure dynamics.
   2nd International Symposium on Computational Mechanics (ISCM II) and

12th International Conference on Enhancement and Promotion of Computational Methods in Engineering and Science (EPMESC XII)
November 30 December 3, 2009, Hong Kong Macau.

7. M. Berezovski, A. Berezovski, J. Engelbrecht
Numerical simulation of wave propagation in materials with microstructure
SIAM Conference on Mathematical Aspects of Materials Science
May 23-26, 2010, Philadelphia, Pennsylvania. (accepted)

Acknowledgments

1. Governing equations

1.1 Elastic waves

Waves correspond to continuous variations of the states of material points representing a medium. In mechanics, the motion of waves is governed by the conservation law for mass, accompanied by conservation laws for linear momentum and energy. These conservation laws complemented by constitutive relations are the basis of the theory of thermoelastic waves in solids (Achenbach, 1973; Graff, 1975; Bedford and Drumheller, 1994; Billingham and King, 2000).

The law of conservation of mass asserts that the mass of a body is invariant under motion, that is, it remains constant in every configuration. The equation of mass conservation, often called the continuity equation in the reference configuration can be written as:

$$\frac{d\rho_0}{dt} = 0, \tag{1.1}$$

where ρ_0 is the density of a material, t is time.

The balance of linear momentum is a statement of Newton's second law of motion, which relates the forces acting on a body to its acceleration:

$$\rho_0 \frac{dv_i}{dt} - \frac{\partial \sigma_{ij}}{\partial x_j} = \rho f_i. \tag{1.2}$$

Here σ_{ij} is the Cauchy stress tensor, v is the particle velocity, f is external body force.

Conservation of angular momentum requires that the Cauchy stress is a symmetric tensor:

$$\sigma_{ij} = \sigma_{ji}. \tag{1.3}$$

These equations are, however, not sufficient to describe the response of a body to a given loading.

For a linear elastic solid it is assumed that the Cauchy stress is a linear function of the infinitesimal strain. A material is said to be isotropic if its mechanical properties can be described without reference to direction. For an isotropic, linear elastic material, the stress-strain law can be written as

$$\sigma_{ij} = 2\mu\varepsilon_{ij} + \lambda\varepsilon_{kk}\delta_{ij}. \tag{1.4}$$

In the preceding equation the two material constants λ and μ are known as Lame's constants, δ_{ij} is the Kronecker symbol, ε_{ij} is the linearized strain tensor in the case

of small deformation:

$$\varepsilon_{ij} = \frac{1}{2}\left(\frac{\partial u_i}{\partial x_j} + \frac{\partial u_j}{\partial x_i}\right). \tag{1.5}$$

The equation of motion (1.2) in the small strain approximation in the absence of body forces can be written in terms of displacements as

$$\rho_0 \frac{\partial^2 u_i}{\partial t^2} = \frac{\partial \sigma_{ij}}{\partial x_j}. \tag{1.6}$$

Substitution for σ_{ij} from Eq. (1.4) in the latter equation yields

$$\rho_0 \frac{\partial^2 u_i}{\partial t^2} = (\lambda + \mu)\frac{\partial^2 u_j}{\partial x_i \partial x_j} + \mu \frac{\partial^2 u_i}{\partial x_j^2}. \tag{1.7}$$

This equation is the starting point for study of elastic wave motion. However, in numerical simulations it is more convenient to use the equation of motion in its original form (1.2).

In one-dimensional case the displacement is a scalar function of coordinate x and time t:

$$u = u(x, t). \tag{1.8}$$

Corresponding strain and particle velocity are determined as partial derivatives of this displacement:

$$\varepsilon(x, t) = \frac{\partial u}{\partial x}, \qquad v(x, t) = \frac{\partial u}{\partial t}. \tag{1.9}$$

One-dimensional wave propagation in the linear elasticity is governed by the balance of linear momentum

$$\rho_0(x)\frac{\partial v}{\partial t} - \frac{\partial \sigma}{\partial x} = 0, \tag{1.10}$$

and the kinematic compatibility condition following from (1.9)

$$\frac{\partial \varepsilon}{\partial t} = \frac{\partial v}{\partial x}. \tag{1.11}$$

The two equations (1.10) and (1.11) contain three unknowns: v, σ and ε. The closure of the system of equations (1.10) and (1.11) is achieved by a constitutive relation, namely, by the stress-strain relation for each material. There are several possibilities for choosing the stress-strain relation which should reflect the properties of the material. The simplest way it to use a linear relationship (Hooke's law)

$$\sigma = \rho c^2 \varepsilon, \tag{1.12}$$

or a weakly nonlinear law (Ostrovsky and Johnson, 2001)

$$\sigma = \rho c^2 \varepsilon (1 + N\varepsilon), \tag{1.13}$$

12

where c is the longitudinal wave velocity and N is a parameter of nonlinearity. More complicated cases of constitutive models are described, for example, by Engelbrecht (1997).

Up to now, wave propagation in a homogeneous medium was considered, which is a well known phenomenon. The corresponding wave equation is the classical example of hyperbolic partial differential equations in textbooks. However, the situation is much more complicated if the medium is inhomogeneous.

Although materials fabrication has long been known, only in the last century it was recognized that the properties of a given material might not be primarily controlled by its chemical composition but rather by its microstructure. Materials microstructures can feature vacancy/solute clusters, dislocations, twins, interfaces, precipitates, ferroelastic, electric, or magnetic domains, and grain structures, characterized by their amount, size, shape, and spatial arrangement. These structural features usually have an intermediate mesoscopic length scale in the range from nanometres to micrometres. The main objective of modern materials science and engineering is to optimize microstructures for desired properties through advanced processing. However, our ability to characterize and predict quantitatively microstructural evolution and hence to yield unambiguous processing-property relationships is rather limited because of the extreme complexity of microstructures and nonlinear interactions of their elements.

Among the other approaches, the material formulation of continuum mechanics (Maugin, 1993) demonstrates explicitly the appearance of microstructural effects. In this representation, the governing equation (the balance of material momentum) can be represented as

$$\frac{\partial P}{\partial t} - \frac{\partial b}{\partial x} = f^{int} + f^{inh}. \tag{1.14}$$

Here the *material momentum P*, the material *Eshelby stress b*, the material *inhomogeneity force* f^{inh}, and the material *internal* force f^{int} defined by (Berezovski, Engelbrecht and Maugin, 2009)

$$P := -\rho_0 u_t u_x, \quad b := -\left(\rho_0 v^2/2 - W + \sigma\varepsilon\right), \tag{1.15}$$

$$f^{inh} := \left(\frac{1}{2}v^2\right)\frac{\partial \rho_0}{\partial x} - \frac{\partial W}{\partial x}\bigg|_{expl}, \quad f^{int} := \sigma u_{xx} - \frac{\partial W}{\partial x}\bigg|_{impl}, \tag{1.16}$$

where W is the free energy, the subscript notations *expl* and *impl* mean, respectively, the derivative keeping the fields fixed (and thus extracting the explicit dependence on x), and taking the derivative only through the fields present in the function.

In order to represent these forces explicitly, the general one-dimensional model based on the Mindlin theory of microstructure (Engelbrecht et al., 2005) is applied. This gives us an excellent possibility to describe main effects most transparently.

1.2 Microstructure modelling

Suppose that the microstructure model is characterized by a quadratic free energy dependence including two internal variables φ, ψ and their space derivatives (Berezovski, Engelbrecht and Maugin, 2009)

$$\overline{W} = \frac{\rho_0 c^2}{2} u_x^2 + A\varphi u_x + \frac{1}{2}B\varphi^2 + \frac{1}{2}C\varphi_x^2 + \frac{1}{2}D\psi^2, \tag{1.17}$$

where c is the elastic wave speed, $A, B, C,$ and D are material parameters.

For simplicity, only the contribution of the second internal variable itself is considered. In this case, the macrostress σ and microstresses η and ζ are calculated as follows:

$$\sigma = \frac{\partial \overline{W}}{\partial u_x} = \rho_0 c^2 u_x + A\varphi, \quad \eta = -\frac{\partial \overline{W}}{\partial \varphi_x} = -C\varphi_x, \quad \zeta = -\frac{\partial \overline{W}}{\partial \psi_x} = 0, \tag{1.18}$$

and the expression for the interactive internal force τ is

$$\tau = -\frac{\partial \overline{W}}{\partial \varphi} = -Au_x - B\varphi. \tag{1.19}$$

The derivative of the free energy with respect to the dual internal variable ψ gives

$$\xi = -\frac{\partial \overline{W}}{\partial \psi} = -D\psi. \tag{1.20}$$

Evolution equations for internal variables can be represented as (Berezovski, Engelbrecht and Maugin, 2009)

$$\dot{\varphi} = -RD\psi, \quad \dot{\psi} = -R(\tau - \eta_x), \tag{1.21}$$

where R is an appropriate constant. Time differentiation of Eq. $(1.21)_1$ and the evolution equation for the dual internal variable $(1.21)_2$ lead to the hyperbolic equation for the primary internal variable

$$\ddot{\varphi} = R^2 D(\tau - \eta_x). \tag{1.22}$$

This allows us to represent the equations of motion both for macro- and microstructure in the form, which includes only primary internal variable

$$u_{tt} = c^2 u_{xx} + \frac{A}{\rho_0}\varphi_x, \tag{1.23}$$

$$I\varphi_{tt} = C\varphi_{xx} - Au_x - B\varphi, \tag{1.24}$$

where $I = 1/(R^2 D)$.

In terms of stresses introduced by Eq.(1.18), the same system of equations is represented as

$$\rho_0 \frac{\partial^2 u}{\partial t^2} = \frac{\partial \sigma}{\partial x}, \tag{1.25}$$

$$I \frac{\partial^2 \varphi}{\partial t^2} = -\frac{\partial \eta}{\partial x} + \tau. \tag{1.26}$$

It is worth to note that the same equations are derived in Engelbrecht, Cermelli and Pastrone (1999) based on different considerations.

The system of equations (1.23) and (1.24) can be also represented in the form of single wave equation (Berezovski, Engelbrecht and Maugin, 2009)

$$u_{tt} = c^2 u_{xx} + \frac{C}{B} \left(u_{tt} - c^2 u_{xx} \right)_{xx} - \frac{I}{B} \left(u_{tt} - c^2 u_{xx} \right)_{tt} - \frac{A^2}{\rho_0 B} u_{xx}. \tag{1.27}$$

More particular cases of the dispersive wave equation can be found in papers by Santosa and Symes (1991); Maugin (1995, 1999); Wang and Sun (2002); Fish et al (2002); Askes and Metrikine (2002); Engelbrecht and Pastrone (2003); Metrikine (2006); Askes et al. (2008). The problem of wave propagation in heterogeneous and microstructured media has different aspects. From physical point of view, the problem consists in the understanding of dispersive wave behavior; from mathematical point of view, the consistent mathematical model is needed to be developed; numerical aspect concerns to how to solve the equations with necessary efficiency and accuracy.

2. Numerical method

2.1 Wave-propagation algorithm

Many numerical methods have been proposed to compute wave propagation in heterogeneous solids (cf. Kampanis, Ekaterinaris and Dougalis (2008)). Standard methods cannot give high accuracy near discontinuities in the material parameters and will often fail completely in problems where the parameters vary drastically on the grid scale. By contrast, solving the Riemann problem at each cell interface properly resolves the solution into waves, taking into account of every discontinuity in parameters, and automatically handling the reflection and transmission of waves at each interface. This is crucial in representing the correct macroscopic behavior. As a result, Riemann-solver methods are quite natural for application. Moreover, the methods are extended easily from linear to nonlinear problems. Exposition of such methods and pointers to a rich literature can be found in many sources (Godlewski and Raviart, 1996; Guinot, 2003; LeVeque, 2002a; Toro, 1997, 2001).

The general idea is the following. Division of a body into a finite number of computational cells requires the description of all fields inside the cells as well as the interaction between neighboring cells. Approximation of wanted fields inside the cells leads to the discontinuities of the fields at the boundaries between cells. This also leads to the appearance of excess quantities, which represent the difference between exact and approximate values of the fields. Interaction between neighboring cells is described by means of fluxes at the boundaries of the cells. These fluxes can be calculated by means of jump relations at the boundaries between cells.

The system of equations (1.10) - (1.12) is a particular case of a conservation law

$$\frac{\partial}{\partial t} q(x,t) + \frac{\partial}{\partial x} f(q(x,t)) = 0, \tag{2.28}$$

where $q(x,t)$ is the vector of variables and $f(q(x,t))$ is the numerical flux. In the linear elastic case

$$q(x,t) = \begin{pmatrix} \varepsilon \\ \rho v \end{pmatrix}, \quad \text{and} \quad f(x,t) = \begin{pmatrix} -v \\ -\rho c^2 \varepsilon \end{pmatrix}. \tag{2.29}$$

2.2 Averaged quantities

A computational grid of cells $C_n = [x_n, x_{n+1}]$ with interfaces $x_n = n\Delta x$ and time levels $t_k = k\Delta t$ can be introduced for the numerical solution. For simplicity, the

grid size Δx and time step Δt are assumed to be constant. Integrating Eq. (2.28) over $C_n \times [t_k, t_{k+1}]$ gives

$$\int_{\Delta x} q(x, t_{k+1})dx = \int_{\Delta x} q(x, t_k)dx - \tag{2.30}$$

$$- \left(\int_{t_k}^{t_{k+1}} f(q(x_{n+1}, t))dt - \int_{t_k}^{t_{k+1}} f(q(x_n, t))dt \right).$$

Introducing the average $\bar{q}_n$ of the exact solution on C_n at time $t = t_k$ and the numerical flux $\bar{f}_n$ that approximates the time average of the exact flux taken at the interface between the cells C_{n-1} and C_n, i.e.

$$\bar{q}_n \approx \frac{1}{\Delta x} \int_{x_n}^{x_{n+1}} q(x, t_k)dx, \quad \bar{f}_n \approx \frac{1}{\Delta t} \int_{t_k}^{t_{k+1}} f(q(x_n, t))dt, \tag{2.31}$$

Eq. (2.30) can be rewritten in the form of a numerical method in the flux-differencing form (LeVeque, 2002a)

$$\bar{q}_n^{k+1} = \bar{q}_n^k - \frac{\Delta t}{\Delta x}(\bar{f}_{n+1}^k - \bar{f}_n^k). \tag{2.32}$$

In general, however, the time integrals cannot be evaluated in the right-hand side of Eq. (2.30) exactly since $q(x_n, t)$ varies with time along each edge of the cell, and we do not have the exact solution to work with. For fully-discrete method the average flux based on the values $\bar{q}^k$ should be approximated.

2.3   Excess quantities and numerical fluxes

The splitting of the body into a finite number of computational cells and averaging all the fields over the cell volumes leads to a situation, which is known in thermodynamics as "endoreversible system" (Hoffmann, Burzler and Schubert, 1997). This means that even if the state of each computational cell can be associated with a corresponding local equilibrium state (and, therefore, temperature and entropy can be defined as usual), the state of the whole body is a non-equilibrium one. The computational cells interact with each other, which leads to the appearance of excess quantities.

In the admitted non-equilibrium description (Muschik and Berezovski, 2004), vector of variables is represented as the sum of averaged (local equilibrium) and excess parts:

$$q = \bar{q} + Q \tag{2.33}$$

Here $\bar{q}$ is the averaged quantity and Q is the corresponding excess quantity. In the linear case, we can rewrite Eq.(2.28) in the form:

$$\frac{\partial}{\partial t}q(x, t) + M\frac{\partial}{\partial x}q(x, t) = 0, \tag{2.34}$$

17

where the matrix M represents a linear operator. For hyperbolic equations the matrix M is diagonalizable. Integrating Eq. (2.34) over the computational cell gives:

$$\frac{\partial}{\partial t} \int_{\Delta x} q dx = M(q^+ - q^-) = M(\bar{q} + Q^+ - \bar{q} - Q^-) = M(Q^+ - Q^-), \qquad (2.35)$$

where superscripts "+" and "-" denote values of the quantities at right and left boundaries of the cell, respectively. The definition of the averaged quantity

$$\bar{q} = \frac{1}{\Delta x} \int_{\Delta x} q dx \qquad (2.36)$$

allow us rewrite the first-order Godunov-type scheme (2.32) in terms of excess quantities

$$(\bar{q})_n^{k+1} - (\bar{q})_n^k = \frac{\Delta t}{\Delta x} \left(MQ_n^+ - MQ_n^- \right), \qquad (2.37)$$
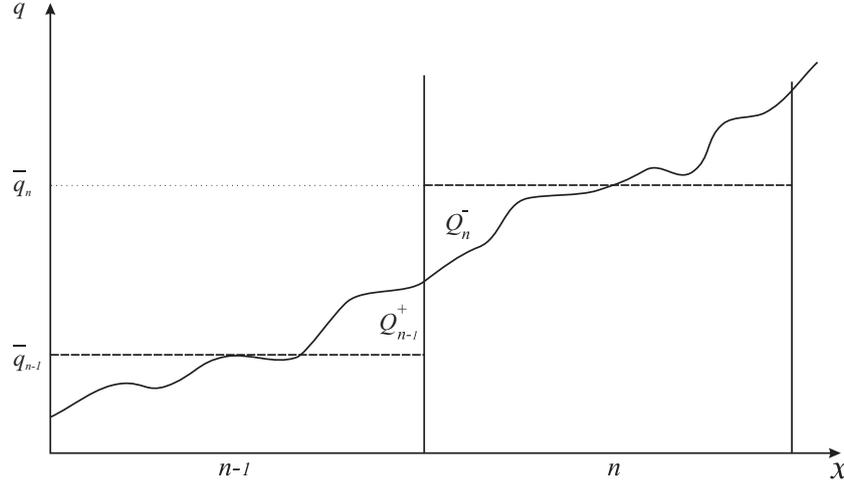
Figure 2.1: Continuity at the boundary of computational cells

Though the excess quantities are determined formally everywhere inside computational cells, we need to know their values only at the boundaries of the cells, where they play the role of numerical fluxes. To determine the values of excess quantities at the boundaries between computational cells, we apply the jump relation (Berezovski and Maugin, 2005), which is reduced in the isothermal case to

$$[\![\bar{q} + Q]\!] = 0. \qquad (2.38)$$

Here $[\![A]\!] = A^+ - A^-$, and $A^\pm$ are the uniform limits of the field A in approaching the boundary from its positive and negative sides, respectively. It should be noted that jump conditions (2.38) can be considered as the *continuity of genuine unknown fields* at the boundaries between computational cells, which is illustrated in Fig. 2.1.

The values of excess quantities at the boundaries between computational cells are not independent (Berezovski and Maugin, 2005). They are connected by Riemann invariants in each particular case.

The representation the wave-propagation algorithm in terms of excess quantities given here is formally identical to the conservative form of the wave-propagation algorithm (Bale et al., 2003).

2.4 Excess quantities at the boundaries between cells in linear elastic case

In the linear elastic case, both stress and velocity are represented as the sum of averaged (local equilibrium) and excess parts:

$$\sigma = \bar{\sigma} + \Sigma, \quad v = \bar{v} + \mathcal{V}. \tag{2.39}$$

Here $\bar{\sigma}$ and $\bar{v}$ are averaged fields and Σ and $\mathcal{V}$ are the corresponding excess quantities.

Therefore, the first-order Godunov-type scheme (Eq. 2.32) can be rewritten in terms of excess quantities

$$(\rho\bar{v})_n^{k+1} - (\rho\bar{v})_n^k = \frac{\Delta t}{\Delta x} \left(\Sigma_n^+ - \Sigma_n^- \right), \tag{2.40}$$

$$\bar{\varepsilon}_n^{k+1} - \bar{\varepsilon}_n^k = \frac{\Delta t}{\Delta x} \left(\mathcal{V}_n^+ - \mathcal{V}_n^- \right). \tag{2.41}$$

Riemann invariants at the interface between computational cells show that the values of excess stresses and excess velocities are connected as (Berezovski, Engelbrecht and Maugin, 2008)

$$\rho_n c_n \mathcal{V}_n^- + \Sigma_n^- \equiv 0, \tag{2.42}$$

$$\rho_{n-1} c_{n-1} \mathcal{V}_{n-1}^+ - \Sigma_{n-1}^+ \equiv 0, \tag{2.43}$$

i.e., the excess quantities depend on each other at the cell boundary.

Rewriting the jump relations (2.39) in the numerical form

$$(\Sigma^+)_{n-1} - (\Sigma^-)_n = (\bar{\sigma})_n - (\bar{\sigma})_{n-1}, \tag{2.44}$$

$$(\mathcal{V}^+)_{n-1} - (\mathcal{V}^-)_n = (\bar{v})_n - (\bar{v})_{n-1}, \tag{2.45}$$

and using the dependence between excess quantities (Eqs. (2.42) and (2.43)), we obtain then the system of linear equations for the determination of excess velocities

$$\mathcal{V}_{n-1}^+ - \mathcal{V}_n^- = \bar{v}_n - \bar{v}_{n-1}, \tag{2.46}$$

$$\mathcal{V}_{n-1}^+ \rho_{n-1} c_{n-1} + \mathcal{V}_n^- \rho_n c_n = \rho_n c_n^2 \bar{\varepsilon}_n - \rho_{n-1} c_{n-1}^2 \bar{\varepsilon}_{n-1}. \tag{2.47}$$

This system of equation can be solved exactly. Then the solution of the global problem can be updated on the next time step by means of Eqs. (2.40) and (2.41)

The algorithm is presented in more detail form in Publication III.

3. Wave propagation in periodic media

3.1 Linear wave propagation in periodic media

The simplest example of heterogeneous media is a periodic medium composed by materials with different properties. As the first case, the propagation of a pulse in a periodic medium composed by alternating layers of dissimilar materials is considered.
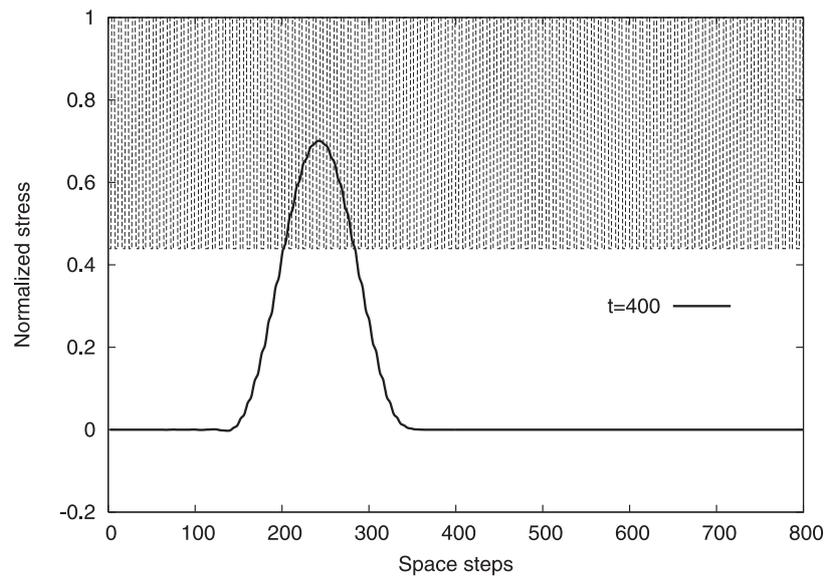
Figure 3.2: Initial pulse shape

The initial pulse shape is presented in Fig. 3.2 where the periodic variation in density is also schematically shown by dashed lines. The wavelength is equal $200\Delta x$ and the periodicity size equals $8\Delta x$.

For the test problem, materials are chosen as polycarbonate ($\rho = 1190 \text{ kg/m}^3$, $c = 4000 \text{ m/s}$) and Al 6061 ($\rho = 2703 \text{ kg/m}^3$, $c = 6149 \text{ m/s}$). Calculations are performed with the Courant-Friedrichs-Levy number equal to 1. The typical result of the simulation for 4000 time steps is shown in Fig. 3.3. A distortion of the pulse shape and a decrease in the velocity of the pulse propagation in comparison of the maximal longitudinal wave velocity in the materials is observed. These results

20
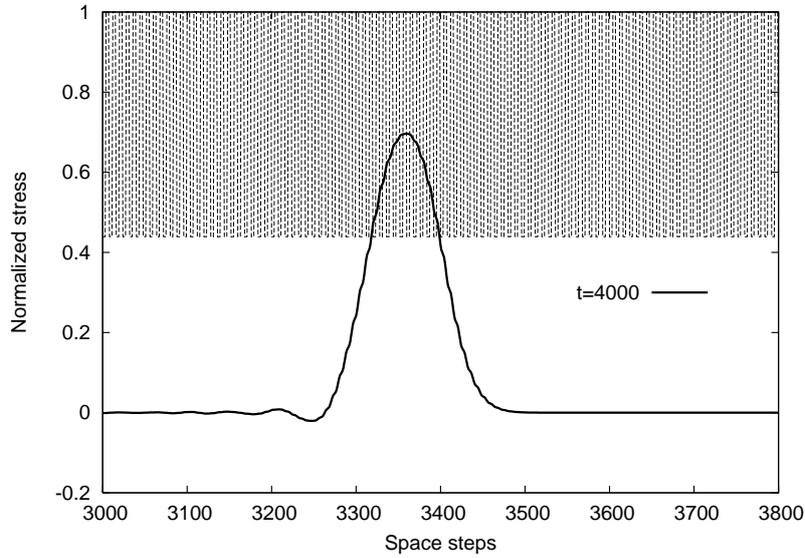
Figure 3.3: Pulse shape at 4700 time step. Linear case

correspond to the prediction of the effective media theory by Santosa and Symes (1991) both qualitatively and quantitatively (Fogarthy and LeVeque, 1999).

More detailed information is published in Publications II and III.

Numerical experiments confirm the dispersive behavior of waves in periodic media with rapidly-varying properties.

3.2 Weakly nonlinear wave propagation in periodic media

In the next example, the influence of materials nonlinearity on the wave propagation is examined. The simple nonlinear stress-strain relation is applied (cf. Ostrovsky and Johnson (2001); Meurer, Qu and Jacobs (2002)) to close the system of Eqs.(1.10) and (1.11) in the case of weakly nonlinear media

$$\sigma = \rho c^2 \varepsilon (1 + N\varepsilon), \qquad (3.48)$$

where N is a parameter of nonlinearity, values and sign of which are supposed to be different for different material materials.

The solution method is almost the same as previously. The approximate Riemann solver for the nonlinear elastic media (Eq.(3.48)) is similar to that used in (LeVeque, 2002b; LeVeque and Yong, 2003). This means that a modified longitudinal wave velocity, $\hat{c}$, following the nonlinear stress-strain relation (3.48) is applied at each time step

$$\hat{c} = c\sqrt{1 + 2N\varepsilon} \qquad (3.49)$$

instead of the piece-wise constant one corresponding to the linear case.

21
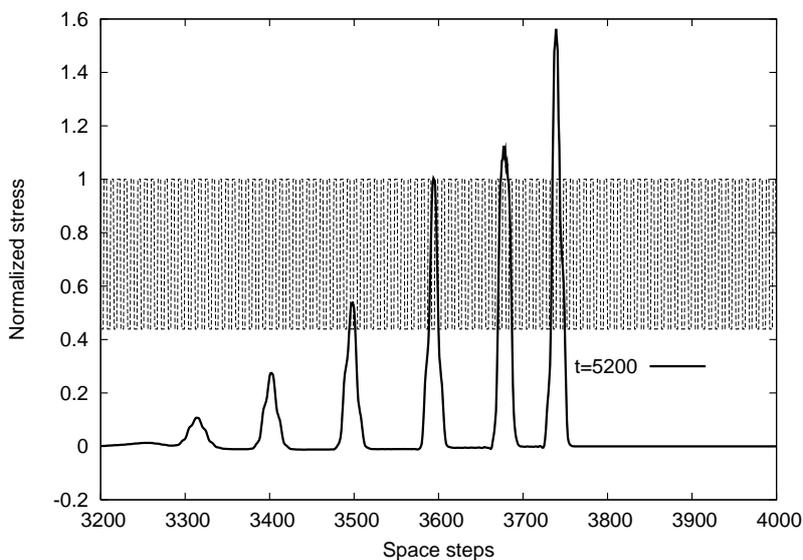
Figure 3.4: Pulse shape at 5200 time step. Nonlinear case

The same pulse shape and the same materials (polycarbonate and Al 6061) as in the case of the linear periodic medium are considered. However, the nonlinear effects appear only for a sufficiently high magnitude of loading. The values of the parameter of nonlinearity N were chosen as 0.24 for Al 6061 and 0.8 for polycarbonate. The result of simulation corresponding to 5200 time steps is shown in Fig. 3.4.

One can observe that an initial bell-shaped pulse is transformed in a train of soliton-like pulses propagating with amplitude-dependent speeds. Such kind of behavior was first reported by LeVeque (2002b), who called these pulses as "stegotons" because their shape is influenced by the periodicity.

In principle, the soliton-like solution could be expected because if we combine the weak nonlinearity (3.48) with the dispersive wave equation in terms of the effective media theory, we arrive at the Boussinesq-type equation

$$\frac{\partial^2 u}{\partial t^2} = (c^2 - c_a^2)\frac{\partial^2 u}{\partial x^2} + \alpha N \frac{\partial u}{\partial x}\frac{\partial^2 u}{\partial x^2} + p^2 c_a^2 c_b^2 \frac{\partial^4 u}{\partial x^4}, \qquad (3.50)$$

which possesses soliton-like solutions. Here u is the displacement, p is the periodicity parameter, c_a and c_b are parameters of the effective media.

These results are published in Publication II and a more detailed analysis is done in Publication III.

Numerical experiments were performed to examine the influence of weak nonlinearity of material on the wave propagation in periodic media and to confirm the emergence of soliton-like wave propagation.

4. Wave propagation in laminates

4.1   Linear wave propagation in laminates

There are three basic length scales in wave propagation phenomena:

- The typical wavelength λ;

- The typical size of the inhomogeneities d;

- The typical size of the whole inhomogeneity domain l.

In the case of infinite periodic media considered in Section 3, the third length scale was absent. Therefore, it may be instructive to consider wave propagation in a body where the periodic arrangement of layers of different materials is confined within a finite spatial domain.
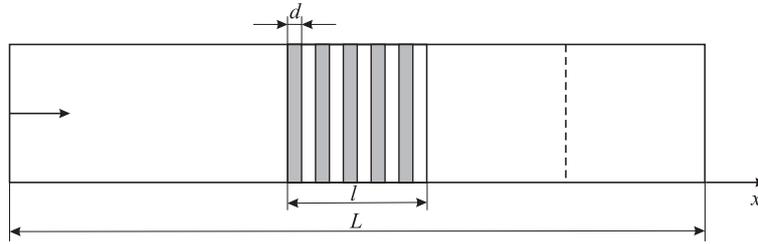
Figure 4.5: Length scales in laminate.

To investigate the influence of the size of the inhomogeneity domain, the shape of the pulse in the homogeneous medium is compared with the corresponding pulse transmitted through the periodic array with a different number of distinct layers (Fig. 4.5).

Different materials Ti ($\rho = 4510\,\text{kg}/\text{m}^3$, $c = 5020\,\text{m/s}$) and Al ($\rho = 2703\,\text{kg}/\text{m}^3$, $c = 5240\,\text{m/s}$) are used in the distinct layers in the numerical simulations of linear elastic wave propagation. The stress pulse the width λ of which corresponds to $100\triangle x$ ($\triangle x$ is the space step) is applied at the left boundary (Fig. 4.5),

$$u_x(0,t) = (1 + \cos(\pi(t - 50\Delta t)/50). \tag{4.51}$$

and the resulting pulse is recorded at $x = 4600\triangle x$. The location is indicated by dashed line in Fig. 4.5.
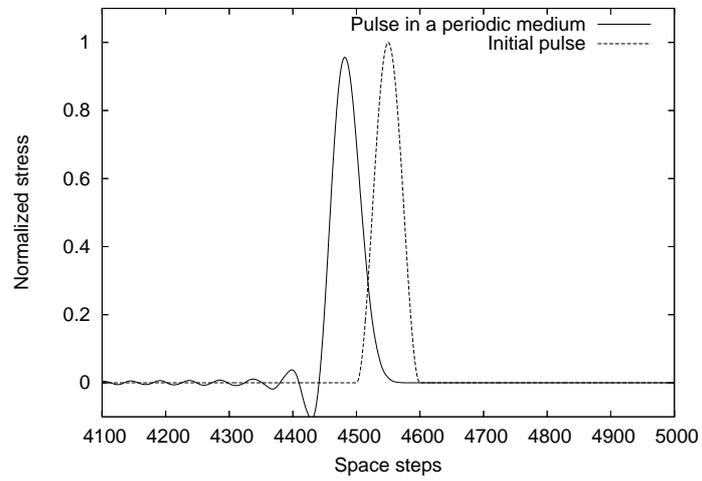
Figure 4.6: Pulse shape at fixed point of 4600 space steps. ($d = 8\triangle x, l = 1000\triangle x$)
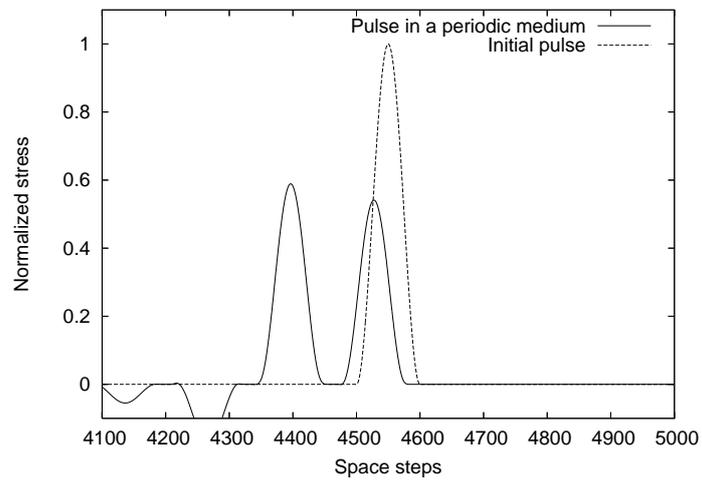
Figure 4.7: Pulse shape at fixed point of 4600 space steps. ($d = 64\triangle x, l = 1000\triangle x$)

The typical results are presented in Figs. 4.6 - 4.7 (solid lines). The reference pulse calculated for homogeneous media is drawn by dashed line. We can observe a strong dispersion of the pulse, i.e., the separation of the wave into components of various frequencies (Fig. 4.7), if the wavelength is comparable with the size of inhomogeneity. This dispersion is not so strong if, vice versa, the size of inhomogeneity d is less than the wavelength λ (Fig. 4.6).

These results are published in Publications II and III.

Thus, waves in laminates demonstrate dispersive behavior, which is governed by relations between characteristic length scales. Taking into account nonlinear effects we have seen the soliton-like wave propagation (Section 3). Both nonlinearity and dispersion effects are observed experimentally in laminates under shock loading.

4.2 Nonlinear wave propagation in laminates under impact loading

In heterogeneous media, scattering due to interfaces between dissimilar materials plays an important role for shock wave dissipation and dispersion (Grady, 1998).

The influence of multiple reflections of internal interfaces on shock wave propagation in the layered composites was clearly illustrated by the shock stress profiles measured by manganin gages.

The geometry of the problem follows the experimental configuration (Zhuang, Ravichandran and Grady, 2003) (Fig. 4.8). To analyze the influence of multiple
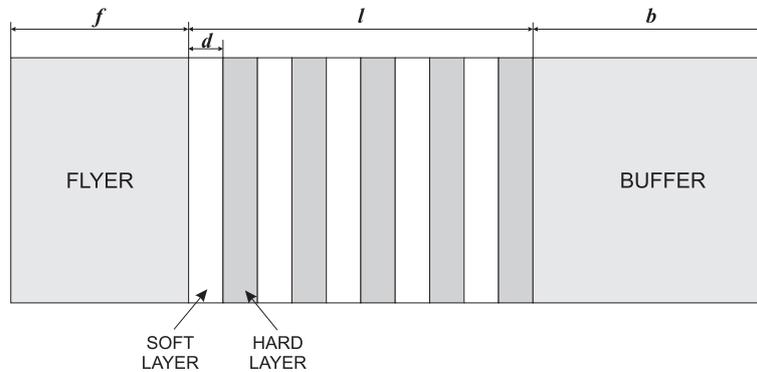
Figure 4.8: Geometry of the problem.

reflections of internal interfaces on shock wave propagation in the layered composites, the initial-boundary value problem of impact loading of a heterogeneous medium composed of alternating layers of two different materials is considered (Berezovski et al., 2006). The impact is provided by a planar flyer of length f which has an initial velocity v_0. A buffer of the same material as the soft component of the specimen is used to eliminate the effect of wave reflection at the stress-free surface. Both left and right boundaries are stress-free.

As previously, a nonlinear stress-strain relation $\sigma(\varepsilon, x)$ for each material (3.48) is applied (cf. Ostrovsky and Johnson (2001); Meurer, Qu and Jacobs (2002))

$$\sigma = \rho c^2 \varepsilon (1 + N\varepsilon), \tag{4.52}$$

where N is a parameter of nonlinearity, values and signs of which are supposed to be different for hard and soft materials. Results of numerical calculations depend crucially on the choice of the parameter of nonlinearity N.
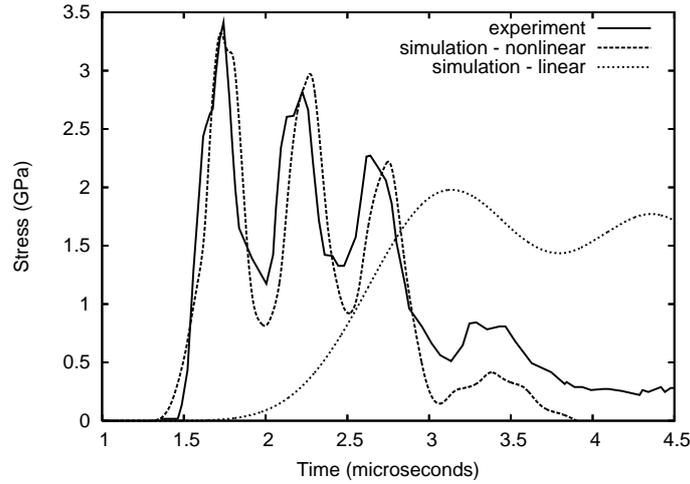
Figure 4.9: Comparison of shock stress time histories corresponding to the experiment 110501

Figure 4.9 shows the stress time histories in the composite, which consists of 16 units of polycarbonate, each 0.37 mm thick, and of 16 units of stainless steel, each 0.19 mm thick. The stress time histories correspond to the distance 3.44 mm from the impact face. Calculations are performed for the flyer velocity 1043 m/s and the flyer thickness 2.87 mm.

The nonlinear parameter N is chosen here to be 2.80 for polycarbonate and zero for stainless steel. Additionally, the stress time history corresponding to the linear elastic solution (i.e., nonlinear parameter N is zero for both components) is shown. It can be seen, that the stress time history computed by means of the considered nonlinear model is very close to the experimental one. It reproduces three main peaks and decreases with distortion, as it is observed in the experiment by Zhuang, Ravichandran and Grady (2003). As it can be seen, the agreement between results of calculations and experiments is achieved by the adjustment of the nonlinear parameter N.

More detailed information and analysis are presented in Publication I, similar results are published in Publications II and III.

Numerical simulations combining scattering effects induced by internal interfaces and physical nonlinearity reproduce the experimentally observed shock response in laminates.

5. Wave propagation in functionally graded materials

Functionally graded materials (FGMs) are composed of two or more phases, that are fabricated so that their compositions vary more or less continuously in some spatial direction and are characterized by nonlinear gradients that result in graded properties. Traditional composites are homogeneous mixtures, and therefore, they involve a compromise between the desirable properties of the component materials.

Studies of the evolution of stresses and displacements in FGMs subjected to a quasistatic load (Suresh and Mortensen, 1998) show that the utilization of structures and geometry of a graded interface between two dissimilar layers can reduce stresses significantly. Such an effect is also important in case of dynamical loading where energy-absorbing applications are of special interest.

We consider the one-dimensional problem in elastodynamics for an FGM slab in which material properties vary only in the thickness direction. It is assumed that the slab is isotropic and inhomogeneous with the following fairly general properties (Chiu and Erdogan, 1999):

$$E(x) = E_0 \left(a\frac{x}{l} + 1 \right)^m \quad \rho(x) = \rho_0 \left(a\frac{x}{l} + 1 \right)^n, \tag{5.53}$$

where ρ is the mass density, l is the thickness, a, m, and n are arbitrary real constants with $a > -1$, E_0 and ρ_0 are the elastic constant and the density at $x = 0$. It is assumed that the slab is at rest for $t \leq 0$. Following Chiu and Erdogan (1999), we consider an FGM slab that consists of nickel and zirconia. The thickness of the slab is $l = 5$ mm, on one surface the medium is pure nickel, on the other surface pure zirconia, and the material properties $E_0(x)$ and $\rho(x)$ vary smoothly in thickness direction. A pressure pulse defined by

$$\sigma_{xx}(l, t) = \sigma_0(H(t) - H(t - t_0)) \tag{5.54}$$

Table 5.1: Properties of materials.

	E (GPa)	ν	ρ (kg/m^3)
ZrO	151	0.33	5331
Ni	207	0.31	8900

27

is applied to the surface $x = l$ and the boundary x=0 is "fixed". Here H is the Heavyside function. The pulse duration is assumed to be $t_0 = 0.2\,\mu s$. The properties of the constituent materials used are given in Table 5.1 (Chiu and Erdogan, 1999).

The material parameters defined by equations (1) and (2) for the FGMs used are Chiu and Erdogan (1999): $a = -0.12354$, $m = -1.8866$, and $n = -3.8866$. The stress is calculated up to $12\,\mu s$ (the propagation time of the plane wave through the thickness $l = 5$ mm is approximately $0.77\,\mu s$ in pure ZrO2 and $0.88\,\mu s$ in Ni). Comparison of the results of the numerical simulation and the analytical solu-
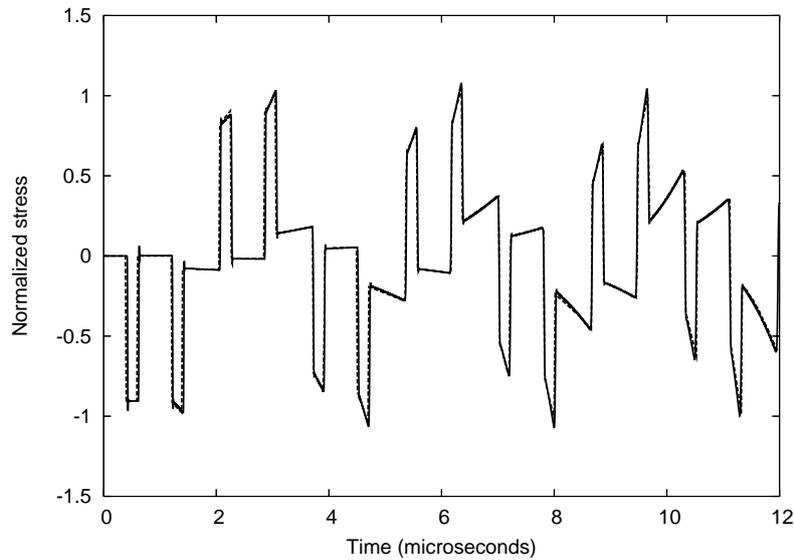
Figure 5.10: Variation of stress with time in the middle of the slab.

tion by Chiu and Erdogan (1999) for the time dependence of the normalized stress σ_{xx}/σ_0 at the location $x/l = 1/2$ is shown in Fig. 5.10.

As one can see, it is difficult to make a distinction between analytical and numerical results. This means that the applied algorithm is well suited for the simulation of wave propagation in FGM.

These results are published in Publications II and III.

Functionally graded materials give examples of materials with non-periodic microstructures. Heterogeneous materials generally exhibit a random distribution of phases according to specific statistical distributions. Microstructural modelling enables us to extend the limits of continuum mechanics to lower scales where size effects are expected.

6. Wave propagation in media with microstructure

6.1 Microstructure modelling

As mentioned in Section 1, the dispersive wave equation based on the Mindlin theory of microstructure is presented in one dimension by Engelbrecht et al. (2005)

$$u_{tt} = c^2 u_{xx} + \frac{C}{B}\left(u_{tt} - c^2 u_{xx}\right)_{xx} - \frac{I}{B}\left(u_{tt} - c^2 u_{xx}\right)_{tt} - \frac{A^2}{\rho_0 B} u_{xx}, \qquad (6.55)$$

where u is the displacement, c is the elastic wave speed, ρ_0 is matter density, A, B, C, and I are material coefficients; subscripts denote derivatives.

As shown in (Engelbrecht et al., 2005), Eq. (6.55) is equivalent to the system of two equations of motion (Engelbrecht, Cermelli and Pastrone, 1999)

$$\rho_0 \frac{\partial^2 u}{\partial t^2} = \frac{\partial \sigma}{\partial x}, \qquad (6.56)$$

$$I \frac{\partial^2 \varphi}{\partial t^2} = -\frac{\partial \eta}{\partial x} + \tau, \qquad (6.57)$$

where the macrostress σ, the microstress η, and the interactive force τ are defined as derivatives of the free energy function

$$\sigma = \frac{\partial W}{\partial u_x}, \quad \eta = -\frac{\partial W}{\partial \varphi_x}, \quad \tau = -\frac{\partial W}{\partial \varphi}, \qquad (6.58)$$

and the quadratic free energy dependence holds

$$W = \frac{\rho_0 c^2}{2} u_x^2 + A \varphi u_x + \frac{1}{2} B \varphi^2 + \frac{1}{2} C \varphi_x^2 + \frac{1}{2} D \psi^2. \qquad (6.59)$$

Here c is the elastic wave speed, as before, A, B, C, and D are material parameters, φ and ψ are dual internal variables (Ván, Berezovski, and Engelbrecht, 2008).

Due to the definitions (6.58) and (6.59), the equations of motion both for macroscale and for microstructure can be represented in the form, which includes only primary internal variable φ (Berezovski, Engelbrecht and Maugin, 2009)

$$u_{tt} = c^2 u_{xx} + \frac{A}{\rho_0} \varphi_x, \qquad (6.60)$$

$$I\varphi_{tt} = C\varphi_{xx} - Au_x - B\varphi, \tag{6.61}$$

where $I = 1/(R^2 D)$ and R is an appropriate constant.

In terms of strain and particle velocity, Eq. (6.60) can be rewritten as

$$\rho_0 v_t = \rho_0 c^2 \varepsilon_x + A\varphi_x. \tag{6.62}$$

The particle velocity and the strain are related by the compatibility condition

$$\varepsilon_t = v_x. \tag{6.63}$$

Similarly, introducing microvelocity w as follows:

$$\varphi_t = w_x, \tag{6.64}$$

which is the compatibility condition at the microlevel, it follows immediately from Eqs. (6.61) and (6.64) that

$$Iw_{tx} = C\varphi_{xx} - A\varepsilon - B\varphi. \tag{6.65}$$

Integrating the latter equation over x, we arrive at (with the accuracy up to arbitrary constant)

$$Iw_t = C\varphi_x - \int (A\varepsilon + B\varphi) dx. \tag{6.66}$$

Thus, we have two coupled systems of equations (6.62), (6.63) and (6.64), (6.66) for the determination of four unknowns: ε, v, φ, and w.

To analyze the capabilities of the model and the role of material constants in the microstructure model, it is needed to solve these systems of equations simultaneously. Numerical simulations are performed by means of a finite-volume numerical scheme modifying the wave-propagation algorithm

$$(\rho\bar{v})_n^{k+1} - (\rho\bar{v})_n^k = \frac{\Delta t}{\Delta x} \left(\Sigma_n^+ - \Sigma_n^- \right) + A\frac{\Delta t}{\Delta x} \left(\Phi_n^+ - \Phi_n^- \right), \tag{6.67}$$

$$\bar{\varepsilon}_n^{k+1} - \bar{\varepsilon}_n^k = \frac{\Delta t}{\Delta x} \left(V_n^+ - V_n^- \right), \tag{6.68}$$

$$\bar{\varphi}_n^{k+1} - \bar{\varphi}_n^k = \frac{\Delta t}{\Delta x} \left(\Omega_n^+ - \Omega_n^- \right), \tag{6.69}$$

$$(I\bar{w})_n^{k+1} - (I\bar{w})_n^k = \frac{C\Delta t}{\Delta x} \left(\Phi_n^+ - \Phi_n^- \right), \tag{6.70}$$

where n and k denote space and time steps, respectively, overbars denote averaged quantities, which are introduced together with excess quantities both for macro- and microfields as follows:

$$\sigma = \bar{\sigma} + \Sigma \quad v = \bar{v} + V, \quad \varphi = \bar{\varphi} + \Phi, \quad w = \bar{w} + \Omega. \tag{6.71}$$

Here Σ is the excess stress, V is the excess velocity, Φ is the excess microstress, and Ω is the excess microvelocity, respectively.

6.2 Results of numerical simulations

As a test problem, the one-dimensional propagation of a pulse is considered. The case of "comparison medium" is analyzed first. In this case, the specimen is assumed homogeneous except of a region of length d, where periodically alternating homogeneous layers of size l are inserted (Fig. 6.11a).
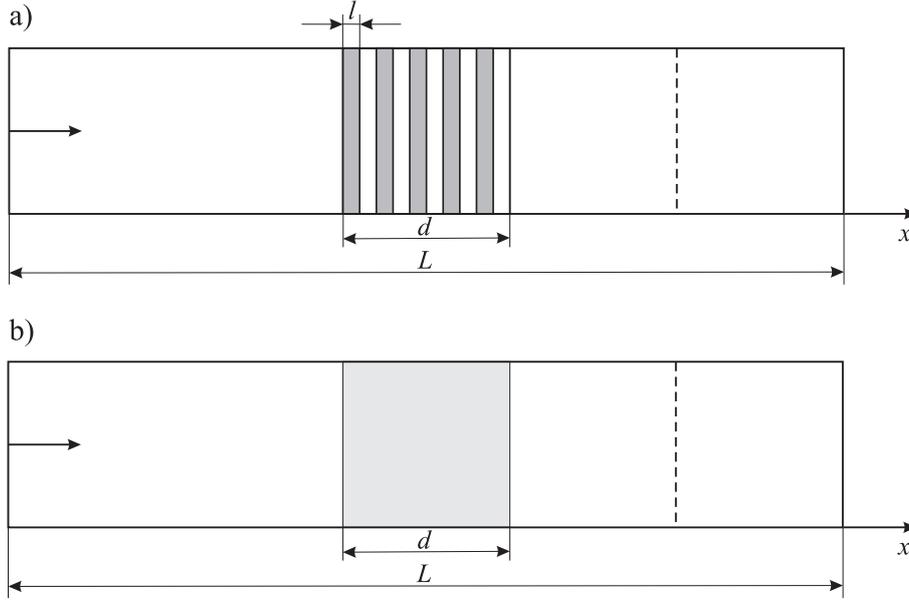
Figure 6.11: Geometry of a test problem.

The density and longitudinal velocity in the specimen are chosen as $\rho = 4510$ kg/m^3 and $c = 5240$ m/s, respectively. The corresponding parameters for the material of the inhomogeneity layers are $\rho_1 = 2703$ kg/m^3 and $c_1 = 5020$ m/s, respectively. Initially, the specimen is at the rest. The shape of the pulse before the crossing of the inhomogeneity region is formed by an excitation of the strain at the left boundary for a limited time period $(0 < t < 100\Delta t)$

$$u_x(0, t) = (1 + \cos(\pi(t - 50\Delta t)/50). \tag{6.72}$$

The arrow in Fig. 6.11 shows the direction of the pulse propagation. The pulse holds its shape up to the entering into the inhomogeneity region. After the interaction with the periodic multilayer, the single pulse is modified because of the successive reflections at each interface between the alternating layers.

Alternatively, the same pulse propagation was simulated by the microstructured model (6.62) - (6.66) (Fig. 6.11b) with $A = 5\rho c^2$. The value of the internal length for the microstructure is kept the same as the size l of periodic layer, as well as density and sound velocity for inhomogeneities: $I = \rho_1, C = Ic_1^2$. The ratio of scales d and λ together with the value of the parameter A determines the contribu-
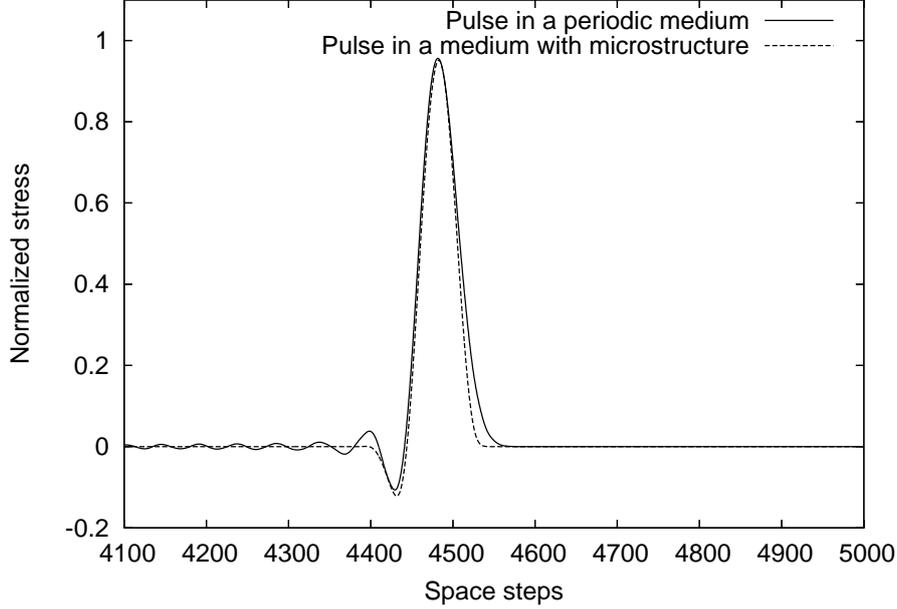
Figure 6.12: Leading transmitted pulses at the inhomogeneity size $l = 8\Delta x$.

tion of the microstructure to macromotion. For relatively long waves (in comparison to the size of inhomogeneity), the shape of the signal is changed slightly, and results of the direct computations and microstructure modelling are in agreement as it can be seen in Fig. 6.12.

However, if the length of the pulse ($\lambda = 100\Delta x$) is comparable with the size of inhomogeneity ($d = 128\Delta x$), the obtained comparison is rather disappointing (Fig. 6.13). Moreover, as extensive numerical experiments show, it cannot be improved by the variation of the values of microstructure parameters.

Therefore, we have to reconsider the microstructure model.

6.2.1 Microstructure model reconstruction

The characteristic property of the microstructure model is the quadratic form of the free energy function (6.59)

$$\overline{W} = \frac{\rho_0 c^2}{2} u_x^2 + A\varphi u_x + \frac{1}{2} B\varphi^2 + \frac{1}{2} C\varphi_x^2 + \frac{1}{2} D\psi^2,\tag{6.73}$$

which is assumed to be convex by default. Convexity requires that the matrix corresponding to this quadratic form

$$M = \begin{pmatrix} \rho_0 c^2 & A & 0 & 0 \\ A & B & 0 & 0 \\ 0 & 0 & C & 0 \\ 0 & 0 & 0 & D \end{pmatrix}\tag{6.74}$$
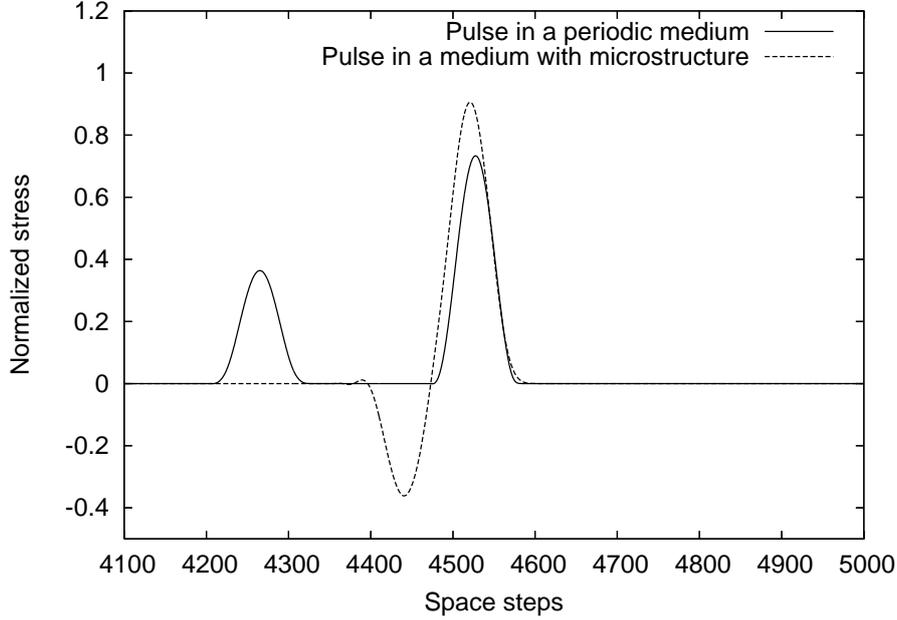
Figure 6.13: Leading transmitted pulses at the inhomogeneity size $l = 128\Delta x$.

must be positive definite. The requirement of positive definiteness results in conditions

$$\rho_0 > 0, \quad \rho_0 c^2 B - A^2 > 0, \quad C > 0, \quad D > 0. \tag{6.75}$$

However, the free energy in the laminated composite analyzed for the comparison with a microstructured medium may be not necessarily convex, while it is convex in each layer. This may be a source of the discrepancy in the results of numerical simulations.

In order to study a more general situation, let us assume that the conditions of convexity (6.75) are not fulfilled completely. Nevertheless, the microstructure model should produce asymptotically stable solutions. In order to verify the generic stability (cf. Ván (2009)), we return to the governing equations of the microstructure model

$$\rho_0 u_{tt} = \rho_0 c^2 u_{xx} + A\varphi_x, \tag{6.76}$$

$$I\varphi_{tt} = C\varphi_{xx} - Au_x - B\varphi, \tag{6.77}$$

and consider exponential plane-wave solutions of the form $u = u_0 e^{\Gamma t + ikx}$, $\varphi = \varphi_0 e^{\Gamma t + ikx}$, where u_0 and φ_0 are constants. Introducing the latter into the system of equations (6.76), (6.77), we get a system of linear equations for u_0 and φ_0

$$\begin{cases} \rho_0 u_0 \Gamma^2 + \rho_0 c^2 u_0 k^2 - A\varphi_0 ik = 0, \\ I\varphi_0 \Gamma^2 + C\varphi_0 k^2 + Au_0 ik + B\varphi_0 = 0. \end{cases} \tag{6.78}$$

33

The condition of existence of a non-trivial solution is the vanishing of the determinant of this system of equations

$$(\rho_0\Gamma^2 + \rho_0 c^2 k^2)(I\Gamma^2 + Ck^2 + B) - A^2 k^2 = 0. \tag{6.79}$$

The requiring asymptotic stability will be reached if $Re\,\Gamma$ is non-positive. This is equivalent to the non-positivity for $Im\,\Gamma^2$.

Let $\Gamma^2 = x + iy$. Then Eq. (6.79) can be represented in the sum of real and imaginary parts

$$(\rho_0 x + \rho_0 c^2 k^2)(Ix + Ck^2 + B) + i\rho_0 y(Ix + Ck^2 + B) + \\ + iIy(\rho_0 x + \rho_0 c^2 k^2) - \rho_0 I y^2 = A^2 k^2. \tag{6.80}$$

The imaginary part should be zero yielding

$$(Ix + Ck^2 + B) + I(x + c^2 k^2) = 0. \tag{6.81}$$

Therefore, the real part of Γ^2 satisfies

$$2Ix = -Ck^2 - B - Ic^2 k^2. \tag{6.82}$$

Inserting the value of the real part of Γ^2 into the real part of Eq. (6.80)

$$(\rho_0 x + \rho_0 c^2 k^2)(Ix + Ck^2 + B) - \rho_0 I y^2 = A^2 k^2, \tag{6.83}$$

we obtain the equation for determining of the imaginary part of Γ^2

$$y^2 = -(Ic^2 k^2 + Ck^2 + B)^2 / 4I^2 - A^2 k^2 / \rho_0 I. \tag{6.84}$$

As it was mentioned, the imaginary part of Γ^2 should be negative. This is achieved by the choice of the negative sign in the square-root of the right-hand side of Eq. (6.84)

$$y = -\sqrt{-(Ic^2 k^2 + Ck^2 + B)^2 / 4I^2 - A^2 k^2 / \rho_0 I}. \tag{6.85}$$

Moreover, the imaginary part is a real number. Therefore, the right-hand side of Eq. (6.84) must be non-negative

$$-(Ic^2 k^2 + Ck^2 + B)^2 / 4I^2 - A^2 k^2 / \rho_0 I \geq 0. \tag{6.86}$$

Rewriting Eq. (6.86) in the form

$$-A^2 k^2 / \rho_0 I \geq (Ic^2 k^2 + Ck^2 + B)^2 / 4I^2, \tag{6.87}$$

we see that the latter condition is satisfied only if $I < 0$.

The condition $I < 0$ is inconsistent with the requirements of convexity of the free energy function and physically questionable. However, the inequality (6.87) is violated for small wave numbers, where the previous pure convex model is valid.

Considering the inequality (6.87) as a constrain for the values of microstructure parameters, we can see that the conservation of hyperbolicity for the equation of motion for microstructure (6.61) yields in the simultaneous negative sign for the coefficient C. Summarizing, we conclude that asymptotically stable solutions are provided for sufficiently large wave numbers by a microstructure model with a (non-convex) free energy function

$$\overline{W} = \frac{\rho_0 c^2}{2} u_x^2 + A\varphi u_x + \frac{1}{2}B\varphi^2 - \frac{1}{2}C\varphi_x^2 - \frac{1}{2}D\psi^2, \tag{6.88}$$

with $C > 0$ and $D > 0$.

Keeping the definitions of stresses, we have in this case

$$\sigma = \frac{\partial \overline{W}}{\partial u_x} = \rho_0 c^2 u_x + A\varphi, \quad \eta = -\frac{\partial \overline{W}}{\partial \varphi_x} = C\varphi_x, \quad \zeta = -\frac{\partial \overline{W}}{\partial \psi_x} = 0. \tag{6.89}$$

The expression for the interactive internal force τ is not changed

$$\tau = -\frac{\partial \overline{W}}{\partial \varphi} = -Au_x - B\varphi. \tag{6.90}$$

The derivative of the free energy with respect to the dual internal variable gives

$$\xi = -\frac{\partial \overline{W}}{\partial \psi} = D\psi. \tag{6.91}$$

Therefore, evolution equations for internal variables φ and ψ (1.21) can be rewritten as

$$\dot{\varphi} = RD\psi, \quad \dot{\psi} = -R(\tau - \eta_x), \tag{6.92}$$

which leads to the hyperbolic equation for the primary internal variable

$$\ddot{\varphi} = -R^2 D(\tau - \eta_x). \tag{6.93}$$

The latter allows us to represent the equations of motion both for macro- and microstructure in the form

$$u_{tt} = c^2 u_{xx} + \frac{A}{\rho_0} \varphi_x, \tag{6.94}$$

$$I\varphi_{tt} = C\varphi_{xx} + Au_x + B\varphi, \tag{6.95}$$

where $I = 1/(R^2 D) > 0$. Comparing with Eq. (6.77), we see the change of signs of last two terms in the right-hand side.

In terms of strain and velocity, Eq. (6.94) is rewritten as

$$\rho_0 v_t = \rho_0 c^2 \varepsilon_x + A\varphi_x. \tag{6.96}$$

The particle velocity and the strain are related by the compatibility condition

$$\varepsilon_t = v_x, \tag{6.97}$$

which form the system of equations for these two variables, as before.

Similarly, introducing microvelocity w as follows:

$$w_x := RD\psi, \tag{6.98}$$

and using Eq. (6.92), we have

$$\varphi_t = w_x, \tag{6.99}$$

which is the compatibility condition at micro-level.

It follows immediately from Eqs. (6.95) and (6.99) that

$$I\dot{w}_x = C\varphi_{xx} + A\varepsilon + B\varphi. \tag{6.100}$$

Integrating the latter equation over x, we arrive at

$$Iw_t = C\varphi_x + \int (A\varepsilon + B\varphi)dx. \tag{6.101}$$

The latter equation differs from Eq. (6.66) only by the sign in the source term in the right-hand side. Results of computations by using Eq. (6.101) instead of Eq. (6.66)
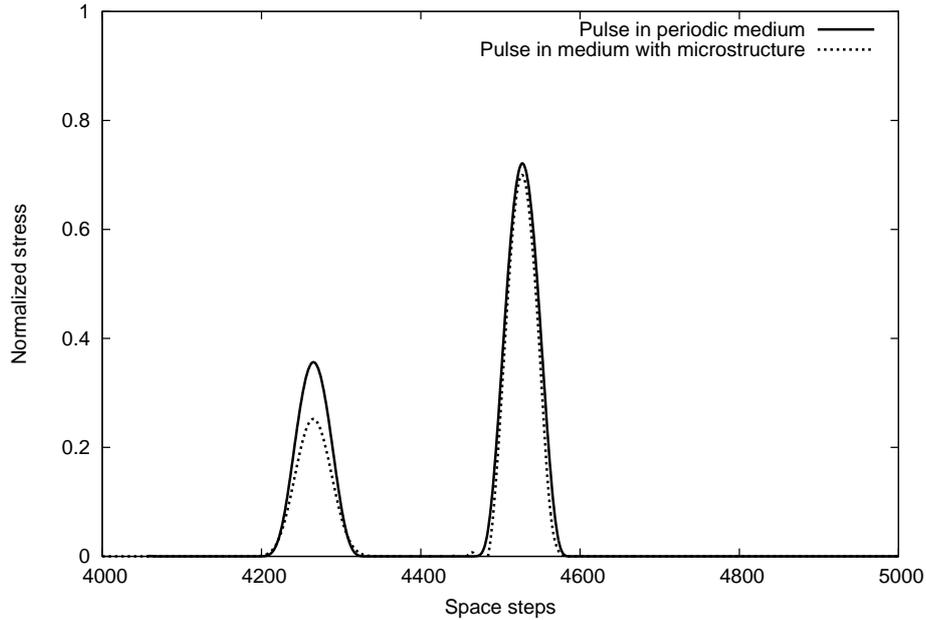
Figure 6.14: Transmitted pulse at the inhomogeneity size $l = 128\Delta x$.

are shown in Fig. 6.14. As one can see, the reconstructed microstructure model is capable of reproducing two leading transmitted pulses in the case of sufficiently short waves (the length of the pulse and the size of inhomogeneity are comparable). The second pulse is smaller than the reference one because of the absence of a reflected trail in the case of the microstructure model.

The coefficient A in the computed microstructure model may be conjectured as related to the variation of the size of inhomogeneity. The corresponding value of the coefficient B is determined by means of the shift of the location of the leading pulse: $B = A^2/(\rho c^2(1 - \alpha^2))$, where α is the value of the Courant number used in the calculation.

Numerical results for various sizes of inhomogeneity are presented in Publication VI. The presented microstructure model looks like a promising variant of the theory, complicated enough to describe various effects of microstructure influence. However, results of numerical simulations show that model should be improved. This manifests the role of numerical simulations in the verification of microstructure models.

First results of model validation are published in Publication IV, results of the improved model are published in Publication V, a more detailed analysis is published in Publication VI.

7. Conclusions

The behavior of many materials of engineering interest (e.g., metals, alloys, granular materials, composites, liquid crystals, polycrystals) is often influenced by an existing or emergent microstructure (e.g., phases in multiphase materials, phase transitions, voids, microcracks, dislocation substructures, texture). In general, the components of such a microstructure have different material properties, resulting in a macroscopic material behavior like in highly anisotropic and inhomogeneous materials.

In dynamic problems, the role of the scale effects is significant. When the wavelength of a traveling signal is comparable with the characteristic size of heterogeneities, successive reflections and refractions of the local waves at the interfaces lead to dispersion and attenuation of the global wave field.

The problem of wave propagation in heterogeneous and microstructured media has different aspects. From the physical point of view, the problem consists in the understanding of dispersive wave behavior; from the mathematical point of view, the consistent mathematical model is needed; numerical aspect concerns to how to solve the equations with necessary efficiency and accuracy.

The aim of the thesis was to construct, validate, and implement an efficient and accurate computational method for the dynamic response of heterogeneous and microstructured materials under an impact load. Wave propagation in periodic media, laminates, functionally graded materials, and media with microstructure were considered under one umbrella.

A modification of the wave-propagation algorithm is applied as a basic tool of numerical simulations due to its physical soundness, accuracy and thermodynamic consistency.

The results of this thesis are:

1. The dispersive behavior of wave propagation in periodic media with rapidly-varying properties is confirmed by numerical experiments.

2. The influence of weak nonlinearity of material on the wave propagation in periodic media is examined. The emergence of soliton-like wave propagation is confirmed.

3. The influence of the size of the inhomogeneity in laminates is investigated. It is shown that if the size of inhomogeneity is comparable with wavelength, the dispersive effect is much stronger than in the case when the size of inhomogeneity is less than the wavelength.

4. The experimentally observed shock response in laminates is reproduced in numerical simulation combining scattering effects induced by internal interfaces and physical nonlinearity.

5. Numerical simulation of wave propagation in functionally graded materials is performed as the example of wave propagation in materials with a non-periodic microstructure.

6. The wave-propagation algorithm for numerical simulation of wave propagation in microstructured media is constructed.

7. The Mindlin-type model is applied for numerical simulation of wave propagation in microstructured media. It is shown that this model is valid for long waves (in comparison to the size of microstructure).

8. The comparison of results for direct numerical simulation in given layered media with the corresponding results obtained by microstructured model leads to the model reconstruction in the case of short waves. It is shown that the reconstructed model is capable of reproducing the wave propagation in microstructured media in the short wave case (the length of the pulse and the size of inhomogeneity are comparable).

Two main points must be stressed. First, the interaction forces between macro- and microstructures are explicitly determined and reflected in the governing equations by dispersive terms. Second, the wave propagation algorithm, elaborated and used for simulation, is a powerful tool for solving the complicated behavior of microstructured solids under dynamical loads. It allows to analyze functionally graded materials and periodically structured laminates from a unified viewpoint and to determine the physical effects with suitable accuracy.

Future studies will be focused in the extension of computations on two-dimensional case and the implementation of front tracking procedure.

Abstract

The aim of the thesis is to construct, validate, and implement an efficient and accurate computational method for the dynamic response of heterogeneous and microstructured materials under an impact load. A modification of the finite volume wave propagation algorithm is used for numerical calculations. A selection of one-dimensional wave propagation problems is presented, the simulation of which exploits the designed numerical scheme. The selection of exemplary problems includes (i) wave propagation in periodic linear and weakly nonlinear media, (ii) linear and nonlinear wave propagation in laminates under an impact load with the comparison with available experimental data, (iii) wave propagation in functionally graded materials, (iv) the comparison of wave propagation in media with explicitly prescribed microstructure and in media with microstructure modeled by internal variables. Main results of the thesis have been presented at seven international conferences and published in papers of journals and proceedings indexed by ISI Web of Science.

Kokkuvõte

Selle töö eesmärk on luua ning rakendada efektiivne ja täpne arvutusmeetod heterogeensete ja mikrostruktuursete materjalide käitumise kirjeldamiseks dünaamilistel koormustel. Numbriliseks simulatsiooniks on tuletatud modifitseeritud lõplike mahtude meetod. On lahendatud hulk lainelevi probleeme ühemõõtmelises seades. Valitud probleemide hulk sisaldab (i) lainelevi perioodilises keskkonnas, (ii) lainelevi lineaarses ja mittelineaarses kihilises keskkonnas löökkoormuse all, (iii) lainelevi funktsionaalselt skaleeritud materjalides, (iv) lainelevi mikrostruktuurses keskkonnas, mida võrreldakse sarnaste tulemustega pidevas keskkonnas modelleeritud mikrostruktuuriga. Käesoleva töö tulemused on esitatud mitmel rahvusvahelisel konverentsil ja avaldatud teadusartiklites rahvusvaheliselt tunnustatud erialaajakirjades ja konverentsikogumikes, mis on indekseeritud ISI Web of Science'i poolt.

References

Achenbach, J.D. (1973). *Wave Propagation in Elastic Solids*. North-Holland, Amsterdam .

Askes, H. and Metrikine, A.V. (2002). One-dimensional dynamically consistent gradient elasticity models derived from a discrete microstructure Part 1: Generic formulation. Eur. J. Mech. A/Solids **21**, 555–572.

Askes, H., Metrikine, A. V., Pichugin, A. V. and Bennett, T. (2008). Four simplified gradient elasticity models for the simulation of dispersive wave propagation. Phil. Mag, **88/28**, 3415-3443.

Baganas, K. (2005). Wave propagation and profile reconstruction in inhomogeneous elastic media. Wave Motion, **42**, 261-273.

Bale, D.S., LeVeque, R.J., Mitran, S., Rossmanith, J.A. (2003). A wave propagation method for conservation laws and balance laws with spatially varying flux functions. SIAM J. Sci. Comp. **24**, 955–978.

Bedford, A., Drumheller, D.S. (1994). *Introduction to Elastic Wave Propagation*. Wiley, New York.

Berezovski, A., Berezovski, M., Engelbrecht, J. (2006). Numerical simulation of nonlinear elastic wave propagation in piecewise homogeneous media. Mater. Sci. Engng. **A 418**, 364–369.

Berezovski, A., Engelbrecht, J., Maugin, G.A. (2008). *Numerical simulation of waves and fronts in inhomogeneous solids.* World Scientific, Singapore.

Berezovski, A., Engelbrecht, J., Maugin, G.A. (2009). One-dimensional microstructure dynamics, In: *Mechanics of microstructured solids: cellular materials, fibre reinforced solids and soft tissues*. (Ganghoffer, J.-F.; Pastrone, F. eds.), pp. 21 − 28, Springer, Series: Lecture Notes in Applied and Computational Mechanics, Vol. 46.

Berezovski, A., Maugin, G.A. (2005). Stress-induced phase-transition front propagation in thermoelastic solids. Eur. J. Mech. - A/Solids **24**, 1–21.

Billingham, J., King, A.C.(2000). *Wave Motion.* Cambridge University Press, Cambridge.

Chiu, T.-C., Erdogan, F. (1999). One-dimensional wave propagation in a functionally graded elastic medium. J. Sound Vibr. **222**, 453–487.

Engelbrecht, J.(1997). *Nonlinear Wave Dynamics. Complexity and Simplicity.* Kluwer, Dordrecht.

Engelbrecht, J., Cermelli, P., Pastrone, F. (1999). Wave hierarchy in microstructured solids. In: Maugin, G.A. (ed.) *Geometry, Continua and Microstructure*, pp. 99–111. Hermann Publ., Paris.

Engelbrecht, J., and Pastrone, F. (2003). Waves in microstructured solids with nonlinearities in microscale. Proc. Estonian Acad. Sci. Phys. Mat. **52**, 12–20.

Engelbrecht, J., Berezovski, A., Pastrone, F., Braun, M. (2005). Waves in microstructured materials and dispersion. Phil. Mag., **85**, 4127–4141.

Fish, J., Chen, W., Nagai, G. (2002). Non-local dispersive model for wave propagation in heterogeneous media: one-dimensional case. Int. J. Numer. Meth. Engng. **54**, 331–346.

Fogarthy, T., LeVeque, R.J. (1999). High-resolution finite-volume methods for acoustics in periodic and random media. J. Acoust. Soc. Am. **106**, 261–297.

Godlewski, E., Raviart, P.-A. (1996). *Numerical Approximation of Hyperbolic Systems of Conservation Laws*. Springer, New York.

Grady, D. (1998). Scattering as a mechanism for structured shock waves in metals. J. Mech. Phys. Solids **46**, 2017–2032.

Graff, K.F. (1975). *Wave Motion in Elastic Solids.* Oxford University Press, Oxford.

Guinot, V. (2003). *Godunov-type Schemes: An Introduction for Engineers*. Elsevier, Amsterdam.

Hoffmann, K.H., Burzler, J.M., Schubert, S. (1997). Endoreversible thermodynamics. J. Non-Equil. Thermodyn. **22**, 311–355.

Kampanis, N. A., Ekaterinaris, J. A. and Dougalis, V. (Eds.) (2008). *Effective Computational Methods for Wave Propagation*. Chapman & Hall/CRC, Boca Raton, FL.

LaMattina B. (2009). The US Army Research Office's Solid Mechanics Perspective. Composites Part B: Engineering **40**, 416.

LeVeque, R.J. (2002a). *Finite Volume Methods for Hyperbolic Problems.* Cambridge University Press, Cambridge.

LeVeque, R.J. (2002b). Finite volume methods for nonlinear elasticity in heterogeneous media. Int. J. Numer. Methods in Fluids **40**, 93–104.

LeVeque, R.J., Yong, D.H. (2003). Solitary waves in layered nonlinear media. SIAM J. Appl. Math. **63**, 1539–1560.

Maugin, G.A. (1993). *Material Inhomogeneities in Elasticity*. Chapman and Hall, London.

Maugin, G.A. (1995). On some generalizations of Boussinesq and KdV systems, Proc. Estonian Acad. Sci. Phys. Mat. **44**, 40–55.

Maugin, G.A. (1999). *Nonlinear Waves in Elastic Crystals*. Oxford University Press, Oxford.

Meurer, T., Qu, J., Jacobs, L.J. (2002). Wave propagation in nonlinear and hysteretic media – a numerical study. Int. J. Solids Struct., **39**, 5585–5614.

Metrikine, A.V. (2006). On causality of the gradient elasticity models. J. Sound Vibr. **297**, 727–742.

Muschik, W., Berezovski, A. (2004). Thermodynamic interaction between two discrete systems in non-equilibrium. J. Non-Equilib. Thermodyn. **29**, 237–255.

Ostrovsky, L. A., Johnson, P. (2001). Dynamic nolinear elasticity in geomaterials. Riv. Nuovo Cimento **34**, 1–46.

Santosa, F., Symes, W.W. (1991). A dispersive effective medium for wave propagation in periodic composites. SIAM J. Appl. Math. **51**, 984–1005.

Suresh, S., Mortensen, A. (1998). *Fundamentals of Functionally Graded Materials*. The Institute of Materials, IOM Communications Ltd., London.

Toro, E.F. (1997). *Riemann Solvers and Numerical Methods for Fluid Dynamics*. Springer, Berlin.

Toro, E.F.(ed.)(2001). *Godunov Methods: Theory and Applications*. Kluwer, New York.

Ván, P., Berezovski, A., Engelbrecht, J. (2008). Internal variables and dynamic degrees of freedom. J. Non-Equilib. Thermodyn. **33**, 235–254.

Ván, P. (2009). Generic stability of dissipative non-relativistic and relativistic fluids. J. Stat. Mech. P02054.

Wang, Z.-P., Sun, C.T. (2002). Modeling micro-inertia in heterogeneous materials under dynamic loading. Wave Motion **36**, 473–485.

Zhuang, S., Ravichandran, G., Grady, D. (2003). An experimental investigation of shock wave propagation in periodically layered composites. J. Mech. Phys. Solids **51**, 245–265.

Appendix A
Publications

Publication I

A.Berezovski, M.Berezovski and J.Engelbrecht

Numerical simulation of nonlinear elastic wave propagation in piecewise homogeneous media,

Numerical simulation of nonlinear elastic wave propagation in piecewise homogeneous media

Arkadi Berezovski*, Mihhail Berezovski, Jüri Engelbrecht

Centre for Nonlinear Studies, Institute of Cybernetics at Tallinn University of Technology, Akadeemia tee 21, 12618 Tallinn, Estonia

Abstract

Systematic experimental work [S. Zhuang, G. Ravichandran, D. Grady, J. Mech. Phys. Solids 51 (2003) 245–265] on laminated composites subjected to high velocity impact loading exhibits the dispersed wave field and the oscillatory behavior of waves with respect to a mean value. Such a behavior is absent in homogeneous solids. An approximate solution to the plate impact in layered heterogeneous solids has been developed in [X. Chen, N. Chandra, A.M. Rajendran, Int. J. Solids Struct. 41 (2004) 4635–4659]. The influence of the particle velocity on many process characteristics was demonstrated. Based on earlier results [A. Berezovski, J. Engelbrecht, G.A. Maugin, Arch. Appl. Mech. 70 (2000) 694–706], numerical simulations of one-dimensional wave propagation in layered nonlinear heterogeneous materials have been performed. The formulated problem follows a conventional experimental configuration of a plate impact. An extension of the high-resolution finite volume wave-propagation algorithm [R.J. LeVeque, Finite Volume Methods for Hyperbolic Problems, Cambridge University Press, 2002] is used. The speed of sound depends nonlinearly on a current stress value in each layer but also on the mismatch properties of layers. Results of numerical simulations capture the experimental data rather well.
© 2005 Elsevier B.V. All rights reserved.

Keywords: Nonlinear elastic waves; Numerical simulation; Finite-volume method; Heterogeneous solids

1. Introduction

Wave propagation in solids can also be characterized as the thermomechanical response of the media. In this context scattering, dispersion and attenuation play an essential role. These phenomena are mostly attributed to material heterogeneity but also to a number of nonlinearities. The nonlinear effects in turn certainly depend on material properties. However, also impedance and geometric mismatch at various length scales have an effect on nonlinearities together with the initial energy of excitation. Although there is a progress in the analysis of wave propagation in heterogeneous materials, the phenomenon of material and geometric dispersion in such media is not fully understood.

The impulsive shock loading in homogeneous media may be divided into three regimes: strong shocks or high pressure, weak shocks or intermediate pressure and elastic or low pressure; the corresponding behavior of solids are respectively hydrodynamic, finite-strain plastic and linear elastic [1]. Though the stress response has been very well understood for homogeneous materials, the same cannot be said for heterogeneous systems. In heterogeneous media, scattering due to interfaces between dissimilar materials plays an important role for shock wave dissipation and dispersion [2].

Diagnostic experiments for the dynamic behavior of heterogeneous materials under impact loading are usually carried out using a plate impact test configuration under a one-dimensional strain state. These experiments are recently reviewed in [3,4]. For almost all the experiments, stress response has shown a sloped rising part followed by an oscillatory behavior with respect to a mean value [3,4]. Such a behavior in the periodically layered systems is consistently exhibited in the systematic experimental work by Zhuang et al. [5]. The specimens used in the shock compression experiments [5] were periodically layered two-component composites prepared by repeating a composite unit as many times as necessary to form a specimen with the desired thickness. A buffer layer of the same material as the soft component of the specimen was used at the other side of the specimen. A window in contact with the buffer layer was used to prevent the free surface from serious damage due to unloading from shock wave reflection at the free surface. Shock

* Corresponding author. Tel.: +372 6204164; fax: +372 6204151.
E-mail address: arkadi.berezovski@cs.ioc.ee (A. Berezovski).

compression experiments were conducted by employing a powder gun loading system, which could accelerate a flat plate flyer to a velocity in range of 400 m/s to about 2000 m/s. In order to measure the particle velocity history at the specimen window surface, a velocity interferometry system was constructed, and to measure the shock stress history at selected internal interfaces, the manganin stress technique was adopted. Four different materials, polycarbonate, 6061-T6 aluminum alloy, 304 stainless steel, and glass, were chosen as components. The selection of these materials provided a wide range of combinations of shock wave speeds, acoustic impedance and strength levels. The influence of multiple reflections of internal interfaces on shock wave propagation in the layered composites was clearly illustrated by the shock stress profiles measured by manganin gages. The origin of the observed structure of the stress waves was attributed to material heterogeneity at the interfaces. For high velocity impact loading conditions, it was fully realized that material nonlinear effects may play a key role in altering the basic structure of the shock wave.

Among the modeling efforts, the mechanical behavior of composites has been extensively investigated using the homogenization approach [6]. Since this approach does not directly consider the interfaces, it is limited in examining the impact behavior, where the wave interactions can be very important.

An approximate solution for layered heterogeneous materials subjected to high velocity plate impact has been developed in [3,4]. For laminated systems under shock loading, shock velocity, density and volume were related to the particle velocity by means of equation of state. The elastic analysis was extended to shock response by incorporating the nonlinear effects through computing shock velocities of the wave trains and superimposing them.

As pointed out in [5], stress wave propagation through layered media made of isotropic materials provides an ideal model to investigate the effect of heterogeneous materials under shock loading, because the length scales, e.g., thickness of individual layers, and other measures of heterogeneity, e.g., impedance mismatch, are well defined.

Since the impact velocity in shock experiments is sufficiently high, various nonlinear effects may affect the observed behavior. That is why we apply numerical simulations of finite-amplitude nonlinear wave propagation to study of scattering, dispersion and attenuation of shock waves in layered heterogeneous materials. The main goal of the paper is to investigate the applicability of the nonlinear description to the shock response of heterogeneous materials.

2. Formulation of the problem

The geometry of the problem follows the experimental configuration [5] (Fig. 1). We consider the initial-boundary value problem of impact loading of a heterogeneous medium composed of alternating layers of two different materials. The impact is provided by a planar flyer of the length f which has an initial velocity v_0. A buffer of the same material as the soft component of the specimen is used to eliminate the effect of wave reflection at the stress-free surface. The densities of the two materials are
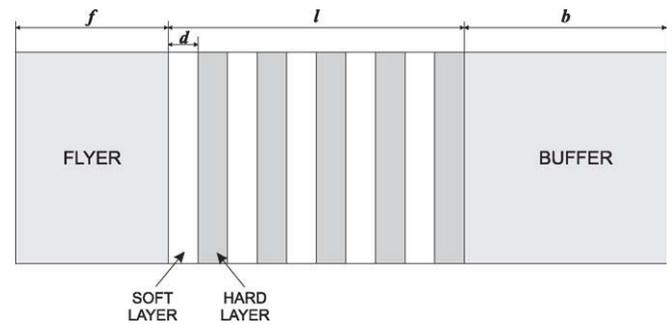
Fig. 1. Geometry of the problem.

different, and the materials response to compression is characterized by the distinct stress–strain relations $\sigma(\varepsilon)$. Compressional waves propagating in the direction of layering are modeled by the one-dimensional hyperbolic system of conservation laws:

$$\rho \frac{\partial v}{\partial t} = \frac{\partial \sigma}{\partial x}, \qquad \frac{\partial \varepsilon}{\partial t} = \frac{\partial v}{\partial x}, \tag{1}$$

where $\varepsilon(x, t)$ is the strain and $v(x, t)$ the particle velocity.

Initially, stress and strain are zero inside the flyer, the specimen, and the buffer, but the initial velocity of the flyer is nonzero:

$$v(x, 0) = v_0, \quad 0 < x < f, \tag{2}$$

where f is the size of the flyer. Both left and right boundaries are stress-free.

Instead of the equation of state as used in [3,4], we apply a more simple nonlinear stress–strain relation $\sigma(\varepsilon, x)$ for each material (cf. [7]):

$$\sigma = \rho c^2 \varepsilon (1 + A\varepsilon), \tag{3}$$

where ρ is the density, c the conventional longitudinal wave speed, A is a parameter of nonlinearity, values of which are supposed to be different for hard and soft materials.

3. Numerical simulations

It is easy to see that the cross-differentiation of Eq. (1) leads to the conventional wave equation, solution of which is well-known, if the corresponding fields are smooth. Assumptions about the smoothness of solutions are not valid near discontinuities in the material parameters. Therefore, standard methods often fail completely, if the parameters vary drastically on the grid size. By contrast, the recently developed high-resolution wave-propagation algorithm [8] has been found well suited for the modeling of wave propagation in rapidly varying heterogeneous media [9]. Within the wave propagation algorithm, every discontinuity in parameters is taken into account by solving the Riemann problem at each interface between discrete elements. The reflection and transmission of waves at each interface are handled automatically for the considered inhomogeneous media.

High-resolution finite-volume methods were originally developed for capturing shock waves in solutions to nonlinear systems of conservation laws, such as the Euler equations of gas dynamics [10]. However, they are also well suited to solving nonlinear wave propagation problems in heterogeneous media

containing many sharp interfaces where coefficients in the equation have discontinuities. Recently, the wave-propagation algorithm was successfully applied to the one-dimensional nonlinear elastic waves in a heterogenous periodic medium consisting of alternating thin layers of two different materials [11,12].

An improved composite wave propagation scheme where a Godunov step is performed after several second-order Lax-Wendroff steps was successfully applied for the two-dimensional thermoelastic wave propagation in media with rapidly varying properties [13–15]. This scheme is also applied here for the solution of the problem (1)–(3). The approximate Riemann solver for the nonlinear elastic media (3) is similar to that used in [11,12]. This means that a modified sound velocity, $\hat{c}$, following the nonlinear stress–strain relation (3) is applied at each time step:

$$\hat{c} = c\sqrt{1 + 2A\varepsilon} \qquad (4)$$

instead of the constant value corresponding to the linear case. Calculations are performed with the Courant number equal to one. Results of the numerical simulations compared with experimental data [5] are presented in the next section.

4. Comparison with experimental data

Fig. 2 shows the measured and calculated stress time history in the composite, which consists of eight units of polycarbonate, each 0.74 mm thick, and of eight units of stainless steel, each 0.37 mm thick. The material properties of components are extracted from [5]: the density $\rho = 1190 \, \text{kg/cm}^3$, the sound velocity $c = 1957 \, \text{m/s}$ for the polycarbonate and $\rho = 7890 \, \text{kg/cm}^3$, $c = 5744 \, \text{m/s}$ for the stainless steel. The stress time histories correspond to the distance 0.76 mm from the impact face. Calculations are performed for the flyer velocity 561 m/s and the flyer thickness 2.87 mm.

Results of numerical calculations depend crucially on the choice of the parameter of nonlinearity A. We choose this parameter from the conditions to match the numerical simulations to experimental results (see Section 5 for the discussion).

Fig. 3. Comparison of particle velocity time histories corresponding to the experiment 112501 [5].

Time histories of particle velocity for the same experiment are shown in Fig. 3. It should be noted that the particle velocity time histories correspond to the boundary between the specimen and the buffer. As one can see both stress and particle velocity time histories are well reproduced by the nonlinear model with the same values of the nonlinear parameter A.

As it is pointed out in [5], the influence of multiple reflections of internal interfaces on shock wave propagation in the layered composites is clearly illustrated by the shock stress time histories measured by manganin gages. Therefore, we focus our attention on the comparison of the stress time histories.

Fig. 4 shows the stress time histories in the composite, which consists of 16 units of polycarbonate, each 0.37 mm thick, and of 16 units of stainless steel, each 0.19 mm thick. The stress time histories correspond to the distance 3.44 mm from the impact face. Calculations are performed for the flyer velocity 1043 m/s and the flyer thickness 2.87 mm.

The nonlinear parameter A is chosen here to be equal 2.80 for polycarbonate and zero for stainless steel. Additionally, the stress time history corresponding to linear elastic solution

Fig. 2. Comparison of shock stress time histories corresponding to the experiment 112501 [5].
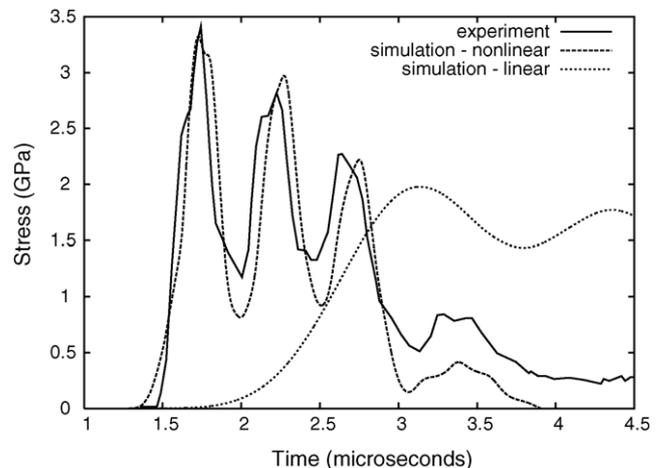
Fig. 4. Comparison of shock stress time histories corresponding to the experiment 110501 [5].

Fig. 5. Comparison of shock stress time histories corresponding to the experiment 110502 [5].
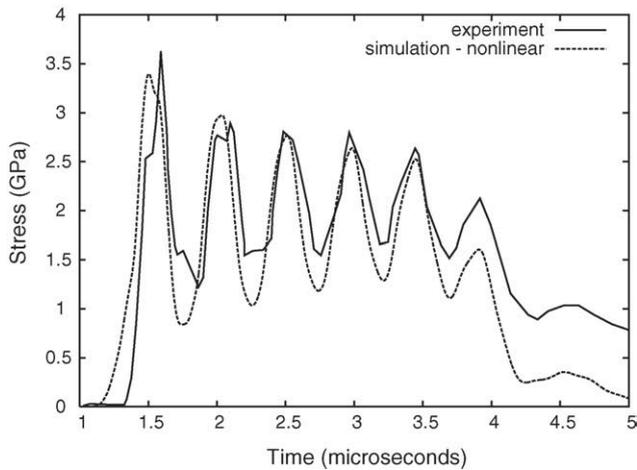
Fig. 6. Comparison of shock stress time histories corresponding to the experiment 112301 [5].

(i.e., nonlinear parameter A is zero for both components) is shown. It can be seen, that the stress time history computed by means of the considered nonlinear model is very close to the experimental one. It reproduces three main peaks and decreases with distortion, as it is observed in the experiment [5].

In Fig. 5 the same comparison is presented for the same composite as in Fig. 4, only the flyer thickness is different (5.63 mm). This means that the shock energy is approximately twice higher than that in the previous case. The nonlinear parameter A is also increased to 4.03 for polycarbonate and remains zero for stainless steel. As a result all six experimentally observed peaks are reproduced well.

In Fig. 6 the comparison of stress time histories is presented for the composite, which consists of sixteen 0.37 mm thick units of polycarbonate and sixteen 0.20 mm thick units of D-263 glass. The material properties of D-263 glass are [5]: the density $\rho = 2510$ kg/cm^3, the sound velocity $c = 5703$ m/s. The distance between the measurement point and the impact face is 3.41 mm. Corresponding flyer velocity is 1079 m/s and the flyer thickness is 2.87 mm. The nonlinear parameter A is chosen to be equal 5.025 for polycarbonate and zero for D-263 glass. Again, the stress time history corresponding to linear elastic solution (i.e., nonlinear parameter is zero for both components) is shown. As one can see, the stress time history corresponding to the nonlinear model reproduces all five peaks with the same amplitude as observed experimentally.

Fig. 7 shows the comparison of stress time histories for composite, which consists of seven units of polycarbonate, each 0.74 mm thick, and seven units of float glass, each 0.55 mm thick. The material properties of float glass are slightly different from those for D-263 glass [5]: the density $\rho = 2500$ kg/cm^3, the sound velocity $c = 5742$ m/s. The stress profiles correspond to the distance 3.37 mm from the impact face, to the flyer velocity 563 m/s, and to the flyer thickness 2.87 mm. The nonlinear parameter A is equal 3.04 for polycarbonate and zero for float glass. The result of numerical simulation coincides with experiment both in amplitude and in shape.
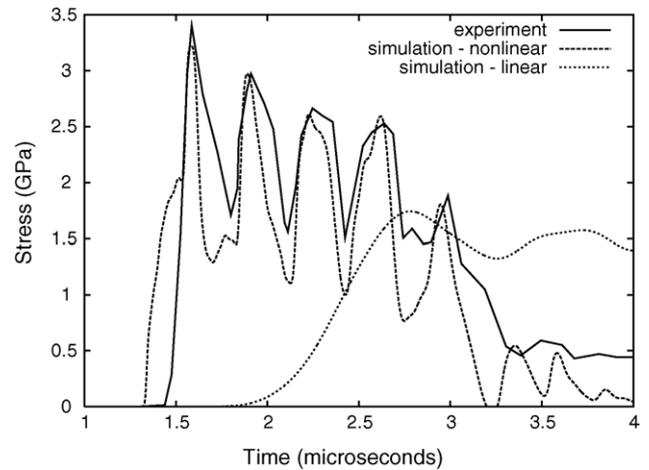
In Fig. 8 the same comparison is presented for the same composite, only the flyer velocity is almost twice higher, namely, 1056 m/s. The value of the nonlinear parameter A is 5.53 for polycarbonate and zero for float glass. It can be seen, that the result of numerical simulation is very close to experimental data. The complicated shape of the experimental stress time history is reproduced as well.

As it can be seen, the agreement between results of calculations and experiments is achieved by the adjustment of the nonlinear parameter A.

5. Discussion

Though the parameter of nonlinearity A looks like a material constant in the Eqs. (3) and (4), numerical simulations show that this parameter depends also on the structure of the specimen. The values of the nonlinear parameter together with the used experimental conditions are given in Table 1. In the table, PC denotes polycarbonate, GS denotes glass, SS denotes 304 stainless steel; the number following the abbreviation of the
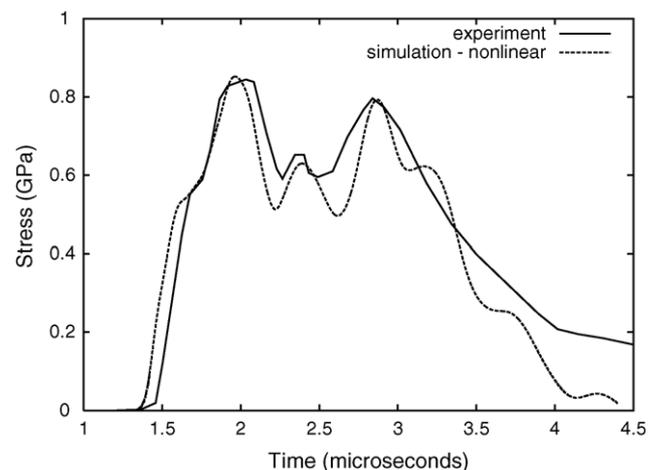
Fig. 7. Comparison of shock stress time histories corresponding to the experiment 120201 [5].

Table 1
Experimental conditions and values of the parameter of nonlinearity

Experiments	Specimen soft/hard	Units	Flyer velocity (m/s)	Flyer thickness (PC) (mm)	Gage position (mm)	A (PC)	A (Other)
110501	PC37/SS19	16	1043	2.87	3.44	2.80	0
110502	PC37/SS19	16	1045	5.63	3.44	4.03	0
112301	PC37/GS20	16	1079	2.87	3.41	5.025	0
120201	PC74/GS55	7	563	2.87	3.37	3.04	0
120202	PC74/GS55	7	1056	2.87	3.35	5.53	0

Table 2
Normalized experimental conditions and nonlinearity parameters

Experiments	Specimen soft/hard	Normalized flyer energy $\check{E}$	Relative impedance mismatch $\check{Z}$	Geometrical factor $\check{G}$	A (PC)	$A\sqrt{\frac{\check{Z}}{\check{E}\check{G}}}$
110501	PC37/SS19	1.00	1.00	1.00	2.80	2.80
110502	PC37/SS19	1.97	1.00	1.00	4.03	2.87
112301	PC37/GS20	1.07	0.316	1.02	5.025	2.71
120201	PC74/GS55	0.29	0.316	1.226	3.04	2.87
120202	PC74/GS55	1.025	0.316	1.226	5.53	2.78

component material represents the layer thickness in hundredths of a millimeter.

It appears that the application of the nonlinear model to only soft material (polycarbonate) is sufficient to reproduce stress profiles at the gage position about 3.4 mm; any hard material can be treated as linear elastic one.

The comparison of the conditions of experiments 110501 and 110502 as well as 120201 and 120202 and the corresponding values of the parameter of nonlinearity A demonstrates the dependence of the parameter A on the impact energy. The influence of the impedance mismatch is clearly follows from the results of simulations corresponding to experiments 110501 and 112301. The dependence on the number of layers is not clear: the difference between the values of the nonlinear parameter in the simulations of experiments 112301 and 120202 can be attributed to the slightly different material properties of float glass and D-263 glass. The effect of the thickness ratio of the layers mentioned in [3] cannot be investigated on the basis of the discussed experimental data, since the thickness ratio was unchanged in the experiments [5].
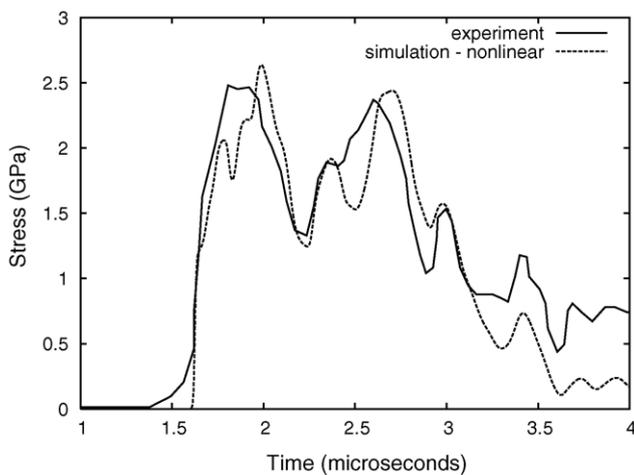
Fig. 8. Comparison of shock stress time histories corresponding to the experiment 120202 [5].

It follows that the nonlinear behavior of the soft material is affected not only by the energy of the impact but also by the scattering induced by internal interfaces. It should be noted that the influence of the nonlinearity is not necessarily small. In the numerical simulations, that match with the experiments, the increase of the actual sound velocity of polycarbonate follows. It may be up to two times in comparison with the linear case. This conclusion is really surprising but supported by the stress time histories. Such an effect but at smaller scale has also been shown by [11,12].

To be able to compare the results of experiments with different geometry and loading conditions we need to have a similarity in the experimental setting. However, experimental data in [5] correspond to various impact energies, impedance mismatches, and number and thickness of units. Therefore, we need to normalize the experimental conditions. First of all, we choose one of the experiments as a representative one. For example, we can choose experiment marked as 110501 as a representative one. Then we relate all other experimental conditions to the conditions of the representative experiment. This means that the impact energy for each experiment should be normalized with respect to the impact energy corresponding to the experiment 110501 resulting in the normalized impact energy $\check{E}$. Similarly, the impedance ratio of hard and soft materials should be normalized with respect to the corresponding ratio for the experiment 110501 to obtain the normalized impedance ratio $\check{Z}$. The geometrical factor can be introduced as follows:

$$G = \frac{mh_2}{h_1 + h_2}, \qquad (5)$$

where m is the gage position, h_1 and h_2 are thicknesses of soft and hard layers, respectively. Its normalized value $\check{G}$ is obtained as described above.

Then one can compute a modified parameter of nonlinearity $\check{A}$:

$$\check{A} = A\sqrt{\frac{\check{Z}}{\check{E}\check{G}}}. \qquad (6)$$

The results of calculations are given in Table 2. As one can see, the modified values of the parameter of nonlinearity

deviate from the mean value (equal to 2.806) less than by 3.5%.

The possibility to calculate the single value of the parameter of nonlinearity means that there exists a similarity in the process under different impact energies, impedance mismatches and geometry. Therefore, the value of the parameter of nonlinearity can be calculated following simple similarity relation (6) from one set of experimental conditions with respect to another.

It should be also noted that the equation of state suggested for the simulation of the plate impact test in [3,4] is simply an approximation of the relation (4) in the case of very small deformations. In fact,

$$\hat{c} = c\sqrt{1 + 2A\varepsilon} \sim c(1 + A\varepsilon) \quad \text{for} \quad A\varepsilon \ll 1. \tag{7}$$

The nonlinear part $A\varepsilon$ can be represented as Av/c at least under condition $dx/dt = c$, which leads to the equation of state:

$$\hat{c} = c + Av, \tag{8}$$

mentioned above. Such kind of equation of state is also condition-dependent, since the particle velocity v depends definitely on the structure of a specimen.

Thus, an application of nonlinear stress–strain relation for materials in numerical simulations of the plate impact problem of a layered heterogeneous medium shows that a good agreement between computations and experiments can be obtained by adjusting the values of the parameter of nonlinearity. In the numerical simulations of the finite-amplitude shock wave propagation in heterogeneous composites, the flyer size and velocity, impedance mismatch of hard and soft materials, as well as the number and size of layers in a specimen were the same as in experiments [5]. Moreover, a nonlinear behavior of materials was also taken into consideration. This means that combining of scattering effects induced by internal interfaces and physical nonlinearity in materials behavior into one nonlinear parameter provides the possibility to reproduce the shock response in heterogeneous media observed experimentally. In this context, parameter A is actually influenced by: (i) the physical nonlinearity of the soft material and (ii) the mismatch of elasticity properties of soft and hard materials. The mismatch effect is similar to the type of nonlinearity characteristic to materials with different

moduli of elasticity for tension and compression. The mismatch effect manifests itself due to wave scattering at the internal interfaces, and therefore, depends on the structure of a specimen. The variation of the parameter of nonlinearity confirms the statement that the nonlinear wave propagation is highly affected by interaction of the wave with the heterogeneous substructure of a solid [5].

The relation between different values of the parameter of nonlinearity is found by means of the normalization of experimental conditions. The obtained similarity means that the same physical mechanism can manifest itself differently depending on the particular heterogeneous substructure.

Acknowledgments

References

[1] R.A. Graham, Solids under High-Pressure Shock Compression: Mechanics, Physics, and Chemistry, Springer, New York, 1993.
[2] D. Grady, J. Mech. Phys. Solids 46 (1998) 2017–2032.
[3] X. Chen, N. Chandra, Comp. Sci. Technol. 64 (2004) 1477–1493.
[4] X. Chen, N. Chandra, A.M. Rajendran, Int. J. Solids Struct. 41 (2004) 4635–4659.
[5] S. Zhuang, G. Ravichandran, D. Grady, J. Mech. Phys. Solids 51 (2003) 245–265.
[6] Z. Hashin, J. Appl. Mech. 50 (1983) 481–505.
[7] T. Meurer, J. Qu, L.J. Jacobs, Int. J. Solids Struct. 39 (2002) 5585–5614.
[8] R.J. LeVeque, J. Comp. Physics 131 (1997) 327–353.
[9] T.R. Fogarty, R.J. LeVeque, J. Acoust. Soc. Am. 106 (1999) 17–28.
[10] R.J. LeVeque, Finite Volume Methods for Hyperbolic Problems, Cambridge University Press, 2002.
[11] R.J. LeVeque, Int. J. Numer. Meth. Fluids 40 (2002) 93–104.
[12] R.J. LeVeque, D.H. Yong, SIAM J. Appl. Math. 63 (2003) 1539–1560.
[13] A. Berezovski, J. Engelbrecht, G.A. Maugin, Arch. Appl. Mech. 70 (2000) 694–706.
[14] A. Berezovski, G.A. Maugin, J. Comp. Physics 168 (2001) 249–264.
[15] A. Berezovski, J. Engelbrecht, G.A. Maugin, Eur. J. Mech. A: Solids 22 (2003) 257–265.

Publication II

A. Berezovski, M. Berezovski, J. Engelbrecht, G.A. Maugin

NUMERICAL SIMULATION OF WAVES AND FRONTS IN INHOMOGENEOUS SOLIDS

A. Berezovski*, M. Berezovski*, J. Engelbrecht*, G.A. Maugin**

*Centre for Nonlinear Studies, Institute of Cybernetics at Tallinn University of Technology, Estonia; **Institut Jean Le Rond d'Alembert, Université Pierre et Marie Curie, Paris, France

e-mail: Arkadi.Berezovski@cs.ioc.ee

Abstract: Dynamic response of inhomogeneous materials exhibits new effects, which often do not exist in homogeneous media. It is quite natural that most of studies of wave and front propagation in inhomogeneous materials are associated with numerical simulations. To develop a numerical algorithm and to perform the numerical simulations of moving fronts we need to formulate a kinetic law of progress relating the driving force and the velocity of the discontinuity. The velocity of discontinuity is determined by means of the non-equilibrium jump relations at the front. The obtained numerical method generalizes the wave-propagation algorithm to the case of moving discontinuities in thermoelastic solids.

Keywords: wave and front propagation, inhomogeneous solids, finite-volume methods

1. Introduction

The understanding of the behavior of materials under very high strain rate loading conditions is vital in many areas of civilian and military applications. So far, the most practical structures/materials to absorb impact energy and resist impact damage are designed in the form of layered composites. Other possibilities are provided by functionally graded materials and shape memory alloys. In order to characterize the dynamic behavior of materials under impact loading, diagnostic experiments are usually carried out using a plate impact test configuration under a one-dimensional strain state. The plate impact test serves the exact purpose of characterizing materials under high-pressure dynamic loading, analogous to that of uniaxial tensile tests under quasi-static loading conditions.

Laminated composites

The major past work in studying wave profiles in alternating layered systems using specifically the plate impact test configuration are summarized recently in Chen and Chandra (2004); Chen *et al.* (2004). For almost all the experiments, stress (or velocity) response have shown an oscillatory behavior in the pulse duration segment. This behavior is conspicuously absent in homogeneous systems. The oscillatory behavior about a mean value in the periodically layered systems are consistently exhibited in the systematic experimental work by Zhuang *et al.* (2003). As pointed out in Zhuang *et al.* (2003), stress wave propagation through layered media made of isotropic materials provides an ideal model to investigate the effect of heterogeneous materials under shock loading, because the length scales, e.g., thickness of individual layers, and other measures of heterogeneity, e.g., impedance mismatch, are well defined. The origin of the observed structure of the stress waves was attributed to material heterogeneity at the interfaces. For high velocity impact loading conditions, it was fully realized that material nonlinear effects may play a key role in altering the basic structure of the shock wave.

Shape memory alloys

A polycrystalline shape memory alloy body subjected to external impact loading will experience deformations that will propagate along the SMA body as stress waves. The experimental investigation concerning impact-induced austenite-martensite phase transformations was reported by Escobar and Clifton (1993). In their experiments, Escobar and Clifton used thin plate-like specimens of Cu-14.44Al-4.19Ni shape-memory alloy single crystal. One face of this austenitic specimen was subjected to an oblique impact loading, generating both shear and compression. As Escobar and Clifton noted, measured velocity profiles provide several indications of the existence of a propagating phase boundary, in particular, a difference between the measured particle velocity and the transverse component of the projectile velocity. This velocity difference, in the absence of any evidence of plastic deformation, is indicative of a stress induced phase transformation that propagates into the crystals from the impact face. The determination of this velocity difference is most difficult from the theoretical point of view, because it depends on the velocity of the moving phase boundary.

In this paper, wave and front propagation is simulated numerically in a one-dimensional case. The propagation is modeled by the one-dimensional hyperbolic system of conservation laws

$$\rho\frac{\partial v}{\partial t} = \frac{\partial \sigma}{\partial x} \qquad\qquad \frac{\partial \varepsilon}{\partial t} = \frac{\partial v}{\partial x} \qquad\qquad (1.1)$$

where ρ is the mass density, ε is the strain, and v the particle velocity.

The densities of the materials may be different, and the materials response to compression is characterized by the distinct stress-strain relations $\sigma(\varepsilon)$. To close the system of Eqs. (1.1), the stress-strain relation for each material can be chosen as linear

$$\sigma = \rho c^2 \varepsilon \qquad\qquad (1.2)$$

or weakly nonlinear

$$\sigma = \rho c^2 \varepsilon (1 + A\varepsilon) \qquad\qquad (1.3)$$

where c is the longitudinal wave velocity and A is a parameter of nonlinearity, values and sign of which are supposed to be different for hard and soft materials. Due to rapidly varying properties, we apply the finite-volume wave-propagation algorithm in its conservative form (Bale *et al.*, 2003) to solve the system of equations (1.1)-(1.2) (or (1.3)). At the moving phase boundary the algorithm is extended as described in Berezovski and Maugin (2005a).

The paper is organized as follows. In the next Section we repeat the classical results for linear wave propagation in periodic media. Then we examine the effect of weak nonlinearity on the material response. The introduction of the nonlinearity allows us to reproduce the shock response in laminated composites observed experimentally. Linear and nonlinear wave propagation in functionally graded materials is considered in the Section 5. Another type of nonlinearity affects the front propagation in shape memory alloys under impact. This nonlinearity is connected to the motion of the phase front.

2.   One-dimensional linear waves in periodic media

As the first example, we consider the propagation of a pulse in a periodic medium composed by alternating layers of dissimilar materials. The initial pulse shape is presented in Figure 1 where the periodic variation in density (normalized by its maximal value) is also schematically shown by dashed lines. Clearly, the wavelength is much larger than the periodicity scale. For the test problem, materials are chosen as polycarbonate ($\rho = 1190\,\mathrm{kg/m^3}$, $c = 4000\,\mathrm{m/s}$) and Al 6061 ($\rho = 2703\,\mathrm{kg/m^3}$, $c = 6149\,\mathrm{m/s}$). Calculations are performed with Courant-Friedrichs-Levy number equal to 1. The result of simulation for 4000 time steps is shown in Figure 2. We observe a distortion of the pulse shape and a decrease in the velocity of the pulse propagation in comparison of the maximal longitudinal wave velocity in the materials. These results correspond to the prediction of the effective media theory by Santosa and Symes (1991) both qualitatively and quantitatively (Fogarthy and LeVeque, 1999).
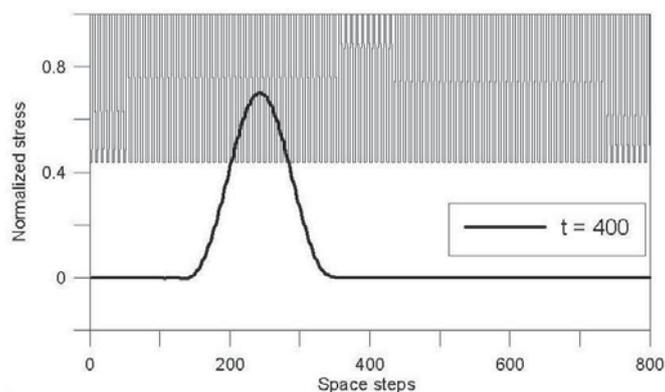
Figure 1. Initial pulse shape
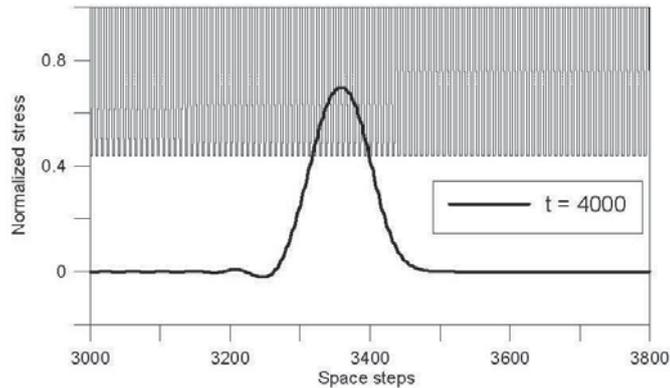
Figure 2. Pulse shape at 4700 time step. Linear case

3. One-dimensional weakly nonlinear waves in periodic media

In the next example, we will see the influence of material nonlinearity on the wave propagation. The approximate Riemann solver for the nonlinear elastic media (Eq. (1.3)) is similar to that used in LeVeque (2002). This means that a modified longitudinal wave velocity, c_1, following the nonlinear stress-strain relation (1.3) is applied at each time step

$$c_1 = c\sqrt{1 + 2A\varepsilon} \tag{3.1}$$

instead of the piece-wise constant one corresponding to the linear case. We consider the same pulse shape and the same materials (polycarbonate and Al 6061) as in the case of the linear periodic medium. However, the nonlinear effects appear only for a sufficiently high magnitude of loading. The values of the parameter of nonlinearity A were chosen as 0.24 for Al 6061 and 0.8 for polycarbonate. The results of simulations corresponding to 5200 time steps are shown in Figure 3.
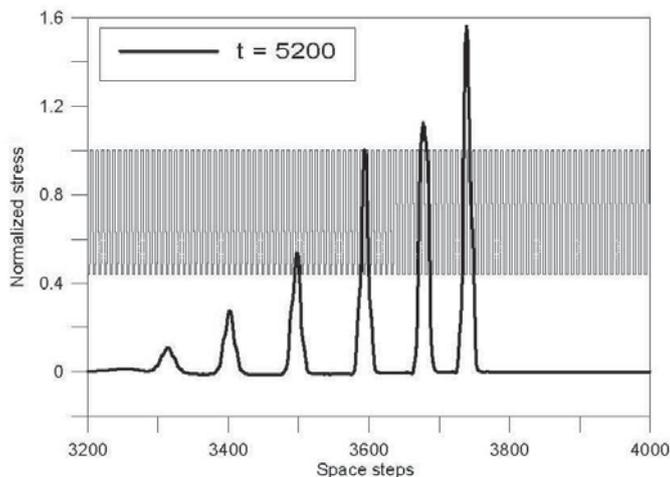
Figure 3. Pulse shape at 5200 time step. Nonlinear case

We observe that an initial bell-shaped pulse is transformed in a train of soliton-like pulses propagating with amplitude-dependent speeds. Such kind of behavior was first reported in LeVeque (2002), who called these pulses as "stegotons" because their shape is influenced by the periodicity.

4. Nonlinear elastic wave in laminates under impact loading

To analyze the influence of multiple reflections of internal interfaces on shock wave propagation in the layered composites, we consider the initial-boundary value problem of impact loading of a heterogeneous medium composed of alternating layers of two different materials (Berezovski *et al.*, 2006). The impact is provided by a planar flyer which has an initial velocity v_0. A buffer of the same material as the soft component of the specimen is used to eliminate the effect of wave reflection at the stress-free surface. Both left and right boundaries are stress-free. As previously, we apply a nonlinear stress-strain relation $\sigma(\varepsilon, x)$ for each material (1.3) (cf. Meurer *et al.*, 2002). Results of numerical calculations depend crucially on the choice of the parameter of nonlinearity A. We choose this parameter from the conditions to match the numerical simulations to experimental results (see discussion in Berezovski *et al.*, 2006).
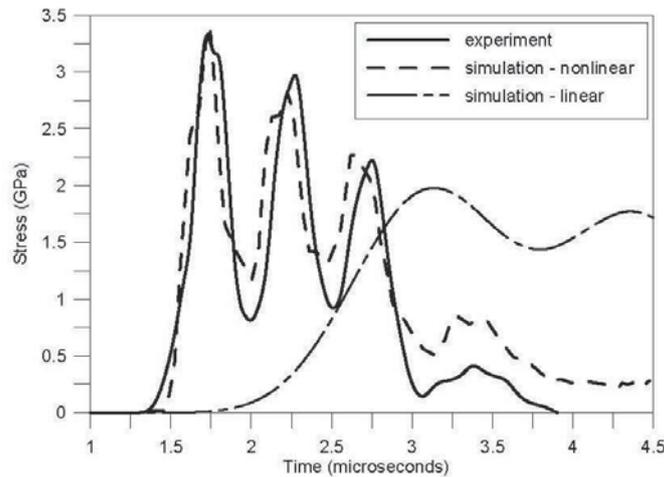
Figure 4. Comparison of shock stress time histories corresponding to the experiment 110501 by Zhuang et al. (2003)

Figure 4 shows the stress time histories in the composite, which consists of 16 units of polycarbonate, each 0.37 mm thick, and of 16 units of stainless steel, each 0.19 mm thick. The stress time histories correspond to the distance 3.44 mm from the impact face. Calculations are performed for the flyer velocity 1043 m/s and the flyer thickness 2.87 mm.

The nonlinear parameter A is chosen here to be 2.80 for polycarbonate and zero for stainless steel. Additionally, the stress time history corresponding to the linear elastic solution (i.e., nonlinear parameter A is zero for both components) is shown. One can see that the stress time history computed by means of the considered nonlinear model is very close to the experimental one. It reproduces three main peaks and decreases with distortion, as it is observed in the experiment by Zhuang *et al.* (2003). As one can see, the agreement between results of calculations and experiments is achieved by the adjustment of the nonlinear parameter A.

5.   Waves in functionally graded materials

Studies of the evolution of stresses and displacements in FGMs subjected to quasi-static loading (Suresh and Mortensen, 1998) show that the utilization of structures and geometry of a graded interface between two dissimilar layers can reduce stresses significantly. Such an effect is also important in the case of dynamical loading where energy-absorbing applications are of special interest. Following Chiu and Erdogan (1999), we consider the one-dimensional problem in elastodynamics for an FGM slab in which material properties vary only in the thickness direction.

It is assumed that the slab is isotropic and inhomogeneous with the following fairly general properties:

$$E(x) = E_0 \left(a\frac{x}{l} + 1\right)^m \qquad\qquad \rho(x) = \rho_0 \left(a\frac{x}{l} + 1\right)^n \qquad (5.1)$$

where l is the thickness, a, m, and n are arbitrary real constants with $a > -1$, E_0 and ρ_0 are the elastic constant and density at $x = 0$. It is assumed that the slab is at rest for $t < 0$. Following Chiu and Erdogan (1999), we consider an FGM slab that consists of nickel and zirconia. The thickness of the slab is $l = 5\,\mathrm{mm}$, on one surface the medium is pure nickel, on the other surface pure zirconia, and the material properties $E(x)$ and $\rho(x)$ vary smoothly in thickness direction. A pressure pulse defined by

$$\sigma(l, t) = \sigma_0(H(t) - H(t - t_0)) \qquad (5.2)$$

is applied to the surface $x = l$ and the boundary $x = 0$ is "fixed". Here H is the Heavyside function. The pulse duration is assumed to be $t_0 = 0.2\,\mu\mathrm{s}$. The properties of the constituent materials used are given in Table 1 (Chiu and Erdogan, 1999). The material parameters for the FGMs used are (Chiu and Erdogan, 1999): $a = -0.12354$, $m = -1.8866$, and $n = -3.8866$. The stress is calculated up to $12\,\mu\mathrm{s}$ (the propagation time of the plane wave through the thickness $l = 5\,\mathrm{mm}$ is approximately $0.77\,\mu\mathrm{s}$ in pure $\mathrm{ZrO_2}$ and $0.88\,\mu\mathrm{s}$ in Ni).

Table 1. *Properties of materials*

Property	Value	Unit	Material
Density	5331	kg/m^3	ZrO$_2$
	8900		Ni
Young modulus	151	GPa	ZrO$_2$
	207		Ni
Poisson's ratio	0.33		ZrO$_2$
	0.31		Ni

Numerical simulations were performed by means of the same algorithm as above. Comparison of the results of the numerical simulation and the analytical solution Chiu and Erdogan (1999) for the time dependence of the normalized stress σ/σ_0 at the location $x/l = 1/2$ is shown in Figure 5. As one can see, it is difficult to make a distinction between analytical and numerical results.
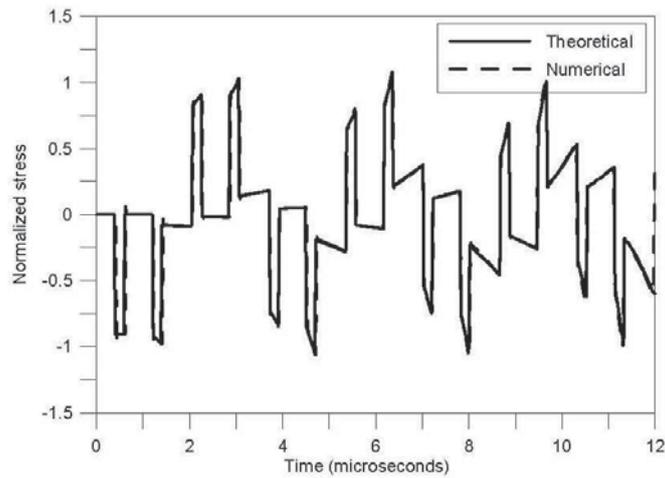
Figure 5. Variation of stress with time in the middle of the slab

Variation of stress in nonlinear case for same materials with the nonlinearity parameter $A = 0.19$ is shown in Figure 6. The amplitude amplification and pulse shape distortion in comparison with linear case is clearly observed. In addition, velocity of a pulse in nonlinear material is increased.
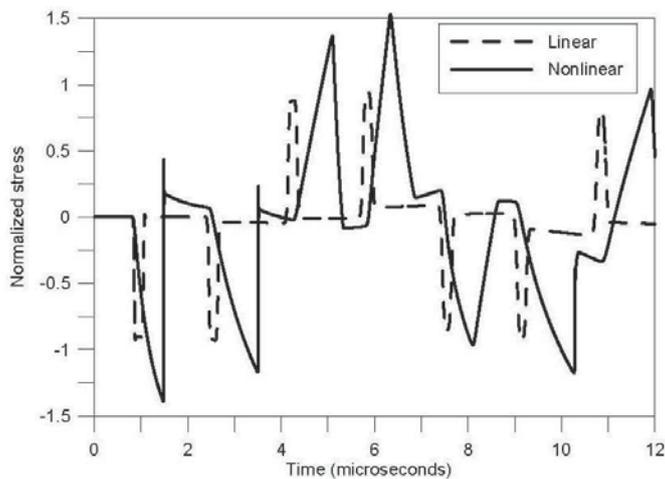
Figure 6. Variation of stress with time in the middle of the slab

6. Phase-transition fronts

In the case of phase-transition front propagation, we consider the boundary value problem of the tensile loading of a 1-D shape memory alloy bar that has uniform cross-sectional area and temperature. The bar occupies the interval $0 < x < L$ in a reference configuration and the boundary $x = 0$ is subjected to the tensile loading. The bar is assumed to be long compared to its diameter so it is under a uniaxial stress state and the stress $\sigma(x, t)$ depends only on the axial position and time. The density of the material ρ is assumed constant. All field variables are averaged over the cross-section of the bar.

At each instant t during a process, the strain $\varepsilon(x,t)$ varies smoothly within the bar except at phase boundaries; across a phase boundary, it suffers jump discontinuity. Away from a phase boundary, balance of linear momentum and kinematic compatibility require the satisfaction of equations (1.1). Suppose that at time t there is a moving discontinuity in strain or particle velocity at $x = \Sigma(t)$. Then one also has the corresponding jump conditions (cf. Abeyaratne et $al.$, 2001)

$$\rho V_\Sigma [v] + [\sigma] = 0 \qquad\qquad V_\Sigma [\varepsilon] + [v] = 0 \qquad\qquad (6.1)$$

where V_Σ is the velocity of the phase-transition front and square brackets denote jumps.

The entropy inequality and the corresponding jump relation read

$$\theta \frac{\partial S}{\partial t} + \frac{\partial q}{\partial x} \geqslant 0 \qquad\qquad V_\Sigma \theta [S] = V_\Sigma f_\Sigma \qquad\qquad (6.2)$$

where the driving traction $f_\Sigma(t)$ at the discontinuity is defined by (cf. Truskinovsky, 1987; Abeyaratne and Knowles, 1990)

$$f_\Sigma = -[W] + \langle \sigma \rangle [\varepsilon] \qquad\qquad (6.3)$$

W is the free energy per unit volume, θ is temperature, S is entropy, and q is heat flux. If f_Σ is not zero, the sign of V_Σ, and hence the direction of motion of discontinuity, is determined by the sign of f_Σ.

Applying the satisfaction of the non-equilibrium jump relation at the phase boundary we obtain the value of the stress jump at the phase boundary (Berezovski and Maugin, 2005b). Having the value of the stress jump, we can determine the material velocity at the moving phase boundary by means of the jump relation for linear momentum (6.1) rewritten in terms of averaged quantities because of the continuity of excess quantities at the phase boundary (Berezovski and Maugin, 2005a).
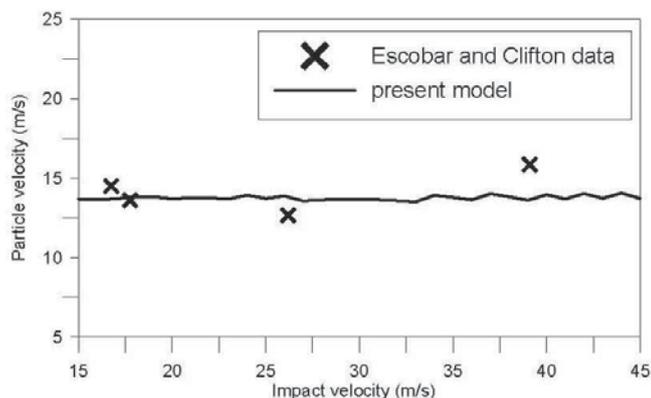
Figure 7. Particle velocity versus impact velocity

To compare the results of modeling with experimental data by Escobar and Clifton (1993), the calculations of the particle velocity were performed for different impact velocities. The results of the comparison are given in Figure 7. As a result, we can see that the computed particle velocity is practically independent of the impact velocity.

7. Conclusions

As we have seen, linear and non-linear wave propagation in media with rapidly-varying properties as well as in functionally graded materials can be successfully simulated by means of the modified wave-propagation algorithm (Berezovski and Maugin, 2001). The applied algorithm is conservative, stable up to Courant number equal to 1, high-order accurate, and thermodynamically consistent. To apply the algorithm to moving singularities, we simply should change the non-equilibrium jump relation for true inhomogeneities to another non-equilibrium jump relation valid for quasi-inhomogeneities.

References

Abeyaratne R., Bhattacharya K., Knowles J.K., 2001, Strain-Energy Functions with Local Minima: Modeling Phase Transformations Using Finite Thermoelasticity, *Nonlinear Elasticity: Theory and Application*, Cambridge University Press, 433-490.

Abeyaratne R., Knowles J.K., 1990, On the Driving Traction Acting on a Surface of Strain Discontinuity in a Continuum, *J. Mech. Phys. Solids*, 38, 345-360.

Bale D.S., LeVeque R.J., Mitran S., Rossmanith J.A., 2003, A Wave Propagation Method for Conservation Laws and Balance Laws with Spatially Varying Flux Functions, *SIAM J. Sci. Comp.*, 24, 955-978.

Berezovski A., Maugin G.A., 2001, Simulation of Thermoelastic Wave Propagation by Means of a Composite Wave-Propagation Algorithm, *J. Comp. Physics*, 168, 249-264.

Berezovski A., Maugin G.A., 2005a, Stress-Induced Phase-Transition Front Propagation in Thermoelastic Solids, *Eur. J. Mech. – A/Solids*, 24, 1-21.

Berezovski A., Maugin G.A., 2005b, On the Velocity of Moving Phase Boundary in Solids, *Acta Mechanica*, 179, 187-196.

Berezovski A., Berezovski M., Engelbrecht J., 2006, Numerical Simulation of Nonlinear Elastic Wave Propagation in Piecewise Homogeneous Media, *Mater. Sci. Engng.*, A 418, 364-369.

Chen X., Chandra N., 2004, The Effect of Heterogeneity on Plane Wave Propagation through Layered Composites, *Comp. Sci. Technol.*, 64, 1477-1493.

Chen X., Chandra N., Rajendran A.M., 2004, Analytical Solution to the Plate Impact Problem of Layered Heterogeneous Material Systems, *Int. J. Solids Struct.*, 41, 4635-4659.

Chiu T.-C., Erdogan F., 1999, One-Dimensional Wave Propagation in a Functionally Graded Elastic Medium, *J. Sound Vibr.*, 222, 453-487.

Escobar J.C., Clifton R.J., 1993, On Pressure-Shear Plate Impact for Studying the Kinetics of Stress-Induced Phase-Transformations, *Mat. Sci. and Engng.*, A 170, 125-142.

Fogarthy T., LeVeque R.J., 1999, High-Resolution Finite-Volume Methods for Acoustics in Periodic and Random Media, *J. Acoust. Soc. Am.*, 106, 261-297.

LeVeque R.J., 2002, Finite Volume Methods for Nonlinear Elasticity in Heterogeneous Media, *Int. J. Numer. Methods Fluids*, 40, 93-104.

Meurer T., Qu J., Jacobs L.J., 2002, Wave Propagation in Nonlinear and Hysteretic Media – A Numerical Study, *Int. J. Solids Struct.*, 39, 5585-5614.

Santosa F., Symes W.W., 1991, A Dispersive Effective Medium for Wave Propagation In Periodic Composites, *SIAM J. Appl. Math.*, 51, 984-1005.

Suresh S., Mortensen A., 1998, *Fundamentals of Functionally Graded Materials*, The Institute of Materials, IOM Communications Ltd., London.

Truskinovsky L., 1987, Dynamics of Nonequilibrium Phase Boundaries in a Heat Conducting Nonlinear Elastic Medium, *J. Appl. Math. Mech.* (PMM), 51, 777-784.

Zhuang S., Ravichandran G., Grady D., 2003, An Experimental Investigation of Shock Wave Propagation in Periodically Layered Composites, *J. Mech. Phys. Solids*, 51, 245-265.

Publication III

A. Berezovski, M. Berezovski, J. Engelbrecht

Waves in inhomogeneous solids,
in: *Applied Wave Mathematics - Selected Topics in Solids, Fluids and Mathematical Methods* E.Quak, T. Soomere (Eds.) Springer, 2009, pp. 55-81.

Waves in Inhomogeneous Solids

Arkadi Berezovski, Mihhail Berezovski and Jüri Engelbrecht

Abstract The paper aims at presenting a numerical technique used in simulating the propagation of waves in inhomogeneous elastic solids. The basic governing equations are solved by means of a finite-volume scheme that is faithful, accurate, and conservative. Furthermore, this scheme is compatible with thermodynamics through the identification of the notions of numerical fluxes (a notion from numerics) and of excess quantities (a notion from irreversible thermodynamics). A selection of one-dimensional wave propagation problems is presented, the simulation of which exploits the designed numerical scheme. This selection of exemplary problems includes (i) waves in periodic media for weakly nonlinear waves with a typical formation of a wave train, (ii) linear waves in laminates with the competition of different length scales, (iii) nonlinear waves in laminates under an impact loading with a comparison with available experimental data, and (iv) waves in functionally graded materials.

1 Introduction

Waves correspond to continuous variations of the states of material points representing a medium. The characteristic feature of waves is their motion. In mechanics the motion of waves is governed by the conservation laws for mass, linear momentum, and energy. These conservation laws, complemented by constitutive relations, are the basis of the theory of thermoelastic waves in solids [1, 3, 9, 19].

Inhomogeneous solids include layered and randomly reinforced composites, multiphase and polycrystalline alloys, functionally graded materials, ceramics and polymers with certain microstructure, etc. Therefore, it is impossible to present a complete theory of linear and nonlinear wave propagation for the full diversity of

Centre for Nonlinear Studies, Institute of Cybernetics at Tallinn University of Technology, Akadeemia tee 21, 12618 Tallinn, Estonia, e-mail: arkadi.berezovski@cs.ioc.ee

possible situations, in so far as geometry, contrast of multiphase properties and loading conditions are concerned.

From a practical point of view, we need to perform numerical calculations. Many numerical methods have been proposed to compute wave propagation in heterogeneous solids, among them, the stiffness matrix recursive algorithm [33, 38] and the spectral layer element method [10, 11] should be mentioned, in addition to more common finite-element, finite-difference, and finite-volume methods.

Here the general idea is the following: division of a body into a finite number of computational cells requires the description of all fields inside the cells as well as the interaction between neighboring cells. Approximation of wanted fields inside the cells leads to discontinuities of the fields at the boundaries between cells. This also leads to the appearance of excess quantities, which represent the difference between the exact and approximate values of the fields. Interaction between neighboring cells is described by means of fluxes at the boundaries of the cells. These fluxes correspond to the excess quantities and, therefore, can be calculated by means of jump relations at the boundaries between cells.

In this paper, we demonstrate how the finite-volume wave-propagation algorithm developed in [27] can be reformulated in terms of the excess quantities and then applied to the wave propagation in inhomogeneous solids. Both original and modified algorithms are stable, high-order accurate, thermodynamically consistent, and applicable both to linear and nonlinear waves.

1.1 Governing equations

The simplest example of heterogeneous media is a periodic medium composed by materials with different properties. One-dimensional wave propagation in the framework of linear elasticity is governed by the conservation of linear momentum [1]

$$\rho(x)\frac{\partial v}{\partial t} - \frac{\partial \sigma}{\partial x} = 0, \tag{1}$$

and the kinematic compatibility condition

$$\frac{\partial \varepsilon}{\partial t} = \frac{\partial v}{\partial x}. \tag{2}$$

Here t is time, x is the space variable, the particle velocity $v = u_t$ is the time derivative of the displacement u, the one-dimensional strain $\varepsilon = u_x$ is the space derivative of the displacement, σ is the Cauchy stress, and ρ is the material density. The compatibility condition (2) follows immediately from the definitions of the strain and the particle velocity.

The two equations (1) and (2) contain three unknowns: v, σ and ε.

The closure of the system of equations (1) and (2) is achieved by a constitutive relation, which in the simplest case is Hooke's law

$$\sigma = \rho(x)c^2(x)\,\varepsilon, \tag{3}$$

where $c(x) = \sqrt{(\lambda(x)+2\mu(x))/\rho(x)}$ is the corresponding longitudinal wave velocity, and $\lambda(x)$ and $\mu(x)$ are the so-called Lamé coefficients. The indicated explicit dependence on the point x means that the medium is materially inhomogeneous.

The system of equations (1)–(3) can be expressed in the form of a conservation law

$$\frac{\partial}{\partial t}q(x,t) + \frac{\partial}{\partial x}f(q(x,t)) = 0, \tag{4}$$

with

$$q(x,t) = \begin{pmatrix} \varepsilon \\ \rho v \end{pmatrix} \quad \text{and} \quad f(x,t) = \begin{pmatrix} -v \\ -\rho c^2 \varepsilon \end{pmatrix}. \tag{5}$$

In the linear case, equation (4) can be rewritten in the form

$$\frac{\partial}{\partial t}q(x,t) + A\frac{\partial}{\partial x}q(x,t) = 0, \tag{6}$$

where the matrix A is given by

$$A = \begin{pmatrix} 0 & -1/\rho \\ -\rho c^2 & 0 \end{pmatrix}. \tag{7}$$

We will solve the system of equations (1)–(3) numerically. Although a numerical solution can be difficult with standard methods, high-resolution finite volume methods based on solving Riemann problems have been found to perform very well on linear hyperbolic systems modeling wave propagation in rapidly-varying heterogeneous media [16].

2 The wave-propagation algorithm

Standard methods cannot give high accuracy near discontinuities in the material parameters and will often fail completely in problems where the parameters vary drastically on the grid scale. By contrast, solving the Riemann problem at each cell interface properly resolves the solution into waves, taking into account every discontinuity in the parameters, and automatically handling the reflection and transmission of waves at each interface. This is crucial in developing the correct macroscopic behavior. As a result, Riemann-solver methods are quite natural for this application. Moreover, the methods extend easily from linear to nonlinear problems. Expositions of such methods and pointers to the rich literature base can be found in many sources [17, 20, 27, 36, 37].

2.1 Averaged quantities

Let us introduce a computational grid of cells $C_n = [x_{n-1/2}, x_{n+1/2}]$ with interfaces $x_{n-1/2} = (n-1)/2\Delta x$ and time levels $t_k = k\Delta t$. For simplicity, the grid size Δx and time step Δt are assumed to be constant. Integrating equation (4) over $C_n \times [t_k, t_{k+1}]$ gives

$$\int_{x_{n-1/2}}^{x_{n+1/2}} q(x, t_{k+1})dx = \int_{x_{n-1/2}}^{x_{n+1/2}} q(x, t_k)dx - \tag{8}$$

$$-\left(\int_{t_k}^{t_{k+1}} f(q(x_{n+1/2}, t))dt - \int_{t_k}^{t_{k+1}} f(q(x_{n-1/2}, t))dt \right).$$

Introducing the average Q_n of the exact solution on C_n at time $t = t_k$ and the numerical flux F_n that approximates the time average of the exact flux taken at the interface between the cells C_{n-1} and C_n, i.e.

$$Q_n \approx \frac{1}{\Delta x} \int_{x_{n-1/2}}^{x_{n+1/2}} q(x, t_k)dx, \quad F_n \approx \frac{1}{\Delta t} \int_{t_k}^{t_{k+1}} f(q(x_{n-1/2}, t))dt, \tag{9}$$

we can rewrite equation (8) in the form of a numerical method in the flux-differencing form

$$Q_n^{k+1} = Q_n^k - \frac{\Delta t}{\Delta x}(F_{n+1}^k - F_n^k). \tag{10}$$

In general, however, we cannot evaluate the time integrals on the right-hand side of equation (8) exactly, since $q(x_{n\pm1/2}, t)$ varies with time along each edge of the cell, and we do not have the exact solution to work with. If we can approximate this average flux based on the values Q^k, then we will have a fully-discrete method.

2.2 Numerical fluxes

Numerical fluxes are determined by means of the solution of the Riemann problem at interfaces between cells. The solution of the Riemann problem (at the interface between cells $n-1$ and n) consists of two waves, which we denote, following [27], $\mathcal{W}_n^I$ and $\mathcal{W}_n^{II}$. The left-going wave $\mathcal{W}_n^I$ moves into cell $n-1$, and the right-going wave $\mathcal{W}_n^{II}$ moves into cell n. The state between the two waves must be continuous across the interface (Rankine-Hugoniot condition) [27]:

$$\mathcal{W}_n^I + \mathcal{W}_n^{II} = Q_n - Q_{n-1}. \tag{11}$$

In the linear case, the considered waves are determined by eigenvectors of the matrix A [27]:

$$\mathcal{W}_n^I = \gamma_n^I r_{n-1}^I, \quad \mathcal{W}_n^{II} = \gamma_n^{II} r_n^{II}. \tag{12}$$

This means that equation (11) is represented as

$$\gamma_n^I r_{n-1}^I + \gamma_n^{II} r_n^{II} = Q_n - Q_{n-1}. \tag{13}$$

Considering the definition of eigenvectors $Ar = \lambda r$, we see that the eigenvector

$$r^I = \begin{pmatrix} 1 \\ \rho c \end{pmatrix} \tag{14}$$

corresponds to the eigenvalue $\lambda^I = -c$ (left-going wave). Similarly, the eigenvector

$$r^{II} = \begin{pmatrix} 1 \\ -\rho c \end{pmatrix} \tag{15}$$

corresponds to the eigenvalue $\lambda^{II} = c$ (right-going wave). Substituting the eigenvectors into equation (13), we have

$$\gamma_n^I \begin{pmatrix} 1 \\ \rho_{n-1} c_{n-1} \end{pmatrix} + \gamma_n^{II} \begin{pmatrix} 1 \\ -\rho_n c_n \end{pmatrix} = Q_n - Q_{n-1}, \tag{16}$$

or, more explicitly,

$$\begin{pmatrix} 1 & 1 \\ \rho_{n-1} c_{n-1} & -\rho_n c_n \end{pmatrix} \begin{pmatrix} \gamma_n^I \\ \gamma_n^{II} \end{pmatrix} = \begin{pmatrix} \bar{\varepsilon}_n - \bar{\varepsilon}_{n-1} \\ \rho \bar{v}_n - \rho \bar{v}_{n-1} \end{pmatrix}. \tag{17}$$

Solving the system of linear equations (17), we obtain the amplitudes of the left-going and right-going waves. Then the numerical fluxes in the Godunov-type numerical scheme are determined as follows:

$$F_{n+1}^k = -\lambda_{n+1}^I \mathcal{W}_{n+1}^I = -c_{n+1} \gamma_{n+1}^I r_n^I, \tag{18}$$

$$F_n^k = \lambda_n^{II} \mathcal{W}_n^{II} = -c_n \gamma_n^{II} r_n^{II}. \tag{19}$$

Finally, the Godunov-type scheme is expressed in the form

$$Q_n^{k+1} = Q_n^k + \frac{\Delta t}{\Delta x} \left(c_{n+1} \gamma_{n+1}^I r_n^I - c_n \gamma_n^{II} r_n^{II} \right). \tag{20}$$

This is the standard form for the wave-propagation algorithm [27].

Within the wave-propagation algorithm, every discontinuity in parameters is taken into account by solving the Riemann problem at each interface between discrete elements. The reflection and transmission of waves at each interface are handled automatically for the considered inhomogeneous media.

2.3 Second-order corrections

The scheme considered above is formally first-order accurate only. To increase the order of accuracy, we rewrite the numerical scheme as

$$Q_n^{k+1} = Q_n^k + \Delta_n^{up} - \frac{\Delta t}{\Delta x}(\tilde{F}_{n+1}^k - \tilde{F}_n^k), \tag{21}$$

where Δ_n^{up} equals the upwind flux (or Godunov flux) obtained from equation (20).

The term $\tilde{F}_n$ is used to update the solution so that second order accuracy is achieved. The flux for the second-order Lax-Wendroff scheme may be written as the Godunov flux plus a correction [27],

$$F_n = \frac{1}{2}A(Q_n + Q_{n-1}) - \frac{\Delta t}{2\Delta x}A(Q_n - Q_{n+1}) = F_n^G + \frac{1}{2}|A|\left(1 - \frac{\Delta t}{\Delta x}|A|\right)\Delta Q_n, \tag{22}$$

where $|A| = A^+ - A^-$. Hence, a natural choice for $\tilde{F}$ is

$$\tilde{F}_n = \frac{1}{2}|A|\left(1 - \frac{\Delta t}{\Delta x}|A|\right)\Delta Q_n = \frac{1}{2}\sum_p |\lambda^p|\left(1 - \frac{\Delta t}{\Delta x}|\lambda^p|\right)\mathcal{W}_n^p. \tag{23}$$

The Godunov-type scheme exhibits strong numerical dissipation, and discontinuities in the solution are smeared, causing low accuracy. The Lax-Wendroff scheme, on the other hand, is more accurate in smooth parts of the solution. However, near discontinuities, numerical dispersion generates oscillations, also reducing the accuracy. A successful approach to suppress these oscillations is to apply flux limiters [16, 23, 24, 25].

2.4 The conservative wave propagation algorithm

For the conservative wave-propagation algorithm [2], the solution of the generalized Riemann problem is obtained by using the decomposition of the flux difference $f_n(Q_n) - f_{n-1}(Q_{n-1})$ instead of the decomposition (11):

$$\mathcal{L}_n^I + \mathcal{L}_n^{II} = f_n(Q_n) - f_{n-1}(Q_{n-1}). \tag{24}$$

The waves $\mathcal{L}^I$ and $\mathcal{L}^{II}$ are still proportional to the eigenvectors of the matrix A

$$\mathcal{L}_n^I = \beta_n^I r_{n-1}^I, \quad \mathcal{L}_n^{II} = \beta_n^{II} r_n^{II}, \tag{25}$$

and the corresponding numerical scheme has the form

$$Q_n^{l+1} - Q_n^l = -\frac{\Delta t}{\Delta x}\left(\mathcal{L}_n^{II} + \mathcal{L}_{n+1}^I\right). \tag{26}$$

The coefficients β^I and β^{II} are determined from the solution of the system of linear equations

$$\begin{pmatrix} 1 & 1 \\ \rho_{n-1}c_{n-1} & -\rho_n c_n \end{pmatrix} \begin{pmatrix} \beta_n^I \\ \beta_n^{II} \end{pmatrix} = \begin{pmatrix} -(\bar{v}_n - \bar{v}_{n-1}) \\ -(\rho c^2 \bar{\varepsilon}_n - \rho c^2 \bar{\varepsilon}_{n-1}) \end{pmatrix}. \tag{27}$$

As it is shown in [2], the obtained algorithm is conservative and second-order accurate on smooth solutions.

3 Excess quantities and numerical fluxes

We could simply apply the numerical scheme described in the previous sections to simulate the wave propagation in periodic media. However, the splitting of the body into a finite number of computational cells and averaging all the fields over the cell volumes leads to a situation known in thermodynamics as "endoreversible system" [22]. This means that even if the state of each computational cell can be associated with a corresponding local equilibrium state (and, therefore, temperature and entropy can be defined as usual), the state of the whole body is a non-equilibrium one. The computational cells interact with each other, which leads to the appearance of excess quantities.

In the admitted non-equilibrium description [32], both stress and velocity are represented as the sum of the averaged (local equilibrium) and excess parts:

$$\sigma = \bar{\sigma} + \Sigma, \quad v = \bar{v} + \mathcal{V}. \tag{28}$$

Here $\bar{\sigma}$ and $\bar{v}$ are averaged fields and Σ and $\mathcal{V}$ are the corresponding excess quantities.

Therefore, we rewrite a first-order Godunov-type scheme (10) in terms of the excess quantities

$$(\rho\bar{v})_n^{k+1} - (\rho\bar{v})_n^k = \frac{\Delta t}{\Delta x}\left(\Sigma_n^+ - \Sigma_n^-\right), \tag{29}$$

$$\bar{\varepsilon}_n^{k+1} - \bar{\varepsilon}_n^k = \frac{\Delta t}{\Delta x}\left(\mathcal{V}_n^+ - \mathcal{V}_n^-\right). \tag{30}$$

Here an overbar denotes averaged quantities, a superscript k denotes a time step, a subscript n denotes the number of the computational cell, while Δt and Δx are time step and space step, respectively.

Though excess quantities are determined formally everywhere inside computational cells, we need to know only their values at the boundaries of the cells, where they play the role of numerical fluxes. To determine the values of the excess quantities at the boundaries between computational cells, we apply the jump relation for the linear momentum [6], which is reduced in the isothermal case to

$$[\bar{\sigma} + \Sigma] = 0. \tag{31}$$

Similarly, the jump relation following from the kinematic compatibility (2) reads

$$[\bar{v} + \mathcal{V}] = 0. \tag{32}$$

It should be noted that the two last jump conditions can be considered as the *continuity of genuine unknown fields* at the boundaries between computational cells, which is illustrated in Fig. 1.
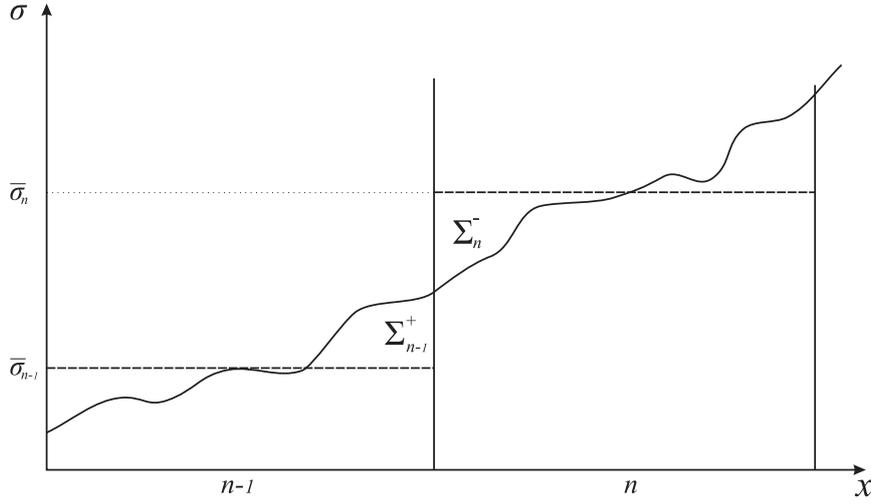
Fig. 1 Stresses in the bulk.

The values of the excess stresses and excess velocities at the boundaries between computational cells are not independent [8]. Considering Riemann invariants at the interface between computational cells, one can see that

$$\rho_n c_n \mathcal{V}_n^- + \Sigma_n^- \equiv 0, \tag{33}$$

$$\rho_{n-1} c_{n-1} \mathcal{V}_{n-1}^+ - \Sigma_{n-1}^+ \equiv 0, \tag{34}$$

i.e., the excess quantities depend on each other at the cell boundary.

3.1 Excess quantities at the boundaries between cells

Rewriting the jump relations (31), (32) in the form

$$(\Sigma^+)_{n-1} - (\Sigma^-)_n = (\bar{\sigma})_n - (\bar{\sigma})_{n-1}, \tag{35}$$

$$(\mathcal{V}^+)_{n-1} - (\mathcal{V}^-)_n = (\bar{v})_n - (\bar{v})_{n-1}, \tag{36}$$

and using the dependence between excess quantities (equations (33) and (34)),

we obtain then the system of linear equations for the determination of the excess velocities

$$\mathcal{V}^+_{n-1} - \mathcal{V}^-_n = \bar{v}_n - \bar{v}_{n-1},$$ (37)

$$\mathcal{V}^+_{n-1}\rho_{n-1}c_{n-1} + \mathcal{V}^-_n\rho_n c_n = \rho_n c_n^2 \bar{\varepsilon}_n - \rho_{n-1}c_{n-1}^2\bar{\varepsilon}_{n-1}.$$ (38)

In matrix notation the latter system of equations has the form

$$\begin{pmatrix} 1 & 1 \\ \rho_{n-1}c_{n-1} & -\rho_n c_n \end{pmatrix} \begin{pmatrix} -\mathcal{V}^+_{n-1} \\ \mathcal{V}^-_n \end{pmatrix} = \begin{pmatrix} -(\bar{v}_n - \bar{v}_{n-1}) \\ -(\rho c^2 \bar{\varepsilon}_n - \rho c^2 \bar{\varepsilon}_{n-1}) \end{pmatrix}.$$ (39)

Comparing the obtained equation with equation (30), we conclude that

$$\beta^I_n = -\mathcal{V}^+_{n-1}, \quad \beta^{II}_n = \mathcal{V}^-_n.$$ (40)

This means that the excess quantities following from non-equilibrium jump relations at the boundary between computational cells correspond to the numerical fluxes in the conservative wave-propagation algorithm.

The representation of the wave-propagation algorithm in terms of the excess quantities given here is formally identical to its conservative form [2]. The advantage of the new representation manifests itself at discontinuities, for which jump relations cannot be reduced to the continuity of true values, e.g., at phase-transition fronts or cracks.

4 One-dimensional waves in periodic media

As the first example, we consider the propagation of a pulse in a periodic medium. The initial form of the pulse is given in Fig. 2, where the periodic variation in density is also shown by dashed lines. For the test problem, the materials are chosen as polycarbonate ($\rho = 1190$ kg/m^3, $c = 4000$ m/s) and Al 6061 ($\rho = 2703$ kg/m^3, $c = 6149$ m/s).

We apply the numerical scheme (29) and (30) for the solution of the system of equations (1)–(3). The corresponding excess quantities are calculated by means of equations (35)–(38).

As it was noted, we can exploit all the advantages of the wave-propagation algorithm, including second-order corrections and transversal propagation terms [24]. However, no limiters are used in the calculations. Suppressing spurious oscillations is achieved by means of using a first-order Godunov step after each three second-order Lax-Wendroff steps. This idea of composition was invented in [29].

Calculations are performed with Courant-Friedrichs-Levy number equal to 1. The simulation result for 4000 time steps is shown in Fig. 3.

We observe a distortion of the pulse shape and a decrease in the velocity of the pulse propagation in comparison to the maximal longitudinal wave velocity in the materials. These results correspond to the prediction of the effective media theory [34] both qualitatively and quantitatively [16].
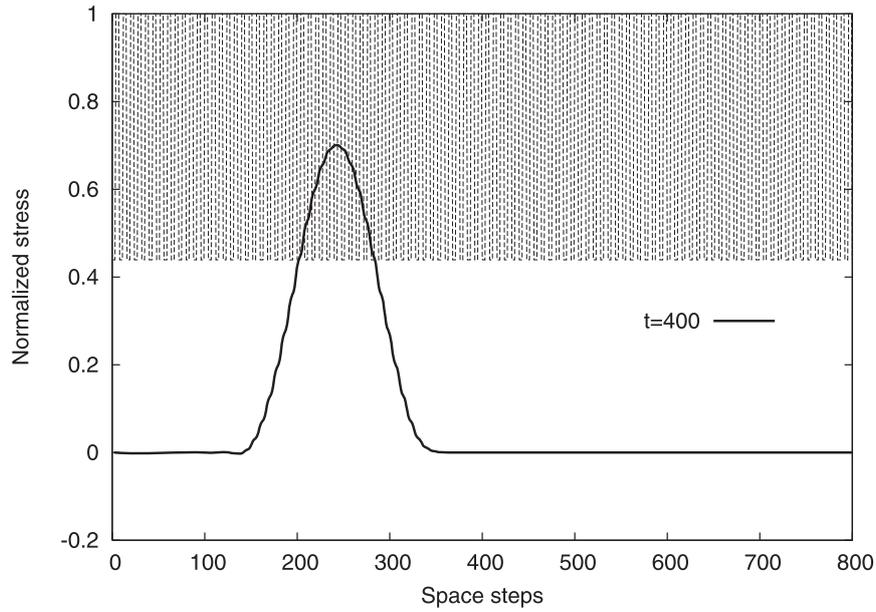
Fig. 2 Initial pulse shape. Reproduced from [5].
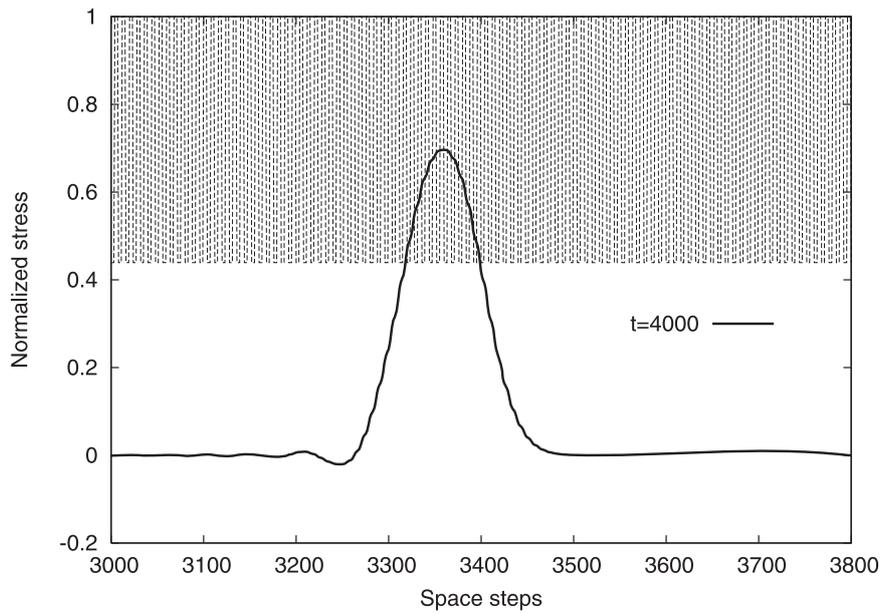
Fig. 3 Pulse shape at time step 4000. Reproduced from [5].

It should be noted that the effective media theory [34] leads to the dispersive wave equation

$$\frac{\partial^2 u}{\partial t^2} = (c^2 - c_a^2)\frac{\partial^2 u}{\partial x^2} + p^2 c_a^2 c_b^2 \frac{\partial^4 u}{\partial x^4}, \tag{41}$$

where u is the displacement, p is the periodicity parameter, and c_a and c_b are parameters of the effective media [15], instead of the wave equation following from equations (1)–(3)

$$\frac{\partial^2 u}{\partial t^2} = c^2 \frac{\partial^2 u}{\partial x^2}. \tag{42}$$

Equation (41) exhibits both *dispersion* (fourth-order space derivative) and the alteration in the longitudinal wave speed.

5 One-dimensional weakly nonlinear waves in periodic media

In the next example, we will see the influence of the materials' nonlinearity on the wave propagation. To close the system of equations (1) and (2) in the case of weakly nonlinear media we apply a simple nonlinear stress-strain relation

$$\sigma = \rho c^2 \varepsilon (1 + B\varepsilon), \tag{43}$$

where B is a parameter of nonlinearity, the values and sign of which are supposed to be different for hard and soft materials.
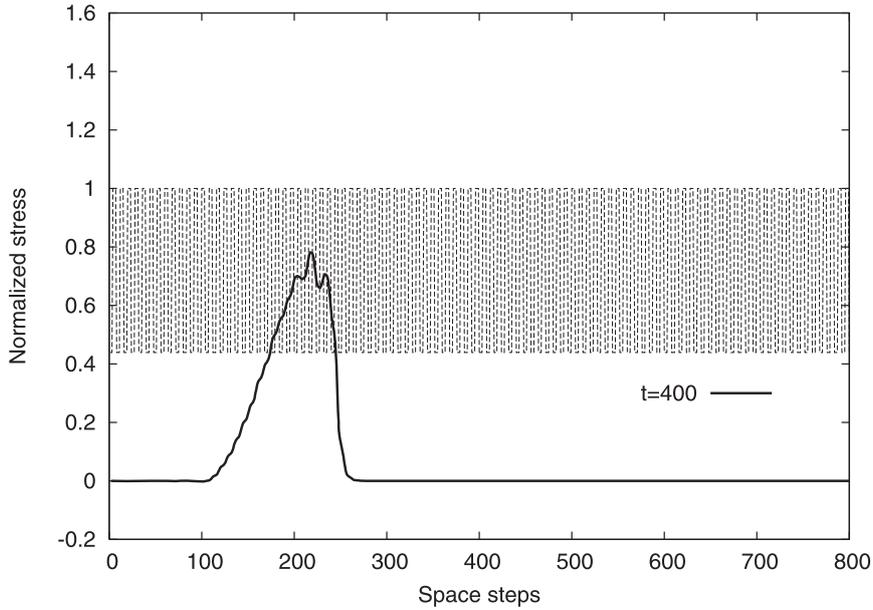
Fig. 4 Pulse shape at time step 400. Nonlinear case.

The solution method is almost the same as before. The approximate Riemann solver for the nonlinear elastic media (equation (43)) is similar to that used in [26, 28]. A modified longitudinal wave velocity $\hat{c}$, following the nonlinear stress-strain relation (43), is applied at each time step in the numerical scheme (29) and (30):

$$\hat{c} = c\sqrt{1 + 2B\varepsilon} \tag{44}$$

instead of the piecewise constant one corresponding to the linear case.

We consider the same pulse shape and the same materials (polycarbonate and Al 6061) as in the case of the linear periodic medium. However, the nonlinear effects appear only for a sufficiently high magnitude of loading. The values of the parameter of nonlinearity B were chosen as 0.24 for Al 6061 and 0.8 for polycarbonate.

The results of the simulations corresponding to 400, 1600, and 5200 time steps are shown in Figs. 4–6.
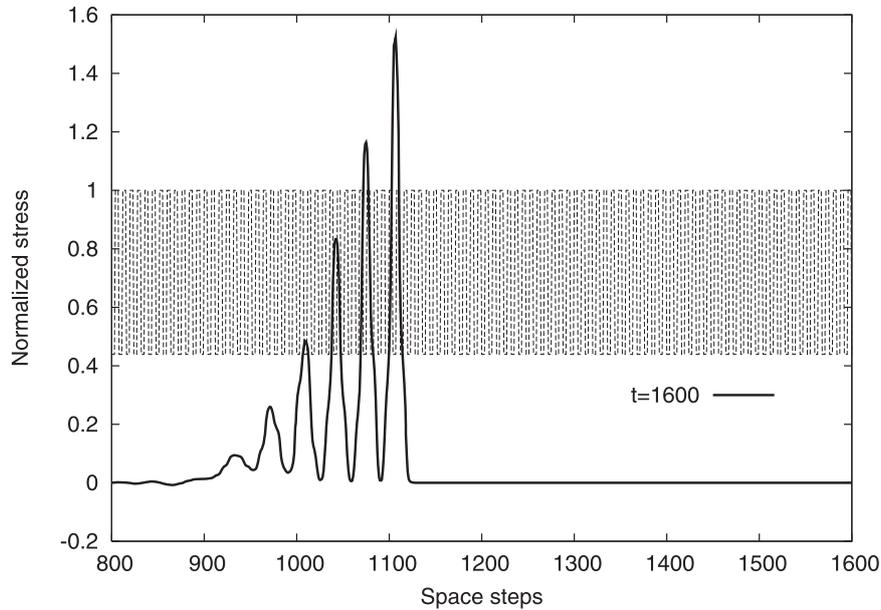
Fig. 5 Pulse shape at time step 1600. Nonlinear case.
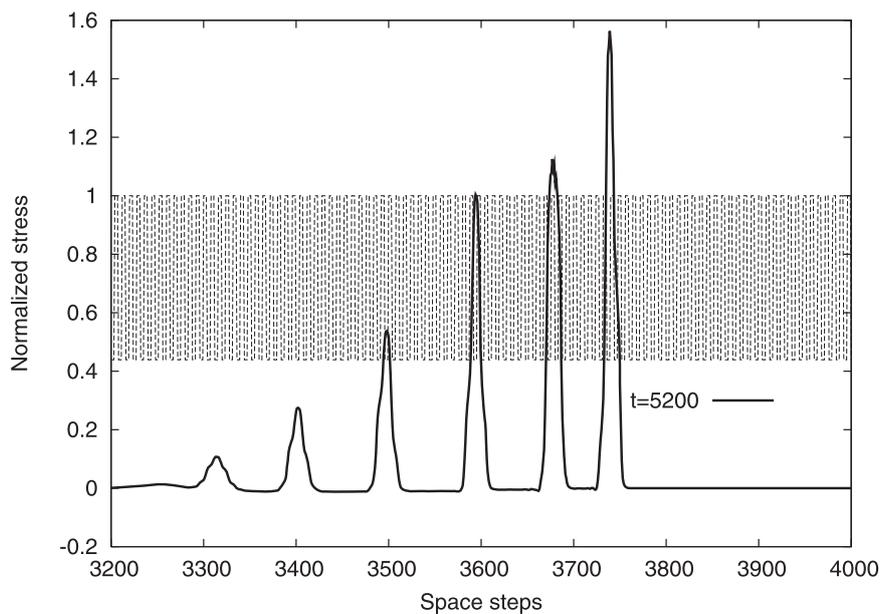
Fig. 6 Pulse shape at time step 5200. Nonlinear case. Reproduced from [5].

We observe that an initial bell-shaped pulse is transformed into a train of soliton-like pulses propagating with amplitude-dependent speeds. Such kind of behavior was first reported in [26], where these pulses were called "stegotons" because their shape is influenced by the periodicity.

In principle, the soliton-like solution could be expected because if we combine the weak nonlinearity (43) with the dispersive wave equation in terms of the effective media theory (41), we arrive at the Boussinesq-type equation

$$\frac{\partial^2 u}{\partial t^2} = (c^2 - c_a^2)\frac{\partial^2 u}{\partial x^2} + \alpha B \frac{\partial u}{\partial x}\frac{\partial^2 u}{\partial x^2} + p^2 c_a^2 c_b^2 \frac{\partial^4 u}{\partial x^4}, \tag{45}$$

which possesses soliton-like solutions.

6 One-dimensional linear waves in laminates

There are three basic length scales in wave propagation phenomena:

– the typical wavelength λ;
– the typical size of the inhomogeneities d;
– the typical size of the whole inhomogeneity domain l.

In the case of infinite periodic media considered above the third length scale was absent. Therefore, it may be instructive to consider wave propagation in a body where the periodic arrangement of layers of different materials is confined within a finite spatial domain.
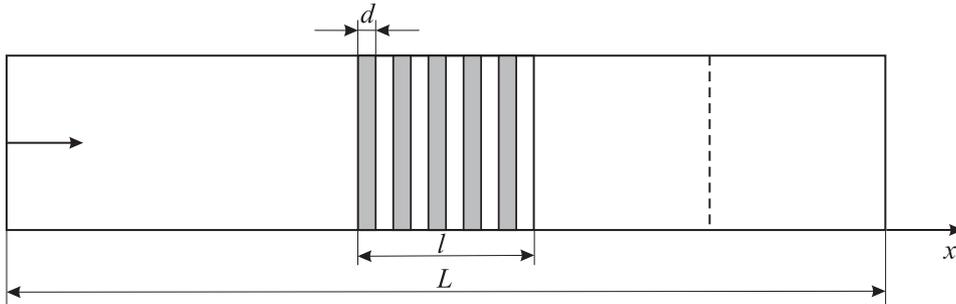
Fig. 7 Length scales in laminate.

To investigate the influence of the size of the inhomogeneity domain, we compare the shape of the pulse in the homogeneous medium with the corresponding pulse transmitted through the periodic array with a different number of distinct layers (Fig. 7).

We use Ti ($\rho = 4510$ kg/m^3, $c = 5020$ m/s) and Al ($\rho = 2703$ kg/m^3, $c = 5240$ m/s) as materials in the distinct layers in the numerical simulations of linear elastic wave propagation.
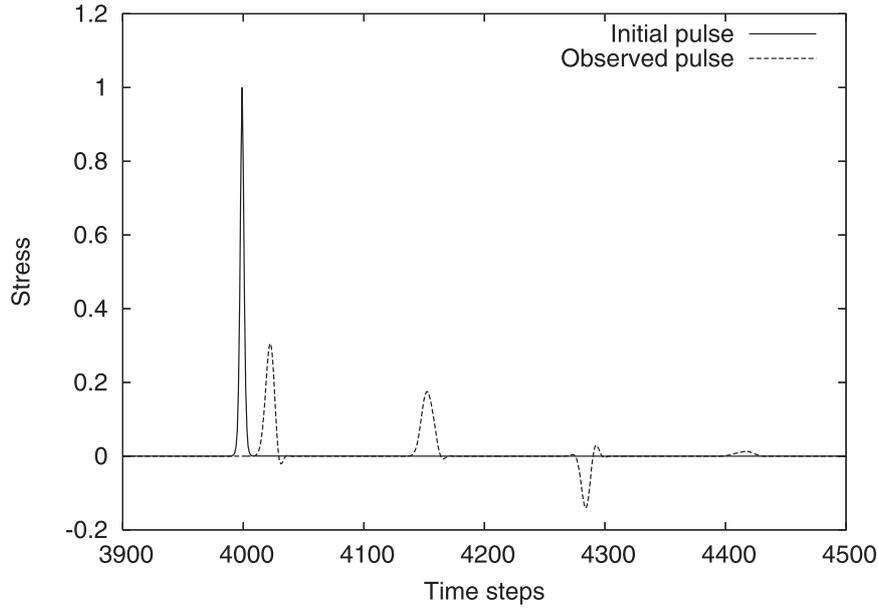
Fig. 8 Pulse shape at 4000 time steps ($d = 64\triangle x, l = 1000\triangle x$).
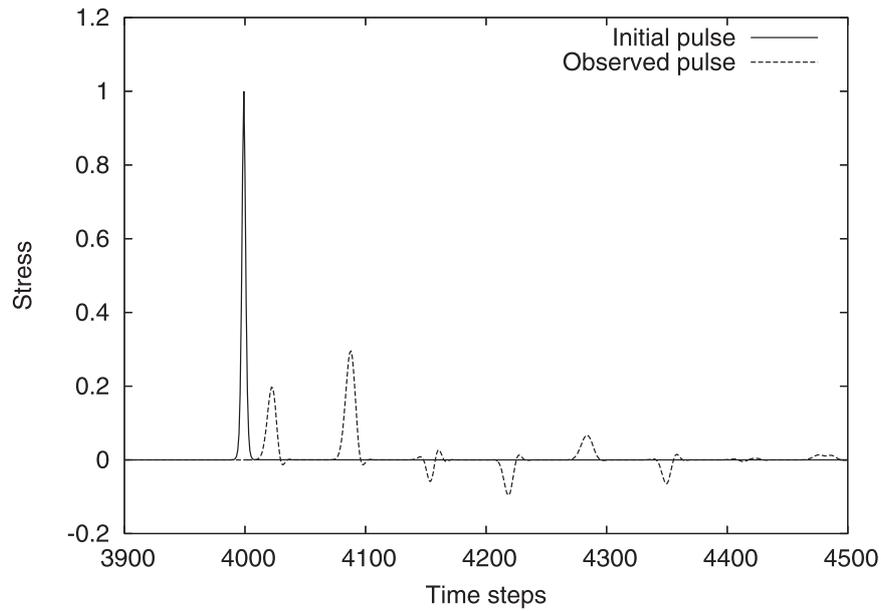
Fig. 9 Pulse shape at 4000 time steps ($d = 32\triangle x, l = 1000\triangle x$).

We apply a stress pulse, the width λ of which corresponds to $30\triangle x$ ($\triangle x$ is the space step)

$$\sigma(t) = \frac{2}{\cosh^2(0.5(t - 15\triangle t))} \tag{46}$$

at the left end of the domain (Fig. 7), and record the resulting pulse at $x = 4000\triangle x$. The location is indicated by the dashed line in Fig. 7.

The results are presented in Figs. 8–10 (dashed lines). The reference pulse calculated for homogeneous media is drawn with a solid line. As can be observed, if
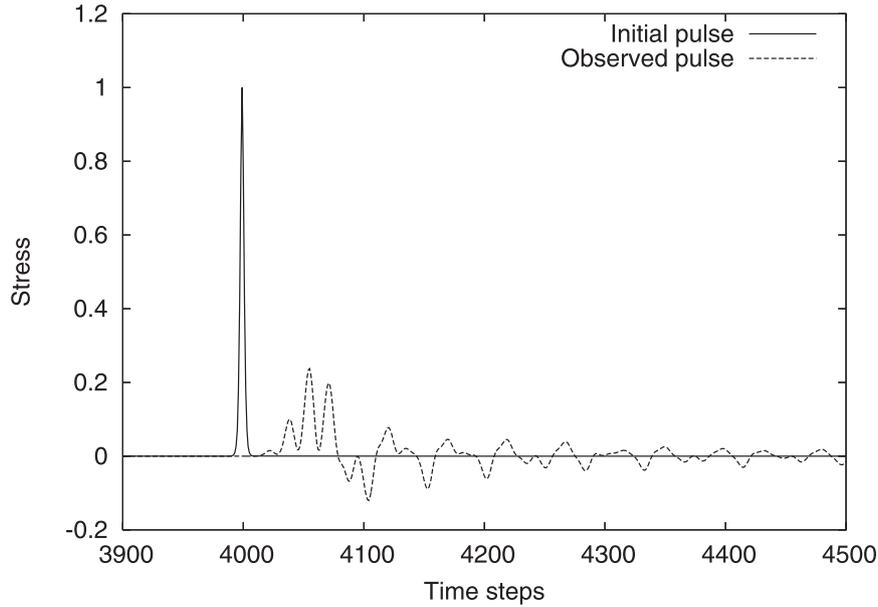
Fig. 10 Pulse shape at 4000 time steps ($d = 8\triangle x, l = 1000\triangle x$).

the wavelength is less then the size of the inhomogeneity ($d \geq \lambda$), we have a strong dispersion of the pulse, i.e., a separation of the wave into components of various frequencies (Figs. 8 and 9). This dispersion is not so strong if, vice versa, the size of the inhomogeneity d is less then the wavelength λ (Fig. 10).

Thus, waves in laminates demonstrate dispersive behavior, which is governed by the relations between the characteristic length scales. Taking into account nonlinear effects, we have seen the soliton-like wave propagation. Both nonlinearity and dispersion effects are observed experimentally in laminates under shock loading.

7 Nonlinear elastic waves in laminates under impact loading

Though the stress response to an impulsive shock loading has been very well understood for homogeneous materials, the same cannot be said for heterogeneous systems. In heterogeneous media, scattering due to interfaces between dissimilar materials plays an important role for shock wave dissipation and dispersion [18].

Diagnostic experiments for the dynamic behavior of heterogeneous materials under impact loading are usually carried out using a plate impact test configuration under a one-dimensional strain state. These experiments were recently reviewed in [12, 13]. For almost all the experiments, the stress response has shown a sloped rising part followed by an oscillatory behavior with respect to a mean value [12, 13]. Such behavior in the periodically layered systems is consistently exhibited in the systematic experimental work [39]. The specimens used in the shock compression experiments [39] were periodically layered two-component composites prepared by repeating a composite unit as many times as necessary to form a specimen with
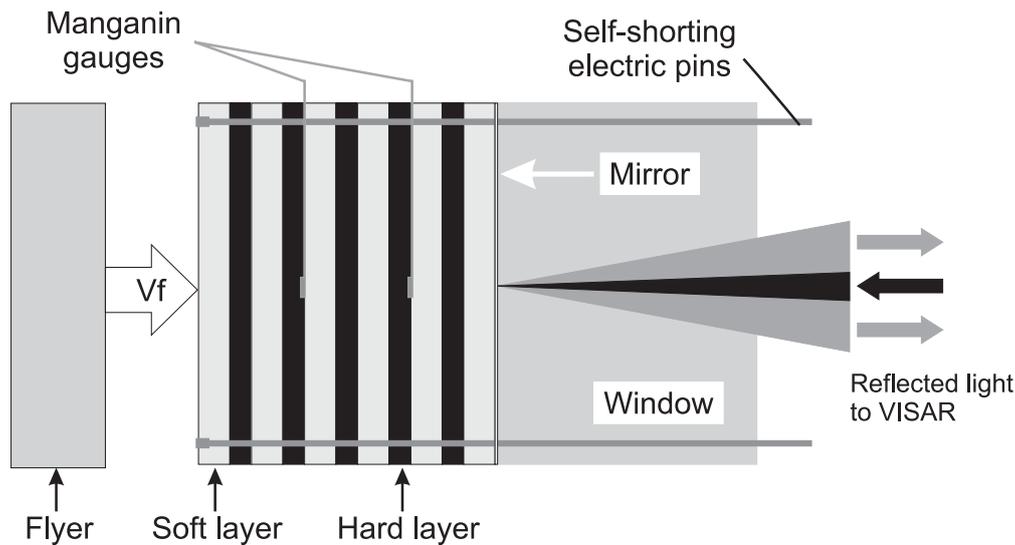
Fig. 11 Experimental setting. Reproduced from [39].

the desired thickness (see Fig. 11). A buffer layer of the same material as the soft component of the specimen was used at the other side of the specimen. A window in contact with the buffer layer was used to prevent the free surface from serious damage due to unloading from shock wave reflection at the free surface. Shock compression experiments were conducted by employing a powder gun loading system, which could accelerate a flat plate flyer to a velocity in the range of 400 m/s to about 2000 m/s. In order to measure the particle velocity history at the specimen window surface, a velocity interferometry system was constructed, and to measure the shock stress history at selected internal interfaces, the manganin stress technique was adopted. Four different materials, polycarbonate, 6061-T6 aluminum alloy, 304 stainless steel, and glass, were chosen as components. The selection of these materials provided a wide range of combinations of shock wave speeds, acoustic impedance and strength levels. The influence of multiple reflections of internal interfaces on shock wave propagation in the layered composites was clearly illustrated by the shock stress profiles measured by manganin gages. The origin of the observed structure of the stress waves was attributed to material heterogeneity at the interfaces. For high velocity impact loading conditions, it was fully realized that material nonlinear effects may play a key role in altering the basic structure of the shock wave.

An approximate solution for layered heterogeneous materials subjected to high velocity plate impact has been developed in [12, 13]. For laminated systems under shock loading, shock velocity, density and volume were related to the particle velocity by means of an equation of state. The elastic analysis was extended to shock response by incorporating the nonlinear effects through computing the shock velocities of the wave trains and superimposing them.

As pointed out in [39], stress wave propagation through layered media made of isotropic materials provides an ideal model to investigate the effect of heterogeneous materials under shock loading, because the length scales, e.g., the thickness of individual layers, and other measures of heterogeneity, e.g., impedance mismatch, are well defined.

Since the impact velocity in shock experiments is sufficiently high, various nonlinear effects may affect the observed behavior. That is why we apply numerical simulations of finite-amplitude nonlinear wave propagation to the study of scattering, dispersion and attenuation of shock waves in layered heterogeneous materials.

The geometry of the problem follows the experimental configuration described in [39] (Fig. 12).
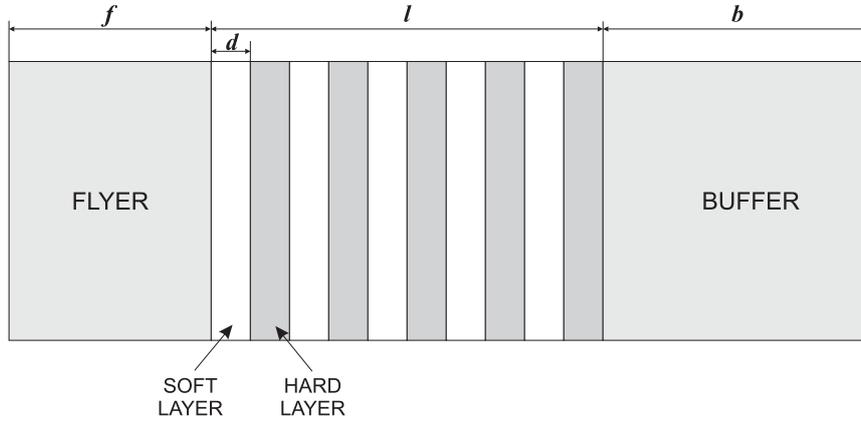
Fig. 12 Geometry of the problem.

We consider the initial-boundary value problem of impact loading of a heterogeneous medium composed of alternating layers of two different materials. The impact is provided by a planar flyer of length L, which has an initial velocity v_0. A buffer of the same material as the soft component of the specimen is used to eliminate the effect of wave reflection at the stress-free surface. The densities of the two materials are different, and the materials' response to compression is characterized by the distinct stress-strain relations $\sigma(\varepsilon)$. Compressional waves propagating in the direction of the layering are modeled by the one-dimensional hyperbolic system of conservation laws (1)–(2).

Initially, stress and strain are zero inside the flyer, the specimen, and the buffer, but the initial velocity of the flyer is nonzero:

$$v(x,0) = v_0, \quad 0 < x < L, \tag{47}$$

where L is the size of the flyer. Both left and right boundaries are stress-free.

Instead of an equation of state like the one used in [12, 13], we apply a simpler nonlinear stress-strain relation $\sigma(\varepsilon, x)$ for each material (43) (cf. [31]):

$$\sigma = \rho c^2 \varepsilon (1 + B\varepsilon), \tag{48}$$

where, as previously, ρ is the density, c is the conventional longitudinal wave speed, and B is a parameter of nonlinearity, the values and signs of which are supposed to be different for hard and soft materials.

We apply the same numerical scheme as in the previous example. The results of the numerical simulations compared with experimental data [39] are presented in the next section.

7.1 Comparison with experimental data

Figure 13 shows the measured and calculated stress time history in the composite, which consists of 8 units of polycarbonate, each 0.74 mm thick, and of 8 units of stainless steel, each 0.37 mm thick. The material properties of the components are extracted from [39]: the density $\rho = 1190$ kg/cm^3 and the sound velocity $c = 1957$ m/s for the polycarbonate; $\rho = 7890$ kg/cm^3 and $c = 5744$ m/s for the stainless steel. The stress time histories correspond to the distance 0.76 mm from the impact face. Calculations are performed for the flyer velocity 561 m/s and the flyer thickness 2.87 mm.
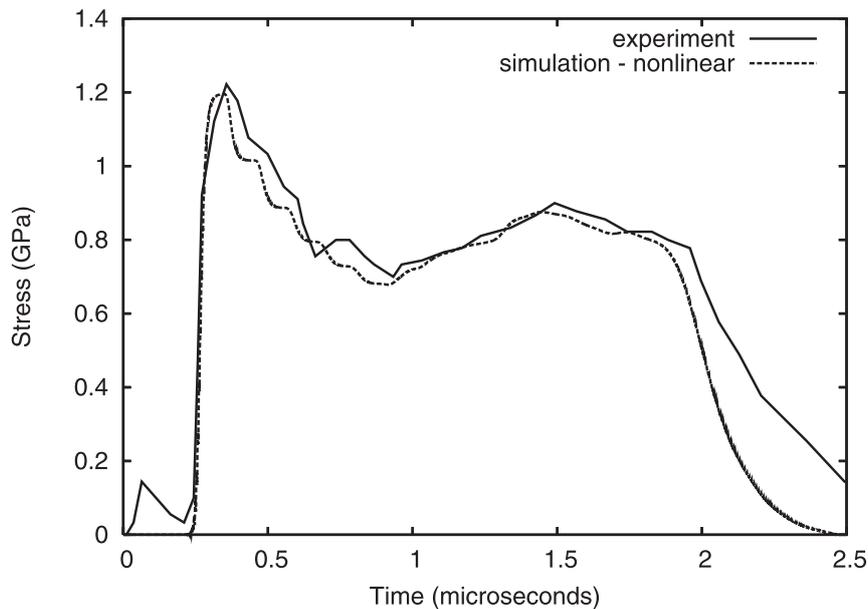
Fig. 13 Comparison of shock stress time histories corresponding to the experiment 112501 [39]. Reproduced from [4].

The results of the numerical calculations depend crucially on the choice of the parameter of nonlinearity B. We choose this parameter from the condition to match the numerical simulations to the experimental results.

Time histories of particle velocity for the same experiment are shown in Fig. 14. It should be noted that the particle velocity time histories correspond to the boundary between the specimen and the buffer. As one can see, both stress and particle velocity time histories are well reproduced by the nonlinear model with the same values of the nonlinearity parameter *B*.
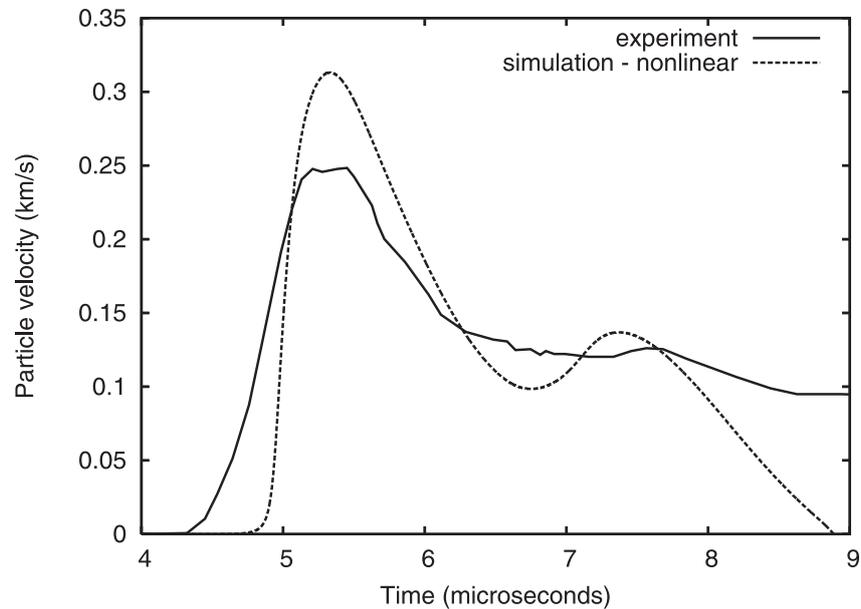
Fig. 14 Comparison of particle velocity time histories corresponding to the experiment 112501 [39]. Reproduced from [4].

As it is pointed out in [39], the influence of multiple reflections of internal interfaces on shock wave propagation in the layered composites is clearly illustrated by the shock stress time histories measured by manganin gages. Therefore, we focus our attention on the comparison of the stress time histories.

Figure 15 shows the stress time histories in the composite, which consists of 16 units of polycarbonate, each 0.37 mm thick, and of 16 units of stainless steel, each 0.19 mm thick. The stress time histories correspond to the distance 3.44 mm from the impact face. Calculations are performed for the flyer velocity 1043 m/s and the flyer thickness 2.87 mm.

The nonlinearity parameter *B* is chosen here to be 2.80 for polycarbonate and zero for stainless steel. Additionally, the stress time history corresponding to the linear elastic solution (i.e., the nonlinearity parameter is zero for both components) is shown. It can be seen that the stress time history computed by means of the considered nonlinear model is very close to the experimental one. It reproduces three main peaks and decreases with distortion, as it is observed in the experiment [39].
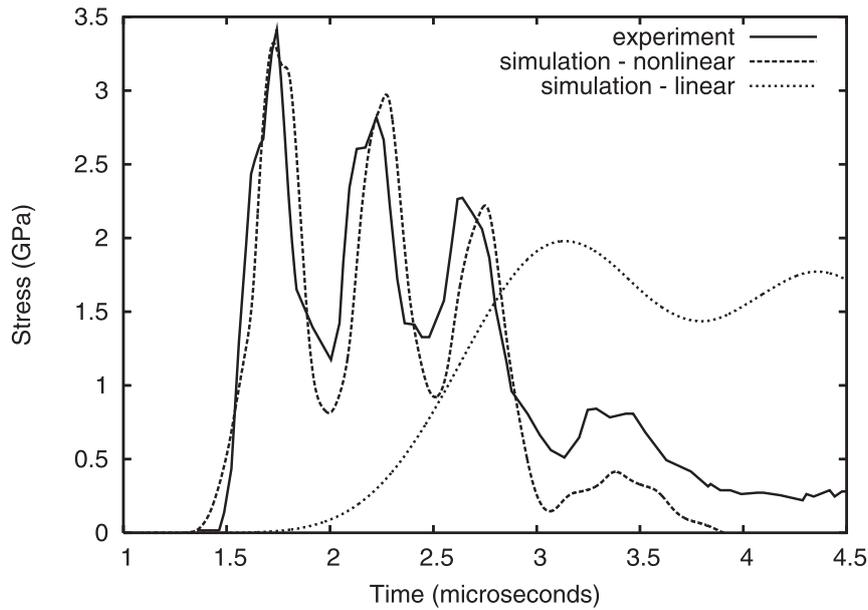
Fig. 15 Comparison of shock stress time histories corresponding to the experiment 110501 [39]. Reproduced from [4].

In Fig. 16 the same comparison is presented for the same composite as in Figure 15, only the flyer thickness is different (5.63 mm). This means that the shock energy is approximately twice as high than that in the previous case. The nonlinearity parameter B is also increased to 4.03 for polycarbonate and remains zero for stainless steel. As a result all 6 experimentally observed peaks are reproduced well.
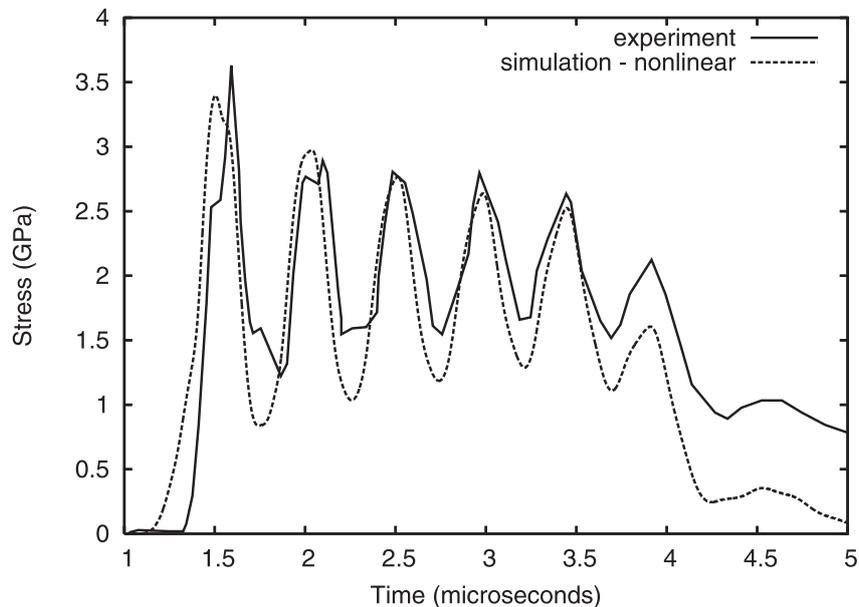
Fig. 16 Comparison of shock stress time histories corresponding to the experiment 110502 [39]. Reproduced from [4].

In Fig. 17 the comparison of stress time histories is presented for the composite consisting of 16 0.37 mm thick units of polycarbonate and 16 0.20 mm thick units of D-263 glass. The material properties of D-263 glass are [39]: the density $\rho = 2510$ kg/cm^3 and the sound velocity $c = 5703$ m/s. The distance between the measurement point and the impact face is 3.41 mm. Corresponding flyer velocity is 1079 m/s and the flyer thickness is 2.87 mm. The nonlinearity parameter B is chosen to be equal 5.025 for polycarbonate and zero for D-263 glass. Again, the stress time history corresponding to the linear elastic solution (i.e., the nonlinearity parameter is zero for both components) is shown. As one can see, the stress time history corresponding to the nonlinear model reproduces all 5 peaks with the same amplitude as observed experimentally.
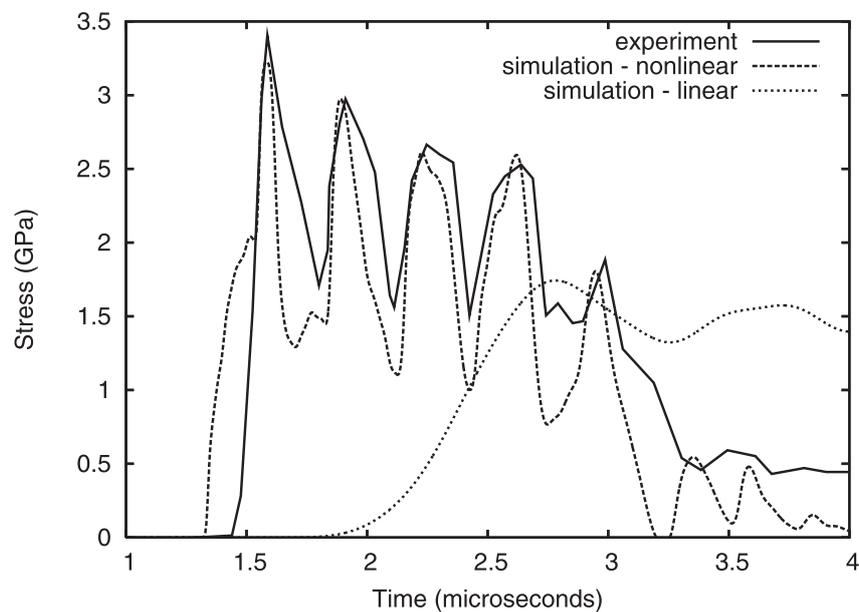
Fig. 17 Comparison of shock stress time histories corresponding to the experiment 112301 [39]. Reproduced from [4].

As it can be seen, the agreement between the results of the calculations and the experiments is achieved by the adjustment of the nonlinearity parameter B.

It follows that the nonlinear behavior of the soft material is affected not only by the energy of the impact, but also by the scattering induced by internal interfaces. It should be noted that the influence of the nonlinearity is not necessarily small. In the numerical simulations, which match with the experiments, the increase of the actual sound velocity of polycarbonate follows. It may be up to two times higher in comparison to the linear case. This conclusion is really surprising, but supported by the stress time histories.

Thus, the application of a nonlinear stress-strain relation for materials in numerical simulations of the plate impact problem of a layered heterogeneous medium shows that a good agreement between computations and experiments can be obtained by adjusting the values of the parameter of nonlinearity [4]. In the numer-

ical simulations of the finite-amplitude shock wave propagation in heterogeneous composites, the flyer size and velocity, the impedance mismatch of hard and soft materials, as well as the number and size of layers in a specimen were the same as in the experiments [39]. Moreover, a nonlinear behavior of materials was also taken into consideration. This means that combining scattering effects induced by internal interfaces and physical nonlinearity in material behavior into one nonlinear parameter, provides the possibility to reproduce the shock response in heterogeneous media observed experimentally. In this context, the parameter B is actually influenced by (i) the physical nonlinearity of the soft material and (ii) the mismatch of the elasticity properties of soft and hard materials. The mismatch effect is similar to the type of nonlinearity characteristic to materials with different moduli of elasticity for tension and compression. The mismatch effect manifests itself due to wave scattering at the internal interfaces, and, therefore, depends on the structure of a specimen. The variation of the parameter of nonlinearity confirms the statement that the nonlinear wave propagation is highly affected by the interaction of the wave with the heterogeneous substructure of a solid [39].

It should be noted that layered media do not exhaust all possible substructures of heterogeneous materials. Another example of a heterogeneous substructure is provided by functionally graded materials.

8 Waves in functionally graded materials

Functionally graded materials (FGMs) are composed of two or more phases that are fabricated so that their compositions vary more or less continuously in some spatial direction and are characterized by nonlinear gradients that result in graded properties. Traditional composites are homogeneous mixtures, and therefore they involve a compromise between the desirable properties of the component materials. Since significant proportions of an FGM contain the pure form of each component, the need for compromise is eliminated. The properties of both components can be fully utilized. For example, the toughness of a metal can be mated with the refractoriness of a ceramic, without any compromise in the toughness of the metal side or the refractoriness of the ceramic side.

Comprehensive reviews of current FGM research may be found in the papers [21] and [30], and in the book [35]. Studies of the evolution of stresses and displacements in FGMs subjected to quasistatic loading [35] show that the utilization of structures and geometry of a graded interface between two dissimilar layers can reduce stresses significantly. Such an effect is also important in the case of dynamical loading, where energy-absorbing applications are of special interest.

We consider the one-dimensional problem in elastodynamics for an FGM slab in which material properties vary only in the thickness direction. It is assumed that the slab is isotropic and inhomogeneous with the following fairly general properties [14]:

$$E'(x) = E'_0 \left(a\frac{x}{l} + 1 \right)^m, \quad \rho(x) = \rho_0 \left(a\frac{x}{l} + 1 \right)^n, \tag{49}$$

where ρ is the mass density, l is the thickness, a, m, and n are arbitrary real constants with $a > -1$, while E_0 and ρ_0 are the elastic constant and density at $x = 0$. The elastic constant E_0 is determined under the assumption that $\sigma_{yy} = \sigma_{zz}$ and the slab is fully constrained at infinity. It can thus be shown that

$$E' = \frac{E(1-v)}{(1+v)(1-2v)},\tag{50}$$

with $E(x)$ and $v(x)$ being the Young modulus and the Poisson ratio of the inhomogeneous material.

It is assumed that the slab is at rest for $t \leq 0$, therefore, the following initial conditions are valid:

$$v(x,0) = 0, \quad \sigma(x,0) = 0.\tag{51}$$

The boundary condition at $x = 0$ is

$$v(0,t) = 0, \quad t > 0 \quad \text{(``fixed'' boundary)}\tag{52}$$

At $x = l$, the slab is subjected to a stress pulse given by

$$\sigma_{xx}(l,t) = \sigma_0 f(t), \quad t > 0,\tag{53}$$

where the constant σ_0 is the magnitude of the pulse, the function f describes its time profile, and without any loss in generality, it is assumed that $|f| \leq 1$.

Following [14], we consider an FGM slab that consists of nickel and zirconia. The thickness of the slab is $l = 5$ mm. On one surface the medium is pure nickel and on the other surface pure zirconia, while the material properties $E_0(x)$ and $\rho(x)$ vary smoothly in thickness direction. A pressure pulse defined by

$$\sigma_{xx}(l,t) = \sigma_0 f(t) = -\sigma_0(H(t) - H(t - t_0)\tag{54}$$

is applied to the surface $x = l$ and the boundary $x = 0$ is "fixed". Here H is the Heaviside function. The pulse duration is assumed to be $t_0 = 0.2 \, \mu s$. The properties of the constituent materials used are given in Table 1 [14].

Material	E (GPa)	v	ρ (kg/m^3)
ZrO	151	0.33	5331
Ni	207	0.31	8900

Table 1 Properties of materials

The material parameters for the FGMs used are [14]: $a = -0.12354$, $m = -1.8866$, and $n = -3.8866$. The stress is calculated up to $12 \, \mu s$ (the propagation time of the plane wave through the thickness $l = 5$ mm is approximately $0.77 \, \mu s$ in pure ZrO2 and $0.88 \, \mu s$ in Ni).
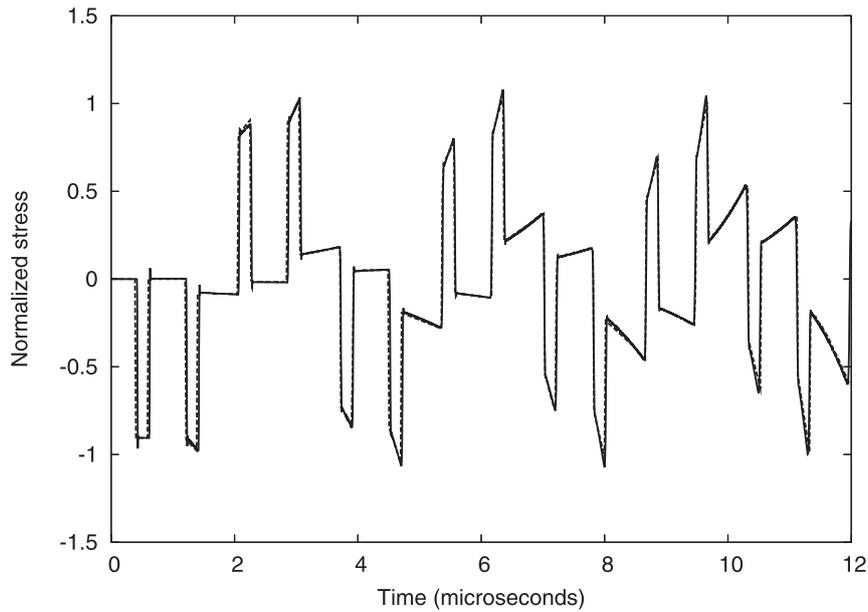
Fig. 18 Variation of stress with time in the middle of the slab. Reproduced from [5].

Numerical simulations were performed by means of the same algorithm as above. The comparison of the results of the numerical simulation and of the analytical solution [14] for the time dependence of the normalized stress σ_{xx}/σ_0 at the location $x/l = 1/2$ is shown in Fig. 18.

As one can see, it is difficult to make a distinction between analytical and numerical results. This means that the applied algorithm is well suited for the simulation of wave propagation in FGM.

A nonlinear behavior for the same materials with the nonlinearity parameter $A = 0.19$ is shown in Figure 19. For the comparison, calculations were performed with the value 0.9 of the Courant number both in the linear and nonlinear case. The amplitude amplification and pulse shape distortion in comparison with the linear case is clearly observed. In addition, the velocity of a pulse in the nonlinear material is increased.

9 Concluding remarks

As we have seen, linear and non-linear wave propagation in media with rapidly-varying properties as well as in functionally graded materials can be successfully simulated by means of the modification of the wave-propagation algorithm based on the non-equilibrium jump relation for true inhomogeneities. It should be emphasized that the used jump relation expresses the continuity of genuine unknown fields at the boundaries between computational cells. The applied algorithm is conservative, stable up to Courant number equal to 1, high-order accurate, and thermodynamically consistent. However, the main advantage of the presented modification of
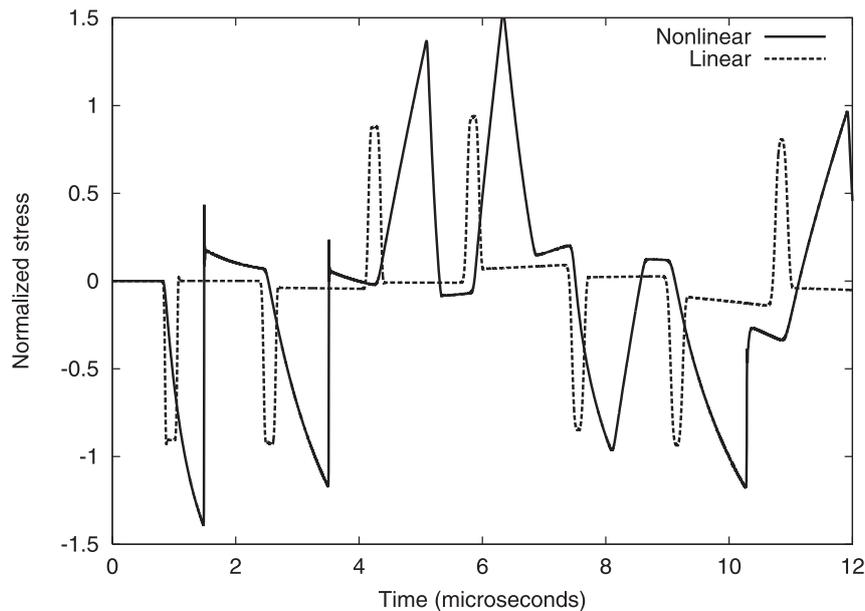
Fig. 19 Variation of stress with time in the middle of the slab. Nonlinear case. Reproduced from [5].

the wave-propagation algorithm is its applicability to the simulation of moving discontinuities. This property is related to the formulation of the algorithm in terms of excess quantities. To apply the algorithm to moving singularities, we simply should change the non-equilibrium jump relation for true inhomogeneities to another non-equilibrium jump relation valid for quasi-inhomogeneities.

References

1. Achenbach, J.D.: Wave Propagation in Elastic Solids. North-Holland, Amsterdam (1973)
2. Bale, D.S., LeVeque, R.J., Mitran, S., Rossmanith, J.A.: A wave propagation method for conservation laws and balance laws with spatially varying flux functions. SIAM J. Sci. Comp. **24**, 955–978 (2003)
3. Bedford, A., Drumheller, D.S.: Introduction to Elastic Wave Propagation. Wiley, New York (1994)
4. Berezovski, A., Berezovski, M., Engelbrecht, J.: Numerical simulation of nonlinear elastic wave propagation in piecewise homogeneous media. Mater. Sci. Eng. **A418**, 364–369 (2006)
5. Berezovski A, Berezovski, M., Engelbrecht, J., Maugin, G.A.: Numerical simulation of waves and fronts in inhomogeneous solids. In: Nowacki, W.K., Zhao, H. (eds.) Multi-Phase and Multi-Component Materials under Dynamic Loading, pp. 71-80. Inst. Fundam. Technol. Research, Warsaw (2007)
6. Berezovski, A., Maugin, G.A.: Simulation of thermoelastic wave propagation by means of a composite wave-propagation algorithm. J. Comp. Physics **168**, 249–264 (2001)

7. Berezovski, A., Maugin, G.A.: Thermoelastic wave and front propagation. J. Thermal Stresses **25**, 719–743 (2002)
8. Berezovski, A., Maugin, G.A.: Stress-induced phase-transition front propagation in thermoelastic solids. Eur. J. Mech. A/Solids **24**, 1–21 (2005)
9. Billingham, J., King, A.C.: Wave Motion. Cambridge University Press (2000)
10. Chakraborty, A., Gopalakrishnan, S.: Various numerical techniques for analysis of longitudinal wave propagation in inhomogeneous one-dimensional waveguides. Acta Mech. **162**, 1–27 (2003)
11. Chakraborty, A., Gopalakrishnan, S.: Wave propagation in inhomogeneous layered media: solution of forward and inverse problems. Acta Mech. **169**, 153–185 (2004)
12. Chen, X., Chandra, N.: The effect of heterogeneity on plane wave propagation through layered composites. Comp. Sci. Technol. **64**, 1477–1493 (2004)
13. Chen, X., Chandra, N., Rajendran, A.M.: Analytical solution to the plate impact problem of layered heterogeneous material systems. Int. J. Solids Struct. **41**, 4635–4659 (2004)
14. Chiu, T.-C., Erdogan, F.: One-dimensional wave propagation in a functionally graded elastic medium. J. Sound Vibr. **222**, 453–487 (1999)
15. Engelbrecht, J., Berezovski, A., Pastrone, F., Braun, M.: Waves in microstructured materials and dispersion. Phil. Mag. **85**, 4127–4141 (2005)
16. Fogarthy, T., LeVeque, R.J.: High-resolution finite-volume methods for acoustics in periodic and random media. J. Acoust. Soc. Am. **106**, 261–297 (1999)
17. Godlewski, E., Raviart, P.-A.: Numerical Approximation of Hyperbolic Systems of Conservation Laws. New York, Springer (1996)
18. Grady, D.: Scattering as a mechanism for structured shock waves in metals. J. Mech. Phys. Solids **46**, 2017–2032 (1998)
19. Graff, K.F.: Wave Motion in Elastic Solids. Oxford University Press (1975)
20. Guinot, V.: Godunov-type Schemes: An Introduction for Engineers. Elsevier, Amsterdam (2003)
21. Hirai, T.: Functionally graded materials. In: Processing of Ceramics. Vol. 17B, Part 2, pp. 292-341. VCH Verlagsgesellschaft, Weinheim (1996)
22. Hoffmann, K.H., Burzler, J.M., Schubert, S.: Endoreversible thermodynamics. J. Non-Equil. Thermodyn. **22**, 311–355 (1997)
23. Langseth, J.O., LeVeque, R.J.: A wave propagation method for three-dimensional hyperbolic conservation laws. J. Comp. Physics **165**, 126–166 (2000)
24. LeVeque, R.J.: Wave propagation algorithms for multidimensional hyperbolic systems. J. Comp. Physics **131**, 327–353 (1997)
25. LeVeque, R.J.: Balancing source terms and flux gradients in high-resolution Godunov methods: the quasi-steady wave-propagation algorithm. J. Comp. Physics **148**, 346–365 (1998)
26. LeVeque, R.J.: Finite volume methods for nonlinear elasticity in heterogeneous media. Int. J. Numer. Methods in Fluids **40**, 93–104 (2002)
27. LeVeque, R.J.: Finite Volume Methods for Hyperbolic Problems. Cambridge University Press (2002)
28. LeVeque, R.J., Yong, D.H.: Solitary waves in layered nonlinear media. SIAM J. Appl. Math. **63**, 1539–1560 (2003)
29. Liska, R., Wendroff, B.: Composite schemes for conservation laws. SIAM J. Numer. Anal. **35**, 2250–2271 (1998)
30. Markworth, A.J., Ramesh, K.S., Parks, W.P.: Modelling studies applied to functionally graded materials. J. Mater. Sci. **30**, 2183–2193 (1995)
31. Meurer, T., Qu, J., Jacobs, L.J.: Wave propagation in nonlinear and hysteretic media – a numerical study. Int. J. Solids Struct. **39**, 5585–5614 (2002)
32. Muschik, W., Berezovski, A.: Thermodynamic interaction between two discrete systems in non-equilibrium. J. Non-Equilib. Thermodyn. **29**, 237–255 (2004)
33. Rokhlin, S.I., Wang, L.: Ultrasonic waves in layered anisotropic media: characterization of multidirectional composites. Int. J. Solids Struct. **39**, 5529–5545 (2002)
34. Santosa, F., Symes, W.W.: A dispersive effective medium for wave propagation in periodic composites. SIAM J. Appl. Math. **51**, 984–1005 (1991)

35. Suresh, S., Mortensen, A.: Fundamentals of Functionally Graded Materials. The Institute of Materials, IOM Communications, London (1998)
36. Toro, E.F.: Riemann Solvers and Numerical Methods for Fluid Dynamics. Springer, Berlin (1997)
37. Toro, E.F. (ed.): Godunov Methods: Theory and Applications. Kluwer, New York (2001)
38. Wang, L., Rokhlin, S.I.: Recursive geometric integrators for wave propagation in a functionally graded multilayered elastic medium. J. Mech. Phys. Solids **52**, 2473–2506 (2004)
39. Zhuang, S., Ravichandran, G., Grady, D.: An experimental investigation of shock wave propagation in periodically layered composites. J. Mech. Phys. Solids **51**, 245–265 (2003)

Publication IV

J. Engelbrecht, A. Berezovski, M. Berezovski

Deformation Waves in Microstructured Materials: Theory and Numerics

Jüri Engelbrecht, Arkadi Berezovski, and Mihhail Berezovski

Centre for Nonlinear Studies, Institute of Cybernetics at Tallinn University of Technology, Tallinn, Estonia

je@ioc.ee

Abstract. A linear model of the microstructured continuum based on Mindlin theory is adopted which can be represented in the framework of the internal variable theory. Fully coupled systems of equations for macro-motion and microstructure evolution are represented in the form of conservation laws. A modification of wave propagation algorithm is used for numerical calculations. Results of direct numerical simulations of wave propagation in periodic medium are compared with similar results for the continuous media with the modelled microstructure. It is shown that the proper choice of material constants should be made to match the results obtained by both approaches.

1. Introduction

The classical theories of continua describe the behaviour of homogeneous materials. In reality, however, materials are always characterized by a certain microstructure at various scales. The character of a microstructure can be regular (like in laminated composites) or irregular (like in polycrystalline solids or alloys). Even more, regularity and irregularity may be combined like for some FGMs. The characteristic scale of a microstructure must always be compared with the spatial scale of excitation. The choice of proper mathematical models is extremely important in order to describe the wave fields with needed accuracy.

In general terms, the starting point for describing a microstructure could be either the discrete or the continuum approach. In the discrete approach the volume elements are treated as point masses with interaction [1]. Or, especially for laminated composites, the effective stiffness theory has been used [2]. The homogenization methods based on properties and geometry of constituents are widely used for static and quasi-static problems [3]. From the viewpoint of continua, the straight-forward modelling leads to assigning all the physical properties to every volume element dV in a solid which means introducing the dependence on space coordinates. Thus, the governing equations are so complicated that can be solved only by numerical methods.

Another way is to separate macro- and microstructure in continua. Then the conservation laws for both structures should be formulated separately [4, 5] or in a

more sophisticated way the microstructural quantities could be introduced into one set of conservation laws for the macrostructure [6]. Quite recently it has been shown that the generalization of such theories can be obtained by using the concept of dual internal variables [7].

To check the capabilities of the theory, it is useful to compare the theoretical predictions with results of direct numerical simulation of wave propagation through a certain known microstructure. In what follows, the derivation of a microstructure model is presented in the one-dimensional setting. The concept of dual internal variables is applied for the physical description of continua with microstructure. The finite volume wave propagation algorithm is used for both direct numerical simulation and the microstructure modeling. Results of direct numerical simulations of wave propagation in a periodically layered medium are compared with similar results for the homogeneous medium with a modelled microstructure.

2. Governing Equations

The governing equations of thermoelasticity are local balance laws for linear momentum and energy [8]. In the one-dimensional case these governing equations are reduced to (no body forces)

$$\frac{\partial}{\partial t}(\rho_0 v) - \frac{\partial \sigma}{\partial x} = 0, \tag{2.1}$$

$$\frac{\partial}{\partial t}\left(\frac{1}{2}\rho_0 v^2 + E\right) - \frac{\partial}{\partial x}(\sigma v - Q) = 0, \tag{2.2}$$

complemented by the second law of thermodynamics

$$\frac{\partial S}{\partial t} - \frac{\partial}{\partial x}(Q/\theta + K) \geq 0. \tag{2.3}$$

Here t is time, ρ_0 is the matter density, v is the physical velocity, σ is the Cauchy stress, E is the internal energy per unit volume, S is the entropy per unit volume, θ is temperature, Q is the material heat flux, and the "extra entropy flux" K vanishes in most cases, but this is not a basic requirement.

3. Internal Variables

Up to now the microstructure was not specified. In the framework of the phenomenological continuum theory it is assumed that the influence of the microstructure on the overall macroscopic behaviour can be taken into account by the introduction of an internal variable φ, which we associate with the integral distributed effect of the microstructure, and a certain dual internal variable ψ. We suppose that the free energy depends on the internal variables φ, ψ and their space derivatives $W = W*(u_x, \varphi, \varphi_x, \psi, \psi_x)$. Then the constitutive equations follow

$$\sigma := \frac{\partial W^*}{\partial u_x}, \quad \tau := -\frac{\partial W^*}{\partial \varphi}, \quad \eta := -\frac{\partial W^*}{\partial \varphi_x}, \quad \xi := -\frac{\partial W^*}{\partial \psi}, \quad \varsigma := -\frac{\partial W^*}{\partial \psi_x}. \quad (3.1)$$

We include into consideration the non-zero extra entropy flux [9]

$$K = -\theta^{-1}\eta\dot{\varphi} - \theta^{-1}\varsigma\dot{\xi}. \tag{3.2}$$

It can be checked that the dissipation inequality in the isothermal case reduces to

$$(\tau - \eta_x)\dot{\varphi} + (\xi - \varsigma_x)\dot{\psi} \geq 0. \tag{3.3}$$

In the non-dissipative case the dissipation inequality can be satisfied by the choice

$$\dot{\varphi} = m(\xi - \varsigma_x), \quad \dot{\psi} = -m(\tau - \eta_x), \tag{3.4}$$

where m is a coefficient. The latter two evolution equations express the duality between internal variables: one internal variable is driven by another one and vice versa.

The simplest free energy dependence is a quadratic function [10]

$$W^* = \frac{\rho_0 c^2}{2}u_x^2 + A\varphi u_x + \frac{1}{2}B\varphi^2 + \frac{1}{2}C\varphi_x^2 + \frac{1}{2}D\psi^2, \tag{3.5}$$

where A, B C, D, and c are material constants.

Here we include only the contribution of the second internal variable itself. In this case, the evolution equation for the internal variable φ is a hyperbolic equation [7]

$$\ddot{\varphi} = m^2 D(\tau - \eta_x). \tag{3.6}$$

4

As a result, we can represent the equations of motion in the form

$$\rho_0 u_{tt} = \rho_0 c^2 u_{xx} + A\varphi_x, \tag{3.7}$$

$$I\varphi_{tt} = C\varphi_{xx} - Au_x - B\varphi, \tag{3.8}$$

where $I = 1/(m^2 D)$ is an internal inertia measure. In terms of stresses introduced by Eq. (3.1), the same system of equations is represented as

$$\rho_0 \frac{\partial^2 u}{\partial t^2} = \frac{\partial \sigma}{\partial x}, \quad I\frac{\partial^2 \varphi}{\partial t^2} = -\frac{\partial \eta}{\partial x} + \tau. \tag{3.9}$$

It is worth to note that same equations are derived in [11] but based on different considerations.

3.1 Single Wave Equation

The governing equations (3.7) and (3.8) can be reduced to one equation. We can determine the first space derivative of the internal variable from Eq. (3.8) and its third derivatives from Eq. (3.7). Inserting the results into the balance of linear momentum (3.7), we obtain a higher order equation [9] with clearly separated wave operators which describe the influence of the microstructure

$$u_{tt} = \left(c^2 - \frac{A}{\rho_0 B}\right)u_{xx} + \frac{C}{B}(u_{tt} - c^2 u_{xx})_{xx} - \frac{I}{B}(u_{tt} - c^2 u_{xx})_{tt}. \tag{3.10}$$

3.2 System of Equations

At the same time, in terms of strain and velocity, Eq. (3.7) is rewritten as

$$\rho_0 v_t = \rho_0 c^2 \varepsilon_x + A\varphi_x. \tag{3.11}$$

The particle velocity and the strain are related by the compatibility condition

$$\varepsilon_t = v_x, \tag{3.12}$$

which form the system of equations for these two variables.

Similarly, introducing a microvelocity w as follows:

$$w_x := -D\psi, \tag{3.13}$$

and using Eq. (3.6) with $m = 1$, we have

$$\varphi_t = w_x, \tag{3.14}$$

that is nothing else but the compatibility condition at micro-level. It follows from Eqs. (3.14) and (3.8) that

$$I\dot{w}_x = C\varphi_{xx} - A\varepsilon - B\varphi. \tag{3.15}$$

Integrating the latter equation over x, we arrive at

$$Iw_t = C\varphi_x - \int (A\varepsilon + B\varphi)\, dx. \tag{3.16}$$

Thus, we have two coupled systems of equations (3.11), (3.12) and (3.14), (3.16) for the determination of four unknowns: $\varepsilon,\ v,\ \varphi$, and w. These two systems of equations are solved numerically to describe the microstructure dynamics.

4 Numerical Simulations

4.1 Algorithm Description

There are many computational methods used to describe wave propagation phenomena (see, e.g. [12]). In our computations we apply a modification of the wave propagation algorithm [13] that was successfully applied to the simulation of wave propagation in inhomogeneous media with rapidly-varying properties [14]. In simulations of wave propagation in a layered medium with known location of inhomogeneities, the numerical scheme is the same as described in [14]. However, the wave propagation algorithm is modified in order to solve the coupled systems of equations in the modelling of the microstructure. This modification is needed to treat the source terms which appeared in equations due to their coupling.

4.2 Linear Waves

As an example, the propagation of a pulse in an one-dimensional medium which can be represented as an elastic bar is analysed. This bar is assumed homogeneous except of a region of length d, where periodically alternating layers of size l are

inserted. The density and longitudinal velocity in the bar are chosen as $\rho_0 = 4510$ kg/m^3 and $c = 5240$ m/s, respectively. The corresponding parameters for the material of the inhomogeneity layers are $\rho_1 = 2703$ kg/m^3 and $c_1 = 5020$ m/s, respectively. The shape of the pulse before the crossing of the inhomogeneity region is formed by an excitation of the strain at the boundary for an limited dimensionless time period ($0 < t < 100$)

$$\varepsilon(0,t) = (1 + \cos(\pi(t-50)/50)).\qquad\qquad(4.1)$$

The time step used in calculations is by definition a unit. The length of the pulse $L = 100\ \varDelta x$ is comparable with the size of inhomogeneity ($l = 128\ \varDelta x$). Using the notion of the bar, it must be stressed that l and L are much smaller than the diameter of the bar [15].

Direct numerical simulation of linear elastic wave propagation in the medium with variable properties shows that the pulse holds its shape up to the entering into the inhomogeneity region. After the interaction with the periodic multilayer, the single pulse is separated into many reflected and transmitted parts as it can be seen in Fig. 4.1. Normalized time shown in Fig. 4.1 is measured in hundreds of time steps. During the propagation in the periodic medium, the amplitude of the pulse is diminished due to multiple reflections.
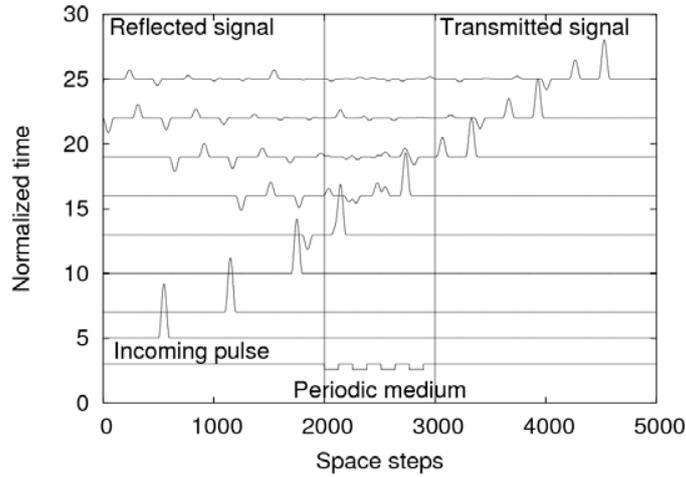
Fig.4.1 Scattering of a pulse by a periodic multilayer.

The same pulse propagation was simulated by the microstructured model described above with the following choice of material parameters: $A = 49\ \rho_0 c^2$, $I = \rho_1$, $C = Ic_1^2$, $B = 24.6\ A^2\rho_0 c^2$. In this case, there is no assumption of periodicity of

microstructure, however, in calculations of the pulse propagation, the internal length l for the microstructure is kept the same as in the case of periodic multilayer. The ratio of scales l and L together with the value of the parameter A determines the contribution of the microstructure to the macromotion.

Here the coupled systems of equations (3.11), (3.12) and (3.14), (3.16) are solved simultaneously. It should be noted that no boundary conditions for the internal variable are prescribed. A non-zero solution for the microstructure is induced due to the coupling.

Results of numerical simulation are presented in Fig.4.2, where the corresponding transmitted pulses from the solution of the problem with periodic multilayer are also shown.
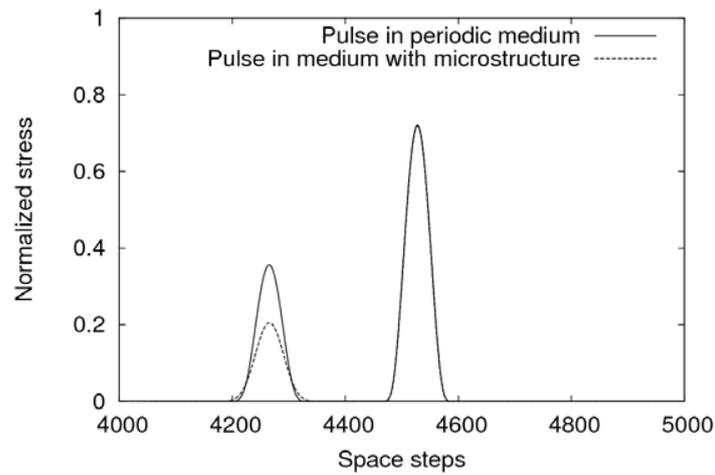
Fig.4.2 Transmitted pulses.

As one can see, the adjustment of material parameters in the microstructure model allows us to reproduce the first pulse with perfect accuracy while the second one is essentially smaller in amplitude, because of the absence of a reflected trail in the case of the microstructure model.

4.3 Weakly Nonlinear Waves

We consider again the propagation of a pulse in a layered 1D medium (elastic bar) where the length of inhomogeneity $l = 4\ \varDelta x$ is much smaller than the length of the pulse $L = 100\ \varDelta x$. The properties of materials are the same as previously with a weak nonlinearity for the less stiff material (cf. [16])

$$\sigma = \rho_0 c^2 u_x \left(1 + N u_x\right),$$ (4.2)

where N is a parameter of nonlinearity.

Direct computations in this weakly nonlinear case ($N = 0.04$) show that the initial bell-shaped pulse is transformed in a train of soliton-like pulses propagating with amplitude-dependent speeds (Fig. 4.3) like for the celebrated KdV case.
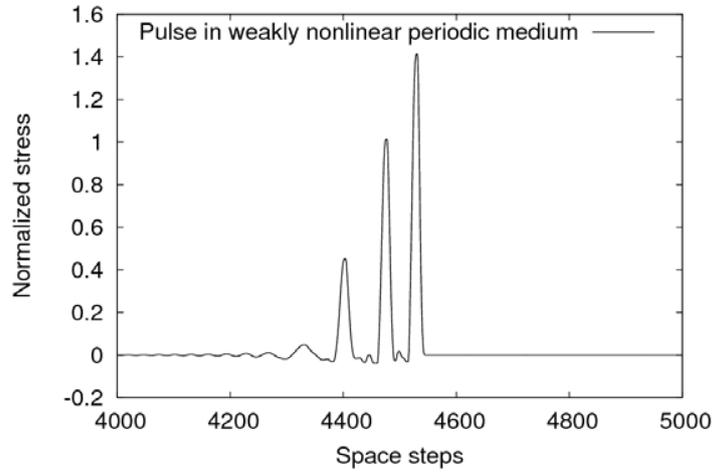
Fig 4.3. Transformation of a bell-shaped pulse in a weakly nonlinear periodic medium (after 4600 time steps).

If we return to the microstructure model then the linear governing equations (3.7), (3.8) must be modified. Instead of the free energy function (3.5), a cubic function is used:

$$W^* = \frac{\rho_0 c^2}{2} u_x^2 + A \varphi u_x + \frac{1}{2} B \varphi^2 + \frac{1}{2} C \varphi_x^2 + \frac{1}{2} D \psi^2$$
$$+ \frac{\rho_0 c^2}{6} M \varphi^3 + \frac{\rho_0 c^2}{6} N u_x^3,$$ (4.3)

where M and N are new material constants (see [17]).

Now the governing equations yield (cf. (3.7), (3.8))

$$\rho_0 u_{tt} = \rho_0 c^2 u_{xx} + \rho_0 c^2 N u_x u_{xx} + A \varphi_x, \tag{4.4}$$

$$I \varphi_{tt} = C \varphi_{xx} + M \varphi_x \varphi_{xx} - A u_x - B \varphi. \tag{4.5}$$

Besides dispersive effects (see [10]), the governing equations (4.4) and (4.5) include also nonlinear effects in macro- and microscale. The dispersive effects are analysed in [10] while the influence of nonlinearities is described in [18]. It is not surprising that the balance between the dispersive and nonlinear effects can occur resulting in emergence of solitons.

For numerical simulation, the system of equations (4.4), (4.5) can be represented in the form of a single (4th order) equation (like Eq. (3.10)). The initial value problem for such a model nonlinear equation is solved by the pseudospectral method [18]. The initial pulse-type excitation leads to the train of solitons similar to that shown in Fig. 4.3.

5 Conclusions

If we know all the details of a given microstructure, namely, size, shape, composition, location, and properties of inclusions as well as properties of a carrier medium, the classical wave theory is sufficient for the description of wave propagation. Usually our knowledge about the microstructure is limited – we know only the characteristic scale of microstructure and its physical properties. Then the accuracy of classical theories is not sufficient and the more advanced theories of continua should be used.

In the paper, we have compared results of direct numerical simulations of wave propagation in given layered media with the corresponding results obtained by a continuous model of the microstructure. The presented model looks like a promising variant of the theory, complicated enough to describe various effects of the microstructure. This model can be naturally extended to include non-linear effects and dissipation [19]. However, numerical simulations demonstrate that the straight-forward numerics and the modelling on the basis of continuum theories need a careful matching of material coefficients.

Some general remarks should be made in addition. The concept of dual internal variables introduced in [7] permits to model consistently microstructure(s) for both dissipative (not analysed here) and non-dissipative processes (see above). Such an approach gives an excellent basis to clarify the structure of generalised continuum theories such like linear Cosserat, micromorphic, and second gradient elasticity theories. This will be a subject of our forthcoming publications.

Once the wavefields in microstructured materials are described with needed accuracy, the respective mathematical models can also be used for solving the inverse problems. In linear cases, the dependence of phase velocities on the microstructure can be used for determining the material properties. In nonlinear cases, when the balance between dispersive and nonlinear effects supports the propaga-

tion of solitary waves, the algorithms for solving the inverse problems can be based on the analysis of shapes of solitary waves. It has been shown namely [17] that the nonlinearity of the microstructure leads to asymmetric solitary waves. This property can be used for constructing an algorithm which determines the parameters of the microstructure from measured asymmetry (see [17]).

References
[1] Maugin, G.A.: Nonlinear Waves in Elastic Crystals. Oxford University Press (1999)
[2] Sun, C.T., Achenbach, J.D., Herrmann, G.: Continuum theory for a laminated medium. J. Appl. Mech. **35,** 467–475 (1968)
[3] Nemat-Nasser, S., Hori, M.: Micromechanics: Overall Properties of Heterogeneous Materials. Elsevier, Amsterdam (1993)
[4] Mindlin, R.D.: Microstructure in linear elasticity. Arch. Rat. Mech. Anal. **16**, 51–78 (1964)
[5] Eringen, A.C., Suhubi, E.S.: Nonlinear theory of micro-elastic solids II. Int. J. Eng. Sci. **2**, 189–203 (1964)
[6] Maugin, G.A.: On the thermomechanics of continuous media with diffusion and/or weak nonlocality. Arch. Appl. Mech. **75**, 723–738 (2006)
[7] Ván, P., Berezovski, A., Engelbrecht, J.: Internal variables and dynamic degrees of freedom. J. Non-Equilib. Thermodyn. **33**, 235–254 (2008)
[8] Nowacki, W.: Thermoelasticity. Pergamon/PWN, Oxford/Warszawa (1962)
[9] Maugin, G.A.: Internal variables and dissipative structures. J. Non-Equilib. Thermodyn. **15**, 173–192 (1990)
[10] Engelbrecht, J., Berezovski, A., Pastrone, F., Braun, M.: Waves in microstructured materials and dispersion. Phil. Mag. **85**, 4127–4141 (2005)
[11] Engelbrecht, J., Cermelli, P., Pastrone, F.: Wave hierarchy in microstructured solids. In: Maugin, G.A. (ed.) Geometry, Continua and Microstructure, pp. 99–111. Hermann Publ., Paris (1999)
[12] Effective Computational Methods for Wave Propagation. Kampanis, N. A., Dougalis, V.A., Ekaterinaris, J.A. (eds.) , Chapman & Hall/CRC, Boca Raton (2008)
[13] LeVeque, R.J.: Finite Volume Methods for Hyperbolic Problems. Cambridge University Press (2002)
[14] Berezovski, A., Engelbrecht, J., Maugin, G.A.: Numerical simulation of waves and fronts in inhomogeneous solids. World Scientific, Singapore (2008)
[15] Lakes, R.S.: Experimental method for study of Cosserat elastic solids and other generalized continua. In: Mühlhaus, H.-B. (ed.) Continuum Models for Materials with Microstructure, pp.1–22. Wiley, New York (1995)
[16] Berezovski, A., Berezovski, M. and Engelbrecht, J.: Numerical simulation of nonlinear elastic wave propagation in piecewise homogeneous media. Mater. Sci. Engng. A **418**, 364–369 (2006)
[17] Janno, J., Engelbrecht J.: An inverse solitary wave problem related to microstructural materials. Inverse Problems, **21**, 2019–2034 (2005)
[18] Engelbrecht, J. Berezovski, A., Salupere, A.: Nonlinear deformation waves in solids and dispersion. Wave Motion, **44**, 493–500 (2007)
[19] Pastrone, F., Cermelli, P. and Porubov, A.: Nonlinear waves in 1-D solids with microstructure. Mater. Phys. Mech. **7**, 9–16 (2004)

Publication V

M. Berezovski, A. Berezovski, J. Engelbrecht
Numerical simulations of one-dimensional microstructure dynamics,
in: Proceedings of the 2nd International Symposium on Computational Mechanics
(ISCM II), November 30 - December 3, 2009, Hong Kong - Macau. (accepted)

Numerical Simulations of One-dimensional Microstructure Dynamics

M. Berezovski*, A. Berezovski, J. Engelbrecht

*Centre for Nonlinear Studies, Institute of Cybernetics at Tallinn University of Technology,
Akadeemia tee 21, 12618 Tallinn, Estonia
Email: mb@cens.ioc.ee*

Abstract. Results of numerical simulations of one-dimensional wave propagation in microstructured solids are presented and compared with the corresponding results of wave propagation in given layered media. A linear microstructure model based on Mindlin theory is adopted and represented in the framework of the internal variable theory. Fully coupled systems of equations for macro-motion and microstructure evolution are rewritten in the form of conservation laws. A modification of wave propagation algorithm is used for numerical calculations. It is shown how the initial microstructure model can be improved in order to match the results obtained by both approaches.

INTRODUCTION

Wave propagation in the medium with microstructure is dispersive [1], [2]. In order to catch the dispersion effects, the classical wave equation for linear elastic wave propagation should be modified. Usually this modification is made by homogenization or continualization methods [3, 4, 5]. Alternatively a generalized continuum theory can be applied [6]. The resulting microstructure models enhance the classical elastic behavior.

As it is recently shown, the concept of dual internal variables [7] can be successfully used for the physical description of the medium with microstructure [8]. Internal variable is associated with the integral distributed effect of the microstructure [9]. In the framework of the internal variable theory, fully coupled systems of equations for macro-motion and microstructure evolution are represented in the form of conservation laws.

However, solution of these equations is not easy task due to their coupling and the absence of natural boundary conditions for internal variable. In addition, parameters of the microstructure model are needed to be determined in each particular case. This is why we performed numerical experiments to compare results of direct numerical calculations of wave propagation in a laminate with prescribed properties and corresponding results obtained for an effective medium with the microstructure modeling. These numerical experiments allowed us to analyze advantages and weaknesses of the model. As a result, we found that some improvements have to be introduced into the microstructure model.

The numerical simulations are performed by means of a finite-volume numerical scheme modifying the wave-propagation algorithm [10] by the introduction of excess quantities instead of numerical fluxes, which simplifies the solution of Riemann problems at boundaries between computational cells at each time step [11]. Source terms are accounted in the jump relations at boundaries between computational cells. The scheme is applied for both macro- and micro-motion. The advantage of the wave-propagation algorithm is high-resolution [12] and the possibility for a natural extension to higher dimensions. It should be emphasized that there is no need for any artificial boundary conditions for the internal variable: the non-trivial solution is provided by the coupling between the macro- and micro-motions.

GOVERNING EQUATIONS

The most general model for the one-dimensional wave propagation in solids with microstructure is presented in [2]. This model is derived independently from the Euler-Lagrange equations for a Mindlin-type material model [13] and from internal variable theory [8]. In the framework of the internal variable theory it is assumed that the influence of the microstructure on the overall macroscopic behavior can be taken into account by the introduction of an internal variable which is associated with the integral distributed effect of the microstructure [9]. In the case of quadratic free energy dependence, the system of two coupled second-order hyperbolic equations for macro- and micromotion is derived as follows [2]:

$$\rho u_{tt} = \rho c^2 u_{xx} + A\varphi_x, \tag{1}$$

$$I\varphi_{tt} = C\varphi_{xx} - Au_{x,} - B\varphi, \tag{2}$$

where u is the macrodisplacement, φ is the internal variable (microdeformation), ρ is the matter density, c is the longitudinal wave velocity at the macrolevel, A, B, C and I are material constants for microstructure, subscripts are used to denote derivatives.

The governing equations (1) and (2) can be represented either as a single fourth-order equation [2] or as a system of four first-order equations. While the former representation is more convenient for theoretical considerations, the latter one is more suitable for numerics. Namely, in terms of strain and velocity, Eq. (1) is rewritten as

$$\rho v_t = \rho c^2 \varepsilon_x + A\varphi_x. \tag{3}$$

The particle velocity $v = u_t$ and the strain $\varepsilon = u_x$ are related by the compatibility condition

$$\varepsilon_t = v_x. \tag{4}$$

Similarly, introducing microvelocity ω we use the compatibility condition at micro-level as follows:

$$\varphi_t = \omega_x. \tag{5}$$

Accounting for Eq. (5) and integrating Eq. (2) over x, we arrive at

$$I\omega_t = C\varphi_x - \int (A\varepsilon + B\varphi)dx. \tag{6}$$

Thus, we have two coupled systems of equations (3), (4), (5) and (6) for the determination of four unknowns: ε, v, φ, and ω. To analyze the capabilities of the model and the role of material constants in the microstructure model, we need to solve these systems of equations simultaneously. It is clear that analytical solutions may be found only in highly simplified asymptotic cases. Therefore, we turn to numerical methods. However, even the numerical solution is not simple and straightforward because of the absence of natural boundary conditions for the internal variable [14] and possible instabilities [15].

As it is mentioned, numerical simulations are performed by means of a finite-volume numerical scheme modifying the wave-propagation algorithm [11]

$$(\rho\bar{v})_n^{k+1} - (\rho\bar{v})_n^k = \frac{\Delta t}{\Delta x}(\Sigma_n^+ - \Sigma_n^-) + A\frac{\Delta t}{\Delta x}(\Phi_n^+ - \Phi_n^-), \tag{7}$$

$$\bar{\varepsilon}_n^{k+1} - \bar{\varepsilon}_n^k = \frac{\Delta t}{\Delta x}(V_n^+ - V_n^-), \tag{8}$$

$$\overline{\varphi}_n^{k+1} - \overline{\varphi}_n^k = \frac{\Delta t}{\Delta x}(\Omega_n^+ - \Omega_n^-), \tag{9}$$

$$(I\overline{\omega})_n^{k+1} - (I\overline{\omega})_n^k = \frac{C\Delta t}{\Delta x}(\Phi_n^+ - \Phi_n^-), \tag{10}$$

where n and k denote space and time steps, respectively, overbars denote averaged quantities which are introduced together with excess quantities both for macro- and microfields as follows:

$$\sigma = \overline{\sigma} + \Sigma, \quad v = \overline{v} + V, \quad \varphi = \overline{\varphi} + \Phi, \quad \omega = \overline{\omega} + \Omega, \quad (\sigma = \rho c^2 \varepsilon). \tag{11}$$

The source terms in Eqs. (3) and (6) are accounted by including them into jump conditions at the boundaries between computational cells which are used for the solution of Riemann problems at each time step, namely,

$$\rho c^2 \varepsilon_{n-1} + A\varphi_{n-1} = \rho c^2 \varepsilon_n + A\varphi_n, \tag{12}$$

$$C\varphi_{n-1} - \left(A\varepsilon_{n-1} + B\varphi_{n-1}\right)\Delta x^2 = C\varphi_n - \left(A\varepsilon_i + B\varphi_n\right)\Delta x^2. \tag{13}$$

We do not apply any boundary conditions for the internal variable due to the coupling between micro- and macromotions.

NUMERICAL SIMULATIONS

To have a reference solution, the propagation of a pulse in a one-dimensional medium which can be represented as an elastic bar is considered first. This bar is assumed homogeneous except of a region of length l, where periodically alternating layers of size d are inserted (Fig. 1).
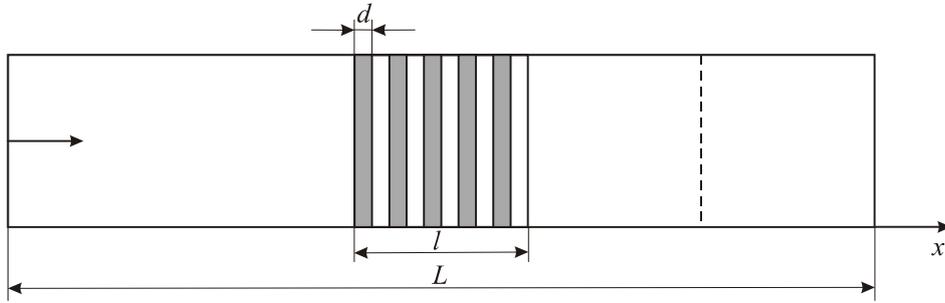
FIGURE 1. Geometry of the bar.

The density and the longitudinal velocity in the bar are chosen as $\rho = 4510$ kg/m^3 and $c = 5240$ m/s, respectively. The corresponding parameters for the material of the inhomogeneity layers are $\rho_1 = 2703$ kg/m^3 and $c_1 = 5020$ m/s, respectively. The shape of the pulse before the crossing of the inhomogeneity region is formed by an excitation of the strain at the boundary for a limited time period ($0 < t < 100\Delta t$)

$$u_x(0,t) = (1 + \cos(\pi(t - 50\Delta t)/50). \tag{14}$$

The length of the pulse ($\lambda = 100\Delta x$) is comparable with the size of inhomogeneity ($d = 128\Delta x$). The pulse holds its shape up to the entering into the inhomogeneity region. The problem is solved directly, i.e., without application of the microstructure model, since the location and properties of substructure are prescribed. The solution shows that after the interaction with the periodic multilayer, the single pulse is separated into many reflected and transmitted parts as it can be seen in Fig. 2.
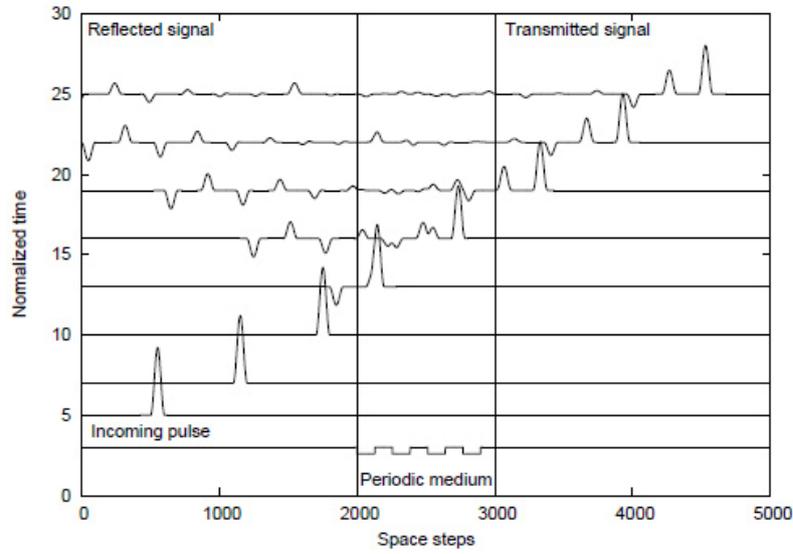
FIGURE 2. Scattering of a pulse by a periodic multilayer.

The dispersion occurs because of the successive reflections at each interface between the alternating layers.

The same pulse propagation was simulated by the microstructure model (3) - (6) with $A = 550\rho c^2$, $I = \rho_I$, $C = Ic_I^2$, $B = 6.7\, A^2/\rho c^2$. In this case, there is no assumption of periodicity, however, in calculations of the pulse propagation, the internal length d for the microstructure is kept the same as in the case of periodic multilayer. The ratio of scales d and λ together with the value of the parameter A determines the contribution of the microstructure to macromotion. The result of the numerical simulation is presented in Fig. 3, where the corresponding transmitted pulses from the solution of the problem with periodic multilayer are also shown.
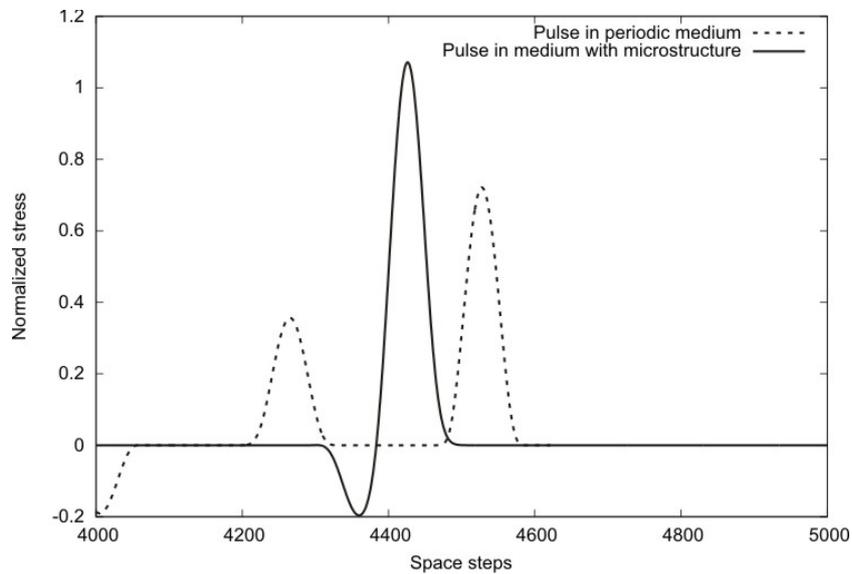
FIGURE 3. Leading transmitted pulses.

The obtained result is rather disappointing. Moreover, as numerous numerical experiments show, it cannot be improved by the varying of the values of microstructure parameters. Therefore, we have to reconsider the microstructure model. It turns out that the change of the sign in source term in Eq. (6) (corresponding to the internal interaction force)

$$I\omega_t = C\varphi_x + \int\left(A\varepsilon + B\varphi\right)dx, \tag{15}$$

leads to a more appropriate result. The corresponding results of computations by using Eq. (15) instead of Eq. (6) are shown in Fig. 4.
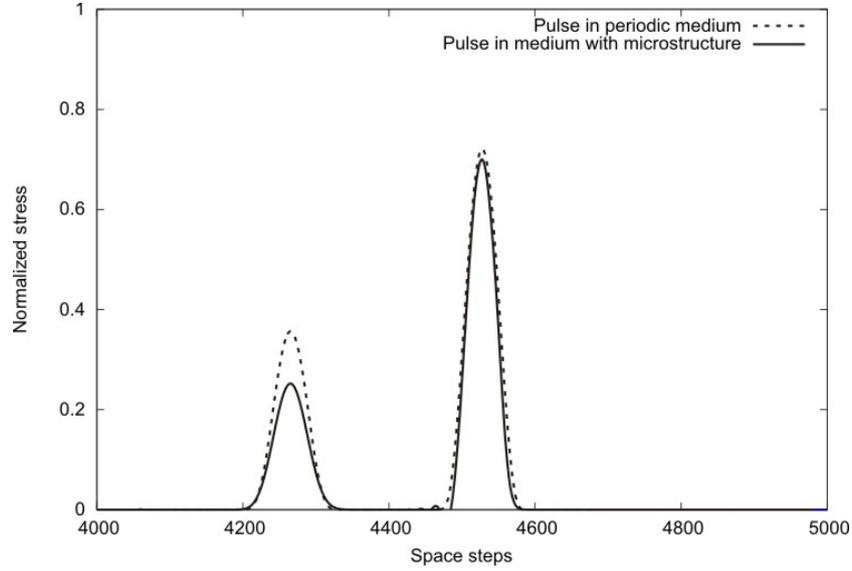
FIGURE 4. Leading transmitted pulses: improved model.

As one can see, the improved microstructure model is capable to reproduce the two leading transmitted pulses in a consistent way. The second pulse is smaller than the reference one because of the absence of a reflected trail in the case of the microstructure model.

The improved model can also reproduce the change in the pulse behavior due to the variation of the size of inhomogeneity ($d = 64\Delta x$ in Fig. 5). The size effect manifests itself in the change of the mutual location of small and big pulses.
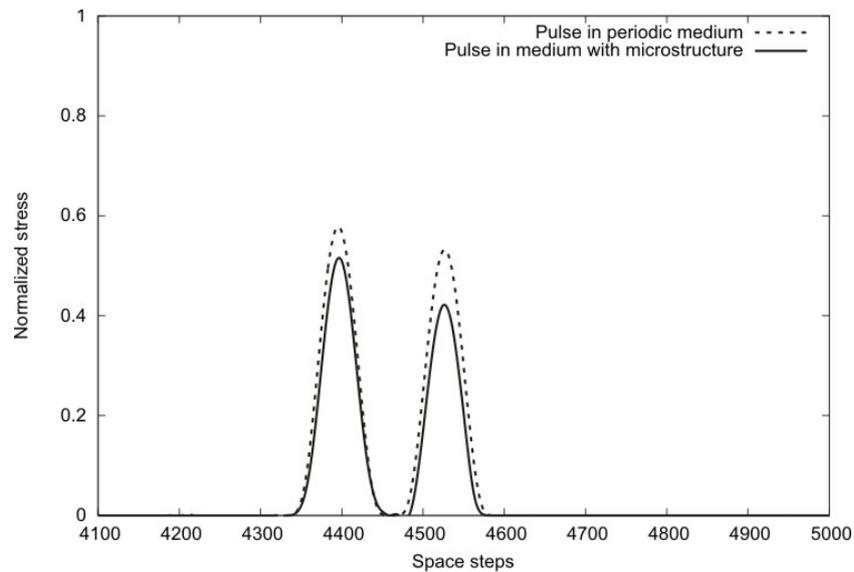
FIGURE 5. Leading transmitted pulses for $d = 64\Delta x$.

CONCLUSIONS

If we know all the details of given microstructure, namely, size, shape, composition, location and properties of inclusions as well as properties of carrier medium, the classical wave equation is sufficient for the description of wave propagation. The less we know concerning the microstructure, the more complicated equation is needed for the equivalent description of waves in the carrier medium which may be considered as simple as possible. In the paper, we have compared results of direct numerical calculations of wave propagation in laminates with the corresponding numerical simulations by using a microstructure model. As it is shown, numerical experiments demonstrate the need for a modification of the applied microstructure model. Nevertheless, the problem of parameters identification remains: some fitting is required to obtain the desirable behavior. At the same time, it is clear that the improved microstructure model qualitatively reproduce the microstructure influence on the macroscopic dynamics.

ACKNOWLEDGMENTS

REFERENCES

1. J.D. Achenbach, C.T. Sun and G. Herrman, *J. Appl. Mech.* **35**, 467–475 (1968).
2. J. Engelbrecht, A. Berezovski, F. Pastrone and M. Braun, *Phil. Mag.* **85**, 4127–4141 (2005).
3. Z. Wang and C.T. Sun, *Wave Motion* **36**, 473–485 (2002).
4. J. Fish, W. Chen and G. Nagai, *Int. J. Numer. Meth. Engng.* **54**, 331–346 (2002).
5. G. Cailletaud, S. Forest, D. Jeulin, F. Feyel, I. Galliet, V. Mounoury, S. Quilici, *Comp. Mater. Sci.* **27**, 351–374 (2003).
6. T. Bennett, I.M. Gitman and H. Askes, *Int. J. Fract.* **148**, 185-193 (2007).
7. P. Van, A. Berezovski and J. Engelbrecht, *J. Non-Equilib. Thermodyn.* **33** 235–254 (2008).
8. A. Berezovski, J. Engelbrecht and G.A. Maugin, „One-dimensional microstructure dynamics" in *Mechanics of microstructured solids: cellular materials, fibre reinforced solids and soft tissues*, edited by J.-F. Ganghoffer, F. Pastrone, Springer, 2009.
9. G.A. Maugin and W.Muschik, *J. Non-Equilib. Thermodyn.* **19**, 217–249 (1994).
10. R.J. LeVeque, *Finite Volume Methods for Hyperbolic Problems*, Cambridge University Press, 2002.
11. A. Berezovski, J. Engelbrecht and G.A. Maugin, *Numerical simulation of waves and fronts in inhomogeneous solids*, World Scientific, Singapore, 2008.
12. D.S. Bale, R.J. LeVeque, S. Mitran and J.A. Rossmanith, *SIAM J. Sci. Comp.* **24**, 955-978 (2003).
13. J. Engelbrecht and F. Pastrone, *Proc. Estonian Acad. Sci. Phys. Math.* **52**, 12-20 (2003).
14. J. D. Kaplunov and A. V. Pichugin, „On rational boundary conditions for higher-order long-wave models" in *IUTAM Symposium on Scaling in Solid Mechanics*, edited by F.M. Borodich, Springer, 2009, pp. 81-90.
15. H. Askes, B.Wang and T. Bennett, *J. Sound Vibr.* **314**, 650-656 (2008).

Publication VI

M.Berezovski, A.Berezovski, J.Engelbrecht
Waves in materials with microstructure: numerical simulation,
Proc. Estonian Acad. Sci., 2010.(accepted)

Waves in materials with microstructure: numerical simulation

Mihhail Berezovski*, Arkadi Berezovski, Jüri Engelbrecht

Centre for Nonlinear Studies, Institute of Cybernetics at Tallinn University of Technology, Akadeemia tee 21, 12618 Tallinn, Estonia

E-mail: misha@cens.ioc.ee

Abstract. Results of numerical experiments are presented in the paper in order to compare direct numerical calculations of wave propagation in a laminate with prescribed properties and corresponding results obtained for an effective medium with the microstructure modeling. These numerical experiments allowed us to analyze advantages and weaknesses of the microstructure model.

Key words: wave propagation, microstructured solids, numerical simulations, internal variables.

1. Background: Microstructure modelling

It is well known that the presence of a microstructure leads to the dispersion of waves propagating in the medium. The most general dispersive wave equation in one dimension is presented by Engelbrecht et al. (2005) based on the Mindlin theory of microstructure

$$u_{tt} = c^2 u_{xx} + \frac{C}{B} \left(u_{tt} - c^2 u_{xx} \right)_{xx} - \frac{I}{B} \left(u_{tt} - c^2 u_{xx} \right)_{tt} - \frac{A^2}{\rho_0 B} u_{xx}, \tag{1}$$

where u is the displacement, c is the elastic wave speed, ρ_0 is matter density, A, B, C, and I are coefficients defined later; subscripts denote derivatives.

More particular cases of the dispersive wave equation can be found in papers by Santosa and Symes (1991); Maugin (1995, 1999); Wang and Sun (2002); Fish et al (2002); Engelbrecht and Pastrone (2003); Metrikine (2006).

---

* Mihhail Berezovski, misha@cens.ioc.ee

As shown in (Engelbrecht et al., 2005), Eq. (1) is equivalent to the system of two equations of motion (Engelbrecht, Cermelli and Pastrone, 1999)

$$\rho_0 \frac{\partial^2 u}{\partial t^2} = \frac{\partial \sigma}{\partial x}, \tag{2}$$

$$I \frac{\partial^2 \varphi}{\partial t^2} = -\frac{\partial \eta}{\partial x} + \tau, \tag{3}$$

where the macrostress σ, the microstress η, and the interactive force τ are defined as derivatives of the free energy function

$$\sigma = \frac{\partial W}{\partial u_x}, \quad \eta = -\frac{\partial W}{\partial \varphi_x}, \quad \tau = -\frac{\partial W}{\partial \varphi}, \tag{4}$$

and the quadratic free energy dependence holds

$$W = \frac{\rho_0 c^2}{2} u_x^2 + A \varphi u_x + \frac{1}{2} B \varphi^2 + \frac{1}{2} C \varphi_x^2 + \frac{1}{2} D \psi^2. \tag{5}$$

Here c is the elastic wave speed, as before, A, B, C, and D are material parameters, φ and ψ are dual internal variables (Ván, Berezovski, and Engelbrecht, 2008).

Due to the definitions (4) and (5), the equations of motion both for macroscale and for microstructure can be represented in the form, which includes only primary internal variable

$$u_{tt} = c^2 u_{xx} + \frac{A}{\rho_0} \varphi_x, \tag{6}$$

$$I \varphi_{tt} = C \varphi_{xx} - A u_x - B \varphi, \tag{7}$$

where $I = 1/(R^2 D)$ and R is an appropriate constant.

In terms of strain and particle velocity, Eq. (6) can be rewritten as

$$\rho_0 v_t = \rho_0 c^2 \varepsilon_x + A \varphi_x. \tag{8}$$

The particle velocity and the strain are related by the compatibility condition

$$\varepsilon_t = v_x, \tag{9}$$

which forms the system of equations for these two variables. Similarly, introducing microvelocity w as follows:

$$\varphi_t = w_x, \tag{10}$$

which is the compatibility condition at the microlevel, we see immediately from Eqs. (7) and (10) that

$$I w_{tx} = C \varphi_{xx} - A \varepsilon - B \varphi. \tag{11}$$

Integrating the latter equation over x, we arrive at (with the accuracy up to arbitrary constant)

$$Iw_t = C\varphi_x - \int (A\varepsilon + B\varphi)dx. \tag{12}$$

Thus, we have two coupled systems of equations (8), (9) and (10), (12) for the determination of four unknowns: ε, v, φ, and w.

The goal of this paper is to examine the validity of the microstructure model. This is achieved by means of the comparison of the results of numerical simulations of a pulse propagation performed by using the microstructure model with the corresponding results of the pulse propagation in a medium with known heterogeneity properties (here referred to as comparison medium).

Next Section is devoted to the description of the high-resolution wave propagation algorithm for the solution of the coupled system of equations (8), (9) and (10), (12). Then the results of numerical simulations for test problems are presented both for microstructured and for comparison media. In last Section, the conclusions are given.

2. Numerical algorithm

2.1. Local equilibrium approximation

Wave propagation in solids is characterized by the values of velocity of the order of 1000 m/s. The corresponding characteristic time is of the order of hundreds or even tens of microseconds, especially in the impact induced events. It is difficult to expect that the corresponding states of material points during such fast processes are equilibrium ones. The hypothesis of local equilibrium is commonly used to avoid the troubles with non-equilibrium states.

The splitting of the body into a finite number of computational cells and averaging all the fields over the cell volumes leads to a situation, which is known in thermodynamics as "endoreversible system" (Hoffmann, Burzler and Schubert, 1997). This means that even if the state of each computational cell can be associated with a corresponding local equilibrium state (and, therefore, temperature and entropy can be defined as usual), the state of the whole body is a non-equilibrium one. The computational cells interact with each other which leads to the appearance of excess quantities (Muschik and Berezovski, 2004) which are introduced here both for macro- and microfields

$$\sigma = \bar{\sigma} + \Sigma \quad v = \bar{v} + V, \quad \varphi = \bar{\varphi} + \Phi, \quad w = \bar{w} + \Omega. \tag{13}$$

Here an overbar denotes averaged quantities, Σ is the excess stress, V is the excess velocity, Φ is the excess microstress, and Ω is the excess microvelocity, respectively.

Integrating Eqs. (8) and (9) over a computational cell, we have, respectively,

$$\rho_0 \frac{\partial}{\partial t} \int_{x_n}^{x_{n+1}} v dx = \bar{\sigma}_n + \Sigma_n^+ + A\bar{\varphi}_n + A\Phi_n^+ - \bar{\sigma}_n - \Sigma_n^- - A\bar{\varphi}_n + A\Phi_n^-$$
$$= \Sigma_n^+ - \Sigma_n^- + A\Phi_n^+ - A\Phi_n^-, \tag{14}$$

$$\frac{\partial}{\partial t} \int_{x_n}^{x_{n+1}} \varepsilon dx = v_n^+ - v_n^- = \bar{v}_n + V_n^+ - \bar{v}_n - V_n^- = V_n^+ - V_n^-. \tag{15}$$

Here $\sigma = \rho_0 c^2 \varepsilon$, and superscripts "+" and "-" denote values at right and left boundaries of the cell, respectively.

Determining the average quantities

$$\bar{v}_n = \frac{1}{\Delta x} \int_{x_n}^{x_{n+1}} v(x,t_k) dx, \quad \bar{\varepsilon}_n = \frac{1}{\Delta x} \int_{x_n}^{x_{n+1}} \varepsilon(x,t_k) dx, \tag{16}$$

we can construct a first-order Godunov-type scheme for the system of Eqs. (8) and (9) in terms of excess quantities

$$(\rho\bar{v})_n^{k+1} - (\rho\bar{v})_n^k = \frac{\Delta t}{\Delta x}\left(\Sigma_n^+ - \Sigma_n^-\right) + A\frac{\Delta t}{\Delta x}\left(\Phi_n^+ - \Phi_n^-\right), \tag{17}$$

$$\bar{\varepsilon}_n^{k+1} - \bar{\varepsilon}_n^k = \frac{\Delta t}{\Delta x}\left(V_n^+ - V_n^-\right), \tag{18}$$

by the finite difference approximation of time derivatives. Here the superscript k denotes time step, the subscript n denotes the number of computational cell, Δt and Δx are time step and space step, respectively.

2.2.   Excess quantities at the boundaries between cells

Though excess quantities are determined formally everywhere inside computational cells, we need to know their values only at the boundaries of the cells, where they play the role of numerical fluxes.

The values of excess quantities are determined from the jump relations providing the continuity of full stresses and velocities at boundaries between computational cells (cf. Berezovski and Maugin (2004))

$$[\![\bar{\sigma} + \Sigma + A(\bar{\varphi} + \Phi)]\!] = 0, \tag{19}$$

$$[\![\bar{v} + V]\!] = 0. \tag{20}$$

where $[\![A]\!] = A^+ - A^-$ denotes the jump of the enclosure at the discontinuity, $A^\pm$ are the uniform limits of A in approaching the discontinuity from the $\pm$ side.

The values of excess stresses and excess velocities at the boundaries between computational cells are not independent. They relate each other at the cell boundary as follows (Berezovski, Engelbrecht and Maugin, 2008):

$$\rho_n c_n V_n^- + \Sigma_n^- \equiv 0, \tag{21}$$

$$\rho_{n-1} c_{n-1} V_{n-1}^+ - \Sigma_{n-1}^+ \equiv 0. \tag{22}$$

As it is shown (Berezovski, Engelbrecht and Maugin, 2008), the excess quantities following from non-equilibrium jump relations at boundaries between computational cells correspond to the numerical fluxes in the conservative wave-propagation algorithm (Bale et.al, 2003). Therefore, the numerical scheme (17) - (22) is the reformulation and generalization of this algorithm in terms of excess quantities. The advantages of the wave-propagation algorithm are high-resolution (LeVeque, 1997, 2002) and the possibility for a natural extension to higher dimensions (Langseth and LeVeque, 2000).

2.3. Excess quantities for internal variables

Since the system of equations (8), (9) and (10), (12) are coupled, we need to solve the system of equations for internal variables (10), (12) simultaneously. Representing the mentioned system of equations in the form

$$\varphi_t = w_x, \tag{23}$$

$$Iw_t = \left(C\varphi - \int \int (A\varepsilon + B\varphi) dx^2 \right)_x, \tag{24}$$

we can construct the corresponding numerical scheme similarly to the case of macromotion

$$\bar{\varphi}_n^{k+1} - \bar{\varphi}_n^k = \frac{\Delta t}{\Delta x} \left(\Omega_n^+ - \Omega_n^- \right), \tag{25}$$

$$(I\bar{w})_n^{k+1} - (I\bar{w})_n^k = \frac{C\Delta t}{\Delta x} \left(\Phi_n^+ - \Phi_n^- \right), \tag{26}$$

where, in its turn, the values of the corresponding excess quantities are determined from the jump relations at boundaries between computational cells

$$\left[\left[C(\bar{\varphi} + \Phi) - (A\varepsilon + B\varphi)\Delta x^2 \right]\right] = 0, \tag{27}$$

$$\left[\left[\bar{w} + \Omega \right]\right] = 0, \tag{28}$$

accompanied with the Riemann invariants conservation

$$c_1 \Phi_{n-1}^+ - \Omega_{n-1}^+ \equiv 0, \tag{29}$$

$$c_1 \Phi_n^- + \Omega_n^- \equiv 0, \tag{30}$$

where a characteristic velocity for microstructure, c_1, is introduced by $C = Ic_1^2$.

2.4. Second order corrections

We can improve the accuracy of the algorithm by introducing second-order correction terms (LeVeque, 2002), which also can be represented in terms of excess quantities both for the macromotion

$$\mathcal{F}_i^I = \frac{1}{2}\left(1 - \frac{\Delta t}{\Delta x}c_i\right)(V_{i-1}^+ + V_i^-), \quad \mathcal{F}_i^{II} = \frac{1}{2}\left(1 - \frac{\Delta t}{\Delta x}c_i\right)(\Sigma_{i-1}^+ + \Sigma_i^-), \tag{31}$$

and for the microstructure

$$\mathcal{G}_i^I = \frac{1}{2}\left(1 - \frac{\Delta t}{\Delta x}\sqrt{C/I}\right)(\Omega_{i-1}^+ + \Omega_i^-), \quad \mathcal{G}_i^{II} = \frac{1}{2}\left(1 - \frac{\Delta t}{\Delta x}\sqrt{C/I}\right)(\Phi_{i-1}^+ + \Phi_i^-). \tag{32}$$

The corresponding Lax-Wendroff schemes have the form

$$(\rho\bar{v})_n^{k+1} - (\rho\bar{v})_n^k = \frac{\Delta t}{\Delta x}\left(\Sigma_n^+ - \Sigma_n^-\right) - \frac{\Delta t}{\Delta x}\left(\mathcal{F}_{n+1}^{II} - \mathcal{F}_n^{II}\right) + A\frac{\Delta t}{\Delta x}\left(\Phi_n^+ - \Phi_n^-\right) - A\frac{\Delta t}{\Delta x}\left(\mathcal{G}_{n+1}^{II} - \mathcal{G}_n^{II}\right), \tag{33}$$

$$\bar{\varepsilon}_n^{k+1} - \bar{\varepsilon}_n^k = \frac{\Delta t}{\Delta x}\left(V_n^+ - V_n^-\right) - \frac{\Delta t}{\Delta x}\left(\mathcal{F}_{n+1}^I - \mathcal{F}_n^I\right), \tag{34}$$

for the macromotion and

$$\bar{\varphi}_n^{k+1} - \bar{\varphi}_n^k = \frac{\Delta t}{\Delta x}\left(\Omega_n^+ - \Omega_n^-\right) - \frac{\Delta t}{\Delta x}\left(\mathcal{G'}_{n+1}^I - \mathcal{G'}_n^I\right), \tag{35}$$

$$(\bar{w})_n^{k+1} - (\bar{w})_n^k = \frac{\Delta t}{\Delta x}\left(\Phi_n^+ - \Phi_n^-\right) - \frac{\Delta t}{\Delta x}\left(\mathcal{G}_{n+1}^{II} - \mathcal{G}_n^{II}\right), \tag{36}$$

for the microstructure.

2.5. Results of numerical simulations

As a test problem, the one-dimensional propagation of a pulse is considered. The case of a comparison medium is analyzed first. In this case, the specimen is assumed homogeneous except of a region of length d, where periodically alternating homogeneous layers of size l are inserted (Fig. 1a).

The density and longitudinal velocity of the main specimen material are chosen as $\rho = 4510$ kg/m^3 and $c = 5240$ m/s, respectively. The corresponding parameters for the material of the inhomogeneity layers are $\rho_1 = 2703$ kg/m^3 and $c_1 = 5020$ m/s, respectively. Initially, the specimen is at the rest. The shape of the pulse before the crossing of the inhomogeneity region is formed by an excitation of the strain at the left boundary for an limited time period ($0 < t < 100\Delta t$)

$$u_x(0,t) = (1 + \cos(\pi(t - 50\Delta t)/50). \tag{37}$$

The length of the pulse is $\lambda = 100\Delta x$. Arrows in Fig. 1 show the direction of the pulse propagation. We consider different cases of the size of inhomogeneity, namely $l = 8\Delta x, 16\Delta x, 32\Delta x, 64\Delta x, 128\Delta x$. The pulse
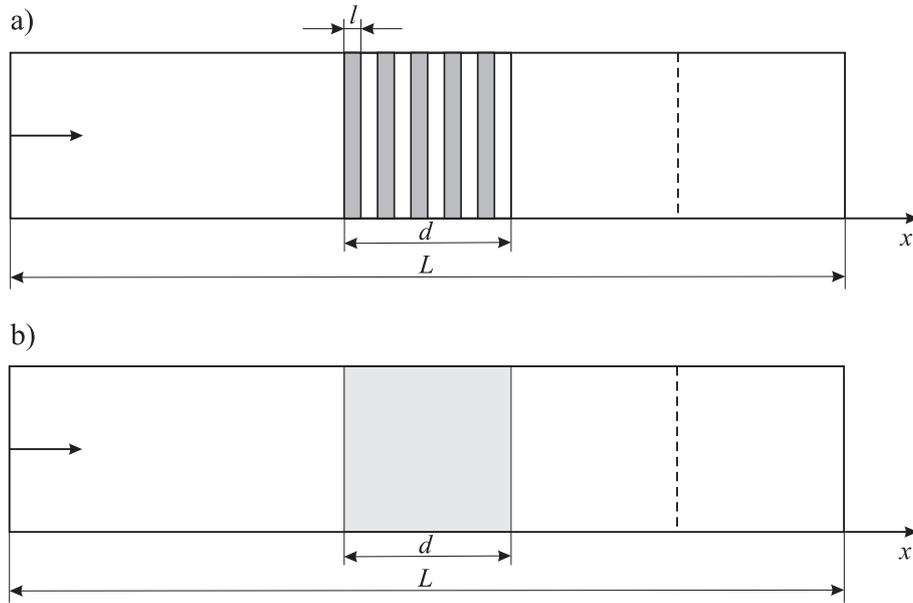
Fig. 1. Geometry of a test problem.

holds its shape up to the entering into the inhomogeneity region. After the interaction with the periodic multilayer, the single pulse is modified because of the successive reflections at each interface between the alternating layers.

Alternatively, the same pulse propagation was simulated by the microstructured model (8) - (12) (Fig. 1b) with the modified sign of the internal interaction force. This means that the equation (12) is replaced by

$$Iw_t = C\varphi_x + \int (A\varepsilon + B\varphi)dx. \tag{38}$$

In these calculations of the pulse propagation, the value of the internal length for the microstructure is kept the same as the size l of periodic layer, as well as density and sound velocity for inhomogeneities: $I = \rho_1, C = Ic_1^2$. The result of the comparison of pulse propagation in laminated and microstructured media is shown in Fig. 2 for the value of the size of inhomogeneity $l = 8\Delta x$. The values of coefficients in the microstructure model are chosen in such a way that location and amplitude of resulting pulses are as close as possible, which leads to the value $A = 19\rho c^2$ in the considered case. The length of the pulse $\lambda = 100\Delta x$ is much larger than the size of inhomogeneity, and the influence of the microstructure is rather small one.

Continuing the calculations we vary the size of inhomogeneity to $l = 16\Delta x$ and $32\Delta x$. The corresponding results are presented in Figs. 3 and 4. Again, the values of the coefficients in the microstructure model were adjusted to keep the location and amplitude of the leading pulse: $A = 97\rho c^2$ and $A = 147\rho c^2$ for $l = 16\Delta x$ and $32\Delta x$, respectively. As we can see, the model is able to reproduce the leading pulse change, but fails in the description of the tail.

Up to now, the size of inhomogeneity was less than the length of the initial pulse. We performed also
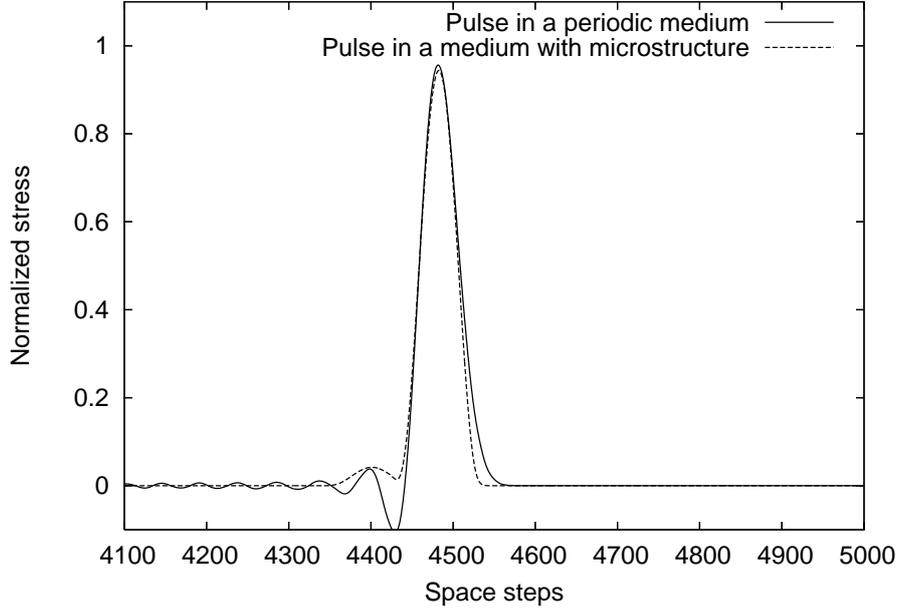
Fig. 2. Transmitted pulse at the inhomogeneity size $l = 8\Delta x$.

numerical experiments where this size is comparable with the length of the pulse: $l = 64\Delta x$ and $128\Delta x$. The corresponding results are presented in Figs. 5 and 6 with the values $A = 665\rho c^2$ and $A = 2059\rho c^2$, respectively. As one can see, if the inhomogeneity size is comparable with the initial pulse length, the ability of the model to reproduce the leading pulse shape is improved. The variation of the coefficient A in the computed microstructure model may be conjectured as related to the variation of the size of inhomogeneity. However, no straightforward relation is observed. As known from theoretical considerations (Engelbrecht et al., 2005), the ratio of the length of the pulse to the scale of the microstructure plays an important role. In terms of dispersion analysis, the problem is related to the difference of dispersion curves. In our calculations the inhomogeneity size is varied according to $2^n, n = 3, ..., 7$, while the length of the initial pulse remains unchanged. This means that we step over from one dispersion curve (for small ratio of the inhomogeneity size to the length of the pulse) to another one (for the ratio of the order of unity). It seems that for limiting cases of the ratio, the value of $A/\rho c^2$ is approximately proportional to 3^n, whereas this is not the case for intermediate values (the most illustrative case corresponds to the value $l = 32\Delta x$). The corresponding value of the coefficient B is determined by means of the shift of the location of the leading pulse: $B = A^2/(\rho c^2(1 - \alpha^2))$, where α is the value of the Courant number used in the calculation.

3. Conclusions

Numerical simulations of a pulse propagation in a laminated medium and in a medium with microstructure were performed to compare the results in order to check the validity of the microstructure model. Mate-
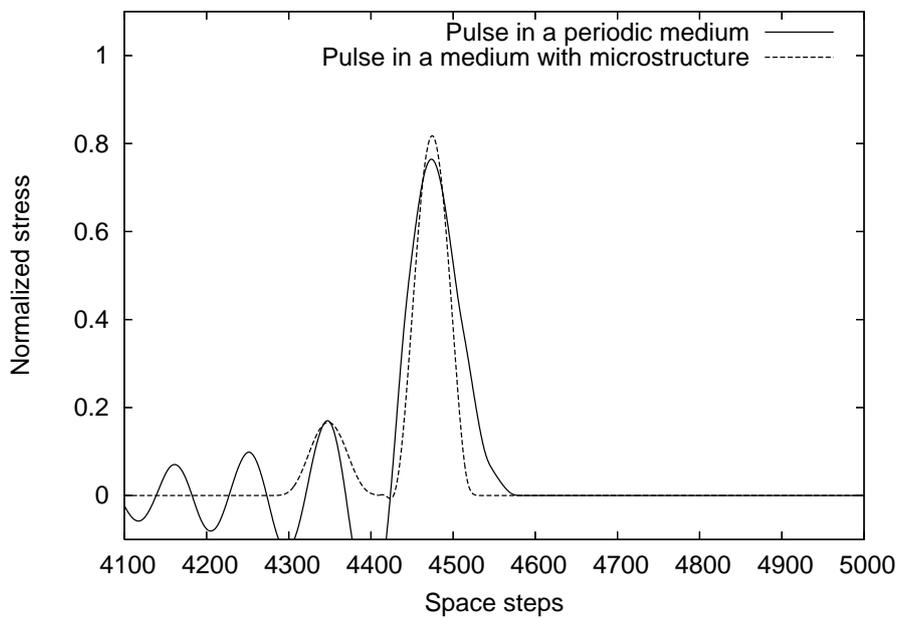
Fig. 3. Transmitted pulse at the inhomogeneity size $l = 16\Delta x$.
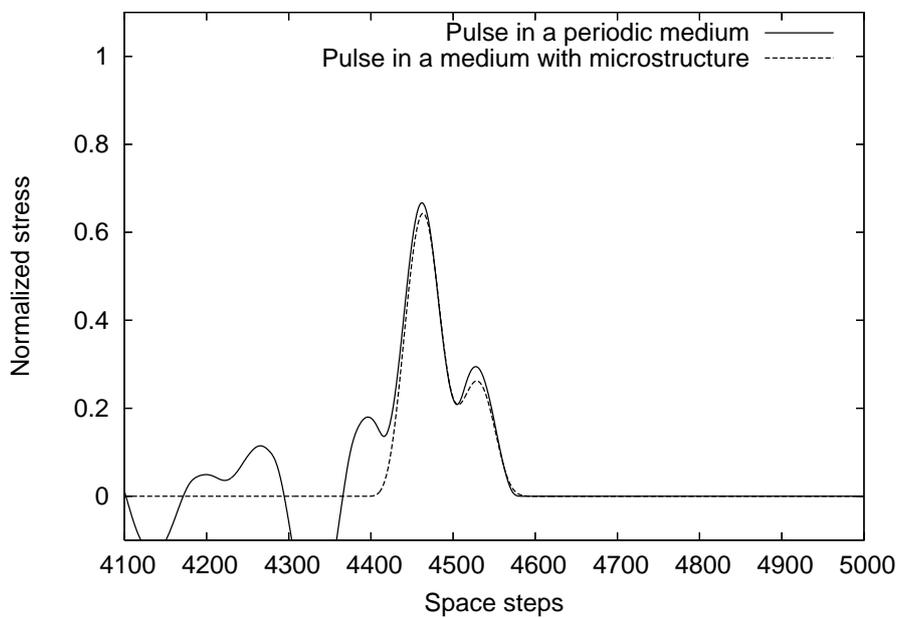
Fig. 4. Transmitted pulse at the inhomogeneity size $l = 32\Delta x$.
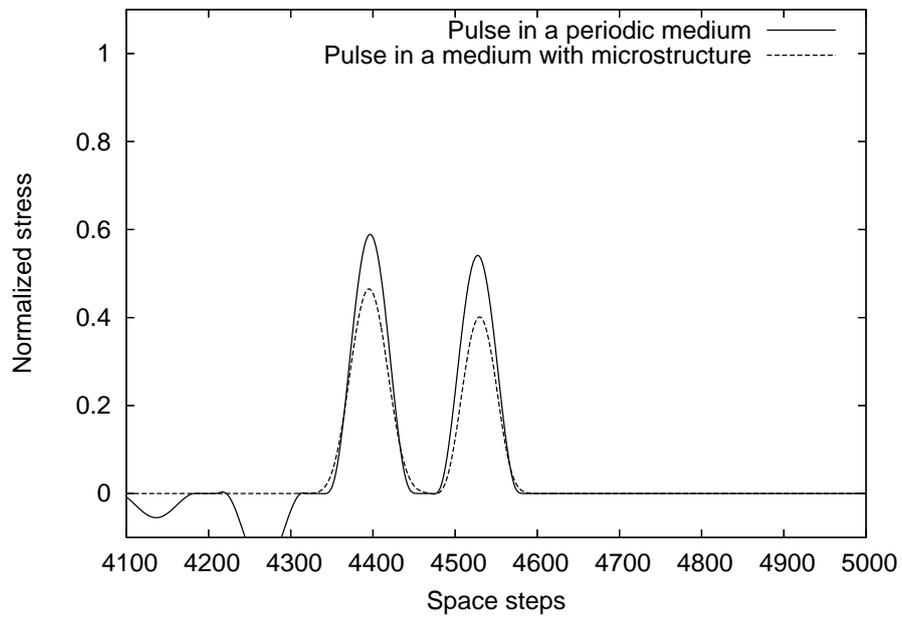
Fig. 5. Transmitted pulse at the inhomogeneity size $l = 64\Delta x$.
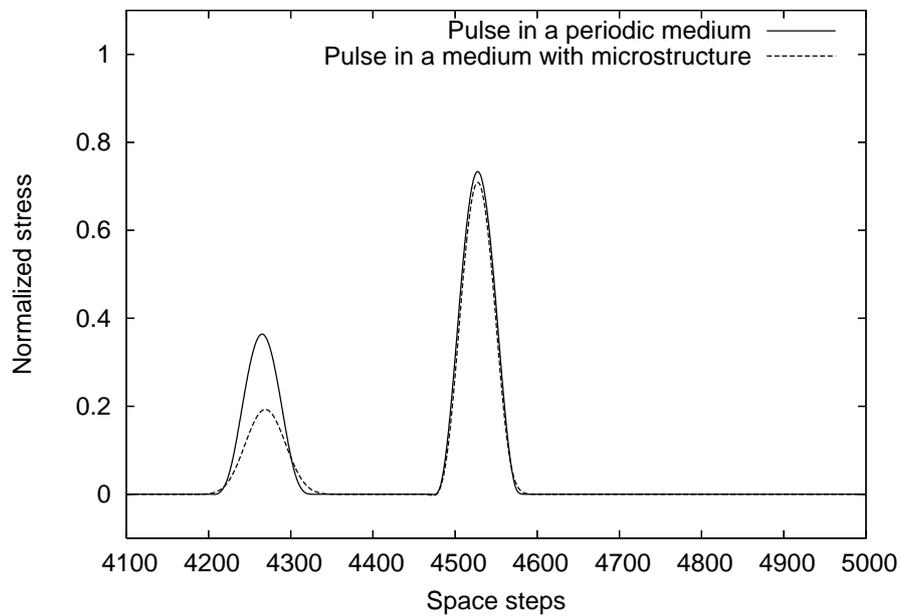
Fig. 6. Transmitted pulse at the inhomogeneity size $l = 128\Delta x$.

rial properties and the characteristic lengths used in calculations were chosen correspondingly to match both cases. The comparison of the results of numerical simulations shows that the coefficients in the improved microstructure model can be adjusted to achieve the accordance of the amplitude and location of the leading transmitted pulses in both cases. This means that the microstructure model is able to describe the wave propagation in complex media. At the same time, it is clear that the influence of the shape and orientation of inclusions needs to be investigated in the framework of two-dimensional formulation.

Acknowledgments

REFERENCES

Bale, D.S., LeVeque, R.J., Mitran, S. and Rossmanith, J.A. A wave propagation method for conservation laws and balance laws with spatially varying flux functions. *SIAM J. Sci. Comp.* **24**, 955–978 (2003).

Berezovski, A., Engelbrecht, J., Maugin, G.A. *Numerical simulation of waves and fronts in inhomogeneous solids.* World Scientific, Singapore (2008).

Berezovski, A. and Maugin, G.A. On the thermodynamic conditions at moving phase-transition fronts in thermoelaric solids. *J. Non-Equilib. Thermodyn.* **29**, 37–51 (2004).

Engelbrecht, J., Berezovski, A., Pastrone, F. and Braun, M. Waves in microstructured materials and dispersion, *Phil. Mag.* **85**, 4127–4141 (2005).

Engelbrecht, J., and Pastrone, F. Waves in microstructured solids with nonlinearities in microscale, *Proc. Estonian Acad. Sci. Phys. Mat.* **52**, 12–20 (2003).

Engelbrecht, J., Cermelli, P., Pastrone, F. Wave hierarchy in microstructured solids. In: Maugin, G.A. (ed.) *Geometry, Continua and Microstructure*, pp. 99–111. Hermann Publ., Paris, (1999).

Fish, J., Chen, W., Nagai, G. Non-local dispersive model for wave propagation in heterogeneous media: one-dimensional case. *Int. J. Numer. Meth. Engng.* **54**, 331–346 (2002).

Hoffmann, K. H., Burzler, J. M. and Schubert, S. Endoreversible thermodynamics, *J. Non-Equil. Thermodyn.* **22**, 311–355 (1997).

Langseth, J.O. and LeVeque, R.J. A wave propagation method for three-dimensional hyperbolic conservation laws, *J. Comp. Physics* **165**, 126–166 (2000).

LeVeque, R.J. Wave propagation algorithms for multidimensional hyperbolic systems, *J. Comp. Physics* **131**, 327–353 (1997).

LeVeque, R.J. *Finite Volume Methods for Hyperbolic Problems,* Cambridge University Press (2002).

Maugin, G.A. On some generalizations of Boussinesq and KdV systems, *Proc. Estonian Acad. Sci. Phys. Mat.* **44**, 40–55 (1995).

Maugin, G.A. *Nonlinear Waves in Elastic Crystals*. Oxford University Press (1999).

Metrikine, A.V. On causality of the gradient elasticity models. *J. Sound Vibr.* **297**, 727–742 (2006).

Muschik, W. and Berezovski, A. Thermodynamic interaction between two discrete systems in non-equilibrium, *J. Non-Equilib. Thermodyn.* **29**, 237–255 (2004).

Santosa, F., Symes, W.W. A dispersive effective medium for wave propagation in periodic composites. *SIAM J. Appl. Math.* **51**, 984–1005 (1991).

Ván, P., Berezovski, A., Engelbrecht, J. Internal variables and dynamic degrees of freedom. *J. Non-Equilib. Thermodyn.* **33**, 235–254 (2008).

Wang, Z.-P., Sun, C.T. Modeling micro-inertia in heterogeneous materials under dynamic loading. *Wave Motion* **36**, 473–485 (2002).

Deformatsioonilained mikrostruktuuriga materjalides: numbriline analüüs

Mihhail Berezovski, Arkadi Berezovski, Jüri Engelbrecht

Lainelevi modelleerimiseks mikrostruktuuriga materjalides on sobiv kasutada Mindlini mudelit, milles olulist rolli omab interaktsioon makro- ja mikrostruktuuri vahel. Kui mikrostruktuur on determineeritud nii nagu kihilistes komposiitmaterjalides, saab lainelevi kirjeldamiseks kasutada klassikalist homogeense materjali mudelit, kuid arvestada tuleb peegeldustega piirpindadelt. Käesolevas artiklis on kasutatud nimetatud mudelite analüüsiks lõplike mahtude meetodit ja võrreldud laineprofiile erinevate mudelite ja erinevate mastaabitegurite ja kihtide geomeetria puhul. Analüüsist selgub interaktsioonitegur, mis seob Mindlini mudelis makro- ja mikrostruktuuri. On näidatud, et see tegur sõltub lainepikkuse ja mastaabiteguri (determineeritud mudelis kihi paksuse) suhtest.

Appendix B
Curriculum vitae

Curriculum vitae

1. Personal data
   Name   Mihhail Berezovski
   Date and place of birth   Born September 01, 1980 in Vladivostok, Russia
   Citizenship   Estonian citizen by birth
   Marrital status   Married to Natalia, Tallinn, Estonia, April 2008

2. Contact information
   Address   Akadeemia tee 21, 12618, Tallinn
   Phone   +372 56 908 550
   E-mail   mihhail.berezovski@gmail.com

3. Education

Educational institution	Graduation year	Education (field of study/degree)
Tallinn University of Technology, Estonia	June 2003	Telecommunications / BSc
Tallinn University of Technology, Estonia	June 2006	Engineering Physics / MSc

4. Language competence / skills (fluent; average; basic skills)

Language	Level
English	Fluent
Russian	Fluent
Estonian	Average

5. Special courses

Period	Educational or other organisation
July 29th - August 27th, 2004	The 14th Jyvaskyla Summer School: "Numerical Simulation of Compressible Flow" University of Jyvaskyla, Jyvaskyla, Finland
September 4 - 8, 2006	CISM course: "Waves in Nonlinear Pre-Stressed Materials" Udine, Italy
August 26th - September 1st, 2007	EPSRC Maths for Engineers Summer School: "Mathematical Modelling and Computational Methods in Solid Mechanics" University of Glasgow, Glasgow, Scotland, UK

6. Professional Employment

Period	Organization	Position
September 2005 - to date	Institute of Cybernetics at Tallinn University of Technology	IT Administrator
September 2003 - September 2005	Institute of Cybernetics at Tallinn University of Technology	Engeneer

7. Scientific work

Papers

  I. A.Berezovski, M.Berezovski and J.Engelbrecht
  Numerical simulation of nonlinear elastic wave propagation in piecewise homogeneous media,
  Mater. Sci. Eng A 2006, **418**, 364-369.

 II. A. Berezovski, M. Berezovski, J. Engelbrecht, G.A. Maugin
  Numerical simulation of waves and fronts in inhomogeneous solids,
  in: Multi-Phase and Multi-Component Materials Under Dynamic Loading, W.K. Nowacki and Han Zhao (Eds.) Inst. Fund. Technol. Res. Warsaw, (EMMC-10 Conference proceedings), 2007, pp. 71-80.

III. A. Berezovski, M. Berezovski, J. Engelbrecht.
  Waves in inhomogeneous solids,
  in: *Applied Wave Mathematics - Selected Topics in Solids, Fluids and Mathematical Methods*, E.Quak, T. Soomere (Eds.) Springer, 2009, pp. 55-81.

IV. J. Engelbrecht, A. Berezovski, M. Berezovski.
  Deformation wave in microstructured materials: theory and numerics,
  in: Proceedings of the IUTAM Symposium on Recent advances of Acoustic Wave in Solids, May 25-28, 2009, Taipei, Taiwan. (accepted)

 V. M. Berezovski, A. Berezovski, J. Engelbrecht.
  Numerical simulations of one-dimensional microstructure dynamics,
  in: Proceedings of the 2nd International Symposium on Computational Mechanics (ISCM II), November 30 - December 3, 2009, Hong Kong - Macau. (accepted)

VI. M.Berezovski, A.Berezovski, J.Engelbrecht.
  Waves in materials with microstructure: numerical simulation,
  Proc. Estonian Acad. Sci., 2010. (accepted)

VII. M.Rousseau, G.A.Maugin and M. Berezovski
  Elements of wave propagation in dynamic materials
  Submitted to Journal of Sound and Vibration

Conference presentations

  I. A. Berezovski, M. Berezovski, J. Engelbrecht
  Numerical Simulation of Non-linear Elastic Wave Propagation in Piecewise Homogeneous Media
  EUROMECH Colloquium 466 Computational and Experimental Mechanics of Advanced Materials
  July 20 - 22, 2005, Loughborough, UK.

 II. A. Berezovski, M. Berezovski, J. Engelbrecht, G.A. Maugin
  Numerical simulation of waves and fronts in inhomogeneous solids
  EMMC-10 Conference
  June 11 - 14, 2007, Kazimierz Dolny, Poland.

III. J. Engelbrecht, A. Berezovski, M. Berezovski
Deformation Wave in Microstructured materials: Theory and Numerics.
IUTAM Symposium on Recent advances of Acoustic Wave in Solids
May 25-28, 2009, Taipei, Taiwan.

IV. M.Rousseau, G.A.Maugin and M. Berezovski
Elements of wave propagation in dynamic materials
7th EUROMECH Solid Mechanics Conference (ESMC2009)
September 7-11, 2009, Lisbon, Portugal.

V. M.Berezovski, A.Berezovski, J.Engelbrecht
Waves in materials with microstructure: numerical simulation
International Conference on Complexity of Nonlinear Waves
October 5-7, 2009, Tallinn, Estonia.

VI. M. Berezovski, A. Berezovski, J. Engelbrecht
Numerical simulations of one-dimensional microstructure dynamics.
2nd International Symposium on Computational Mechanics (ISCM II)
and 12th International Conference on Enhancement and Promotion of
Computational Methods in Engineering and Science (EPMESC XII)
November 30 December 3, 2009, Hong Kong Macau.

VII. M. Berezovski, A. Berezovski, J. Engelbrecht
Numerical simulation of wave propagation in materials with microstructure
SIAM Conference on Mathematical Aspects of Materials Science
May 23-26, 2010, Philadelphia, Pennsylvania.(accepted)

8. Defended theses
Internet access by ADSL technology, BSc, Tallinn University of Technology, 2003
Numerical simulation of elastic wave propagation in layered nonlinear media, MSc, Tallinn University of Technology, 2006

9. Fields of research interests
Computational methods, solid mechanics, materials with microstructure, composite materials.

10. Participation in projects

01.01.04 - 31.12.06	Estonian Science Foundation grant 5765, Numerical simulation of wave propagation in materials with internal interfaces
01.01.03 - 31.12.07	Estonian Block Grant 0322521s03, Nonlinear dynamics and stress analysis
01.01.07 - 31.12.10	Estonian Science Foundation grant 7037, Multiscale dynamics in microstructured solids
01.01.08 - 31.12.13	EEstonian Block Grant 0140077s08, Nonlinear dynamics and complex systems

Elulookirjeldus

1. Isikuandmed
   Ees- ja perekonnanimi   Mihhail Berezovski
   Sünniaeg ja -koht   01.09.1980, Vladivostok, Venemaa
   Kodakondsus   Eesti
   Perekonnaseis   Abielus

2. Kontaktandmed
   Aadress   Akadeemia tee 21, 12618, Tallinn
   Telefon   +372 56 908 550
   E-posti aadress   mihhail.berezovski@gmail.com

3. Hariduskäik

Õppeasutus	Lõpetamise aeg	Haridus (eriala/kraad)
Tallinna Tehnikaülikool	2003	Telekommunikatsioon / BSc
Tallinna Tehnikaülikool	2006	Tehniline füüsika / MSc

4. Keelteoskus(alg-, kesk- või kõrgtase)

Keel	Tase
Inglise	kõrgtase
Vene	kõrgtase
Eesti	kesktase

5. Täiendusõpe

Õppimise aeg	Täiendusõppe läbiviija nimetus
29.07 - 27.08.2004	The 14th Jyvaskyla Summer School: "Numerical Simulation of Compressible Flow" University of Jyvaskyla, Jyvaskyla, Finland
4-8.09.2006	CISM course: "Waves in Nonlinear Pre-Stressed Materials" Udine, Italy
26.04 - 01.09.2007	EPSRC Maths for Engineers Summer School: "Mathematical Modelling and Computational Methods in Solid Mechanics" University of Glasgow, Glasgow, Scotland, UK

6. Teenistuskäik

Töötamise aeg	Tööandja nimetus	Ametikoht
2005 - tänaseni	Küberneetika Instituut	Arvutisüsteemi administraator
2003 - 2005	Küberneetika Instituut	Insener

7. Teadustegevus
   Teadusartiklite, konverenstsiteeside ja konverentsiettekannete loetelu on toodud ingliskeelse CV juures.

8. Kaitstud lõputööd
   Internet access by ADSL technology, BSc, Tallinna Tehnikaülikool, 2003
   Numerical simulation of elastic wave propagation in layered nonlinear media, MSc, Tallinna Tehnikaülikool, 2006

9. Teadustöö põhisuunad
   Computational methods, solid mechanics, materials with microstructure, composite materials.

10. Osalus uurimisprojektides

01.01.04 - 31.12.06	Estonian Science Foundation grant 5765, Numerical simulation of wave propagation in materials with internal interfaces
01.01.03 - 31.12.07	Estonian Block Grant 0322521s03, Nonlinear dynamics and stress analysis
01.01.07 - 31.12.10	Estonian Science Foundation grant 7037, Multiscale dynamics in microstructured solids
01.01.08 - 31.12.13	Estonian Block Grant 0140077s08, Nonlinear dynamics and complex systems